

THE DEVELOPMENT OF A SHIP EMISSION PREDICTION MODEL FOR
SHIPS TRANSITING ICE-COVERED WATERS

By Joshua Veber

A thesis submitted to the School of Graduate Studies in partial fulfillment of requirements
for the degree of

Master of Engineering

Department of Ocean and Naval Architectural Engineering

Faculty of Engineering and Applied Science

Memorial University of Newfoundland and Labrador

October 2023

St. John's, Newfoundland & Labrador

Abstract

Marine traffic in ice-covered waters is increasingly becoming a common practice with improved access to the Arctic, new ship technology, and commercial interests, including shipping and resource extraction. Currently, ships transiting in ice are exempt from carbon emissions reporting while in ice due to a limited understanding of ship performance in ice and a lack of fairness compared with ships operating in open water. Therefore, the first stage in clarifying this area is to design an empirical emissions estimator for ships in ice. The lack of environmental reporting, specifically regarding level ice thickness, is first addressed by evaluating a method for statistically estimating sea ice thickness. The technique uses a model-tested ship performance equation to estimate level ice thickness from collected field data from the full-scale ship. The Canadian Coast Guard ship (CCGS) CCGS Henry Larsen was used to evaluate this method, and results were compared against Canadian Ice Service (CIS) ice charts for validation. Existing empirical performance models were compared with the CCGS Henry Larsen field data to investigate the limitations of predicting ship emissions in ice. A new empirical method was proposed, drawing on the existing prediction methods, and scaled using the CCGS Henry Larsen performance model. The International Maritime Organization (IMO) has extensive regulations for evaluating ship emissions of ships transiting open water. These regulations were adapted to the developed ice performance model to predict fuel consumption and carbon emissions for vessels transiting in ice-covered water. The complete model developed provides innovative methods for determining environmental conditions and predicting emissions for ships in ice.

Acknowledgments

I would like to acknowledge the Natural Sciences and Engineering Research Council (NSERC)/ Husky Energy (Cenovus) Industrial Research Chair in Safety at Sea for their financial support. I would also like to gratefully acknowledge the support of the National Research Council of Canada (NRC) for the provision of research and experimental data.

A much-appreciated acknowledgment to my supervisors, including – Dr. Brian Veitch for allowing me the opportunity to continue my education under his direction and guidance, Dr. David Molyneux for his expertise and knowledge on matters related to ship performance operating in ice, and Dr. Thomas Browne for his support on the issues of relevant marine regulations and collaboration with the NRC.

I would also like to give a special mention to various industry professionals for their continued support and advice throughout my degree – Jeffrey Brown for his technical support with accessing ship field data, Jungyong Wang for his assistance in analyzing and incorporating model test data from the NRC, and Dan Olford for his expertise on IMO regulations regarding emissions of ships at sea.

Thank you to my engineering team and manager William Andrews at the Canadian Coast Guard (CCG), for their continued support throughout my education and for fostering my interest in the marine industry.

Lastly, I would like to thank my family, parents Paul and Denise, and Sister Sarah, for their continued support and instilling a desire to learn and build on my professional engineering career.

Contents

ABSTRACT.....	II
ACKNOWLEDGMENTS	III
CONTENTS.....	IV
LIST OF FIGURES	VII
LIST OF TABLES	IX
LIST OF ABBREVIATIONS AND SYMBOLS	X
1 INTRODUCTION	1
1.1 OVERVIEW	1
1.2 BACKGROUND.....	1
1.3 PURPOSE	3
2 LITERATURE REVIEW	5
2.1 EMPIRICAL ICE RESISTANCE MODELS	5
2.1.1 <i>Vance</i>	7
2.1.2 <i>Lewis</i>	7
2.1.3 <i>Zahn & Philips</i>	8
2.1.4 <i>Lindqvist</i>	9
2.1.5 <i>Keinonen</i>	9
2.1.6 <i>Riska</i>	11
2.1.7 <i>Semi-Empirical Summary</i>	11
2.2 SHIP PROPULSION.....	13
2.3 MARINE EMISSIONS REGULATIONS	15
2.3.1 <i>Marine Fuel Consumption</i>	16
2.3.2 <i>IMO EEDI & CII</i>	17
2.3.3 <i>CIS Ice Charts</i>	20
2.4 CCGS HENRY LARSEN.....	22
2.4.1 <i>Type 1200 Model Tests</i>	24

2.4.2	<i>Full-scale Data</i>	28
3	METHODOLOGY	30
3.1	STATISTICAL APPROACH FOR ESTIMATION SEA ICE THICKNESS	30
3.2	EMPIRICAL ICE RESISTANCE COMPARISON	35
3.3	ESTIMATING PROPULSIVE EFFICIENCY	37
4	RESULTS.....	39
4.1	ICE THICKNESS ESTIMATES	39
4.1.1	<i>Validating Method in Open Water Transit</i>	40
4.1.2	<i>Statistical Ice Estimate Results</i>	42
4.1.3	<i>Special Cases</i>	48
4.2	MODIFIED EMPIRICAL ICE PREDICTION MODEL	51
4.2.1	<i>Analysis of Existing Empirical Models</i>	52
4.2.2	<i>Factorial Design Experiment</i>	55
4.2.3	<i>Validating Modified Keinonen Model</i>	62
4.3	REGRESSION SHIP PROPULSION EFFICIENCIES.....	64
4.3.1	<i>Thrust Estimates</i>	65
4.3.2	<i>Propeller Efficiency</i>	71
4.4	EMISSIONS PREDICTIONS.....	78
4.4.1	<i>Fuel Consumption</i>	78
4.4.2	<i>Complete emissions prediction model</i>	80
5	DISCUSSIONS.....	81
5.1	PRACTICAL APPLICATION OF EQUIVALENT-LEVEL ICE.....	81
5.2	LIMITATIONS	82
5.3	FUTURE APPLICATIONS	84
5.3.1	<i>Simulator Training</i>	85
5.3.2	<i>Route Planning Optimization</i>	87
5.4	FUTURE IMPROVEMENTS.....	88
6	CONCLUSIONS.....	90

7	REFERENCES	91
8	APPENDIX A – CCGS HENRY LARSEN DATA SEGMENT ANALYSIS.....	94

List of Figures

Figure 1 - CCGS Henry Larsen in Deception Bay, QC, on October 31, 2022.	23
Figure 2 - Open water resistance curve for full-scale ship, ITTC 57.....	26
Figure 3 - TT Sense ® mounted on CCGS Henry Larsen port shaft.	29
Figure 4 - Route plot for segments #11 and #12.	31
Figure 5 - Full-scale RPM (Left) and Speed (Right) for duration of segments #11 and #12.	31
Figure 6 - Plot of all 22 data segments located around the northwest peninsula of Newfoundland.	40
Figure 7 - Map of open water segment.	41
Figure 8 - Open water estimated ice thickness for model validation.	41
Figure 9 - Plot of segment #14 route in the Strait of Belle Isle.	43
Figure 10 - CIS Ice Chart for NE Newfoundland Waters March 3rd, 2022 (Canadian Ice Service, 2022) © Her Majesty the Queen in Right of Canada, as represented by the Minister of Environment Canada, [2022].	44
Figure 11 - Ice thickness estimate for segment #14.	46
Figure 12 - Segment #1 ice thickness estimate resembling open water.	49
Figure 13 - Estimated Ice Thickness for Dataset 19.	51
Figure 14 - Empirical resistance estimates for CCGS Henry Larsen at an ice thickness of 0.5m.	54
Figure 15 - Empirical resistance estimates for CCGS Henry Larsen at an ice thickness of 1m	54
Figure 16 - Empirical resistance estimates for CCGS Henry Larsen at an ice thickness of 1.5m	55
Figure 17 - Half-normal plot to identify statistically significant terms StatEase®	58
Figure 18 - Pareto graph showing the t-value of most significant terms StatEase®	59
Figure 19 - Normal plot of residuals. The assumption of normality is valid.	60
Figure 20 - Residual vs predicted plot. Residuals are evenly distributed and within limits.	61

Figure 21 - Modified Keinonen model used to predict the resistance of CCGS Henry Larsen in 1m level ice at speeds from 0.5-5m/s.....	62
Figure 22 - Modified Keinonen model used to predict the resistance of MT Sotka in 0.54m level ice at speeds from 0.5-5m/s.....	64
Figure 23 - Regression analysis of CCGS Henry Larsen thrust deduction for all 22 data segments. Thrust deduction as a function of ship speed and ice thickness.....	66
Figure 24 - CCGS Henry Larsen thrust deduction curves based on regression equation of speed and ice thickness. Curves are shown at speeds ranging from 1m/s to 5m.s in thicknesses up to 1m.	68
Figure 25 - Plot of CCGS Henry Larsen thrust measured and predicted for data segment #14.....	69
Figure 26 - Thrust predictions for data segment #3.....	70
Figure 27 - Motor power estimated using a regression scaling factor.	73
Figure 28 - Propeller performance curves in open water, CCGS Henry Larsen full scale propellers.....	74
Figure 29 - Motor power estimated using propeller efficiency curves.	75
Figure 30 - CCGS Henry Larsen Power Predictions using scaled behind hull efficiency and propeller curves for segment #14.....	77
Figure 31 - Fuel Consumption and carbon emissions for CCGS Henry Larsen segment #14.....	79

List of Tables

Table 1 - Conversion factors between fuel consumption and CO ₂ emissions (International Maritime Organization, 2018).....	17
Table 2 - Table of data segments used for statistical estimation of sea ice thickness.	32
Table 3 - Summary of statistical ice thickness estimates and ice chart comparison. Additional Details provided in Appendix A – CCGS Henry Larsen Data Segment Analysis.....	47
Table 4 - Parameters for chosen empirical methods.	56
Table 5 - Design of experiments factors.	57
Table 6 - Empirical prediction parameters for the MT Sotka (Erceg & Ehlers, 2017).	63
Table 7 - CCGS Henry Larsen propeller specifications (Wang, 2023).....	73

List of Abbreviations and Symbols

IMO	International Maritime Organization
B	Beam
c	Concentration
CCG	Canadian Coast Guard
CCGS	Canadian Coast Guard Ship
CII	Carbon Intensity Index
CIS	Canadian Ice Service
D	Propeller Diameter [m]
ECCC	Environment & Climate Change Canada
EEDI	Energy Efficiency Design Index
EEOI	Energy Efficiency Operational Index
F_h	Ice Thickness Froude Number
g	Gravitational Constant [m/s^2]
GHG	Green House Gases
HFO	Heavy Fuel Oil
h_i	Ice Thickness [m]
H_v	Equivalent Ice Thickness [m]
IMO	International Maritime Organization
J	Advance Coefficient
n	Propeller RPM
NRC	National Research Council of Canada
OCRE	Ocean Coastal and River Engineering
POLARIS	Polar Operational Limit Assessment Risk Indexing System
R_B	Ice Buoyancy Resistance [N]
R_{BR}	Icebreaking Resistance [N]

R_C	Ice Crushing Resistance [N]
R_I	Ice Resistance [N]
R_{IT}	Total Ice Resistance [N]
R_{OW}	Open Water Resistance [N]
R_{IO}	Risk Index Outcome
R_{IV}	Risk Index Value
ρ_i	Ice Density [kg/m ³]
ρ_s	Saltwater Density [kg/m ³]
S_N	Ice Strength Number
SOLAS	Safety of Life at Sea
STW	Speed Through Water [m/s]
σ_f	Flexural Ice Strength [Pa]
t	Thrust Deduction Factor
T_E	Effective Thrust [N]
V_S	Ship Speed [m/s]

1 Introduction

1.1 Overview

The marine industry is experiencing increasing pressure to mitigate the level of emissions from maritime transportation and to push towards a greener global fleet. The emissions must be considered in all shipping aspects, including ice-covered water operations. This research proposes an emissions model to predict fuel consumption and emissions for ships transiting ice-covered water. It is tested and validated against full-scale ship data.

Emissions in the marine industry are the measure of carbon dioxide mass produced by a ship during regular operation. As climate change becomes an ever-impending threat, the global consensus is that technology must evolve to adapt, produce less emissions, and slow its effects. As one of the largest global producers of emissions, the marine industry has an onus to reduce its impacts in the coming years. The marine industry is also known to use heavy fuel oils which the emissions and pArcticles emitted can accelerate local ice melting in the Arctic.

1.2 Background

Current regulations express some limitations and allocations on advanced navigation such as in ice due to complex modelling and a need for fair regulating. Therefore, research must be conducted to refine these conditions and improve the adaptation of regulations in the marine industry. The International Maritime Organization (IMO) regulates the emissions permitted by ships through two standards: the Energy

Efficiency Design Index (EEDI) and the Carbon Intensity Index (CII). The EEDI is a term for a ship's design efficiency. It is primarily used in design calculations to estimate the emissions profile of a ship before construction (International Maritime Organization, 2018). The EEDI remains constant. However, it can be modified if ships undergo refits to modify machinery or improve fuel types.

The CII, in contrast, is an operational parameter that must be reported to the IMO annually (International Maritime Organization, 2022). It is calculated by the ratio of the mass of carbon dioxide emissions over the capacity times distance traveled. Capacity is considered a ship's deadweight, or in the case of passenger vessels and ro-ro ferries, the gross tonnage is used. Ships are exempt from reporting their CII when transiting in ice. As such, the regulations do not apply to the portion of a ship's voyage through ice.

The IMO does consider a limited scope of full-scale ships through an ice-capable factor. However, this is limited to ice strengthened ice classes of cargo vessels up to 1A super (International Maritime Organization, 2018), and instead offers relaxation of the CII regulation to icebreakers while transiting open water. The IMO recognizes that not all ships are designed equal, and their mission parameters may position them with an emission disadvantage. However, it still does not consider the time these ships operate in ice as part of the CII calculation.

Research has been conducted on ship emissions in ice by developing a route-optimizing agent for ice-covered water (Browne, et al., 2022). This research aimed to develop a goal-based route optimizer; one such goal was minimizing fuel consumption. This model was based on the Keinonen method for ship performance (Keinonen, Browne, Revill, & Reynolds, 1996), and the emissions estimates were determined by the work of

Frederking (Frederking, 2003). No further justification was used to validate the accuracy of the emissions predictions in the route-optimizing research. This assumption was adequate given the objective of optimizing routes where the difference in emission production between routes is more critical than the actual mass of carbon dioxide produced.

The research in this thesis was conducted through a collaboration among Memorial University, the National Research Council (NRC) of Canada, and the Canadian Coast Guard (CCG). Two primary sources of input data are used to develop this analysis, both of which are based on the Canadian Coast Guard Ship (CCGS) CCGS Henry Larsen. The NRC developed and tested a 1:20 scaled model of the CCGS Henry Larsen in their open water and ice tow tank laboratories. These tests resulted in open water performance based on ITTC-57 method and regression-based ice performance parameters, which are the base of the operational parameters for statistical ice thickness estimates made in this thesis. The full-scale running data was supplied by a joint NRC and CCG full-scale measurement campaign on the CCGS Henry Larsen (Wang, et al., 2023). The collection of position and propulsion parameters from this ship, measured over an extended period, provided the necessary running data for estimating sea ice thickness and predicting emission outputs in this thesis.

1.3 Purpose

This research aimed to develop an emissions prediction model and statistical ice thickness estimator for ships transiting in ice. The objective was to create a model that could be applied to a broad scope of vessels with different hull shapes and performance

capabilities. The approach to achieving this model was to evaluate existing methods for individual components of ship performance and marine emissions through validation with full-scale ship operational data as well as environmental data including ice conditions. Regression analysis was used to apply modifications and adapt existing prediction models to ice-covered sea conditions.

2 Literature Review

A literature review was conducted to find and evaluate scholarly works relevant to the project. This review was conducted using Memorial University's library One Search tool, Google Scholar, and through discussions with relevant industry professionals. Some key search words included: *Ice navigation; Ice resistance; marine emissions; ship performance model; ice forecasting; marine propulsion; propeller design; and ship efficiency*. Preference was placed on the most relevant research within the last decade; however, considering the limited research in specific fields, exceptions were made so as not to exclude essential or unique information. This consideration is applied to research on ice resistance as many of the most cited works in this area exceed 25 years. The following section highlights the key literature by categorizing fundamental research objectives, including ice resistance models, ship propulsion, marine emissions, and CCGS Henry Larsen.

2.1 Empirical Ice Resistance Models

Ships transiting ice face a highly variable environment that is often difficult to model using conventional ice resistance methods. One of the most frequent methods for estimating ship ice performance is calculating the resistance in equivalent-level ice. This term refers to a generalization of the ice cover in terms of a single uniform value for thickness which incorporates the different aspects, including ice thickness, snow cover, and

pressure, among other variables. This method provides a simple qualitative value for evaluating a specific hull form's performance characteristics.

Many published works have presented semi-empirical based models, often generated using full-scale and model test data to estimate ship performance in equivalent-level ice. These methods are often employed in ship design as a qualitative concept development tool to evaluate ice-breaker designs. For this research, the semi-empirical models were evaluated against verified ship performance models to evaluate their accuracy.

Several publications independently review these empirical models and evaluate their performance. The report “Review of ship ice interaction mechanics” provides a comprehensive historical overview of the existing models (Daley & Riska, 1990). However, this publication does not provide insight into the validity of these models and merely indicates the evolution of the models with time. The equations for these models get progressively more complex with time and incorporate increasingly more performance variables. It is also evident that the existing empirical methods are based on performance regression instead of physics-based models (Daley & Riska, 1990).

A comparison of the more commonly used methods is presented in the paper “Semi-empirical level ice resistance prediction methods” (Erceg & Ehlers, 2017). This review evaluates the predictions of ice resistance using six empirical models against field data from four ships. The analysis determined that the empirical models are inconclusive and that no single model was sufficient to predict the captured data, despite all models estimating within the vicinity of the measured values (Erceg & Ehlers, 2017). However, a lack of field data used in the analysis results in this inconclusiveness. The results were only plotted for a single ice thickness, and the paper does not address the thickness as a changing variable.

It was determined that all six methods be evaluated in this research project to enable a comparison of the CCGS Henry Larsen's results with those of the four ships presented in the publication by Erceg & Ehlers (2017).

The following sub-sections detail the specific empirical equations considered; their origins and fundamental attributes are highlighted.

2.1.1 Vance

The empirical model developed by Vance was derived from full-scale trials on the USCG Katmai Bay. The equation comprises two components which are summarized as ice submersion and speed dependence. This model is known to typically predict higher increasing values with higher ice strength, which alluded to conditions experienced during the trials (Vance, 1980).

The most significant drawback of this model is its limited scope. Unlike the following methods, Vance's model is exclusively based on one ship during one test period.

2.1.2 Lewis

Lewis' model was developed using full-scale trial data for four ships ranging in length from 39.6m to 295.7m (Lewis, Debord, & Bulat, 1982). The consideration of multiple model hulls was an improvement over Vance. However, there remained some issues with the results of this model. It is noted that the intercept values or ice friction predictions are typically higher than Lewis' prediction. This finding is assumed to have

resulted from two ships not having low friction coatings and a high level of snow cover during the trials.

The significant contribution of Lewis to the progression of empirical models is the consideration of two ship scale terms and two ice parameters. However, the limitations do not make it the most reliable prediction model.

2.1.3 Zahn & Philips

Unlike the previous two methods, Zahn & Philips (1987) based their prediction model on model test data instead of full-scale trials. This approach was an attempt to prove that ship ice model testing was a valid method for determining ship ice resistance. However, like its predecessors, the common flaw is that this model is based solely on one ship, the USCG Mobile Bay (Zahn & Philips, 1987). As such, there was no method for determining the effects of the ship parameters and the friction component. This method also stands out from the rest because the resistance was found to be dependent on velocity squared as opposed to linear. As a result, the predictions at higher speeds are often much higher than the other methods.

Zahn suggested the model was appropriate to be applied to ships outside the Bay class used for the analysis (Zahn & Philips, 1987). However, they also developed a linearly fitted regression equation as an alternative, which is not considered.

2.1.4 Lindqvist

Lindqvist was the first to develop an empirical method for ship design to estimate ship ice resistance before model testing (Lindqvist, 1989). Lindqvist's objective was to develop a simple equation for ship ice resistance, including three primary breaking terms: ice crushing, breaking by bending, and submergence. The model approximates the hull as flat surfaces and elements of ice deflection and trim are ignored to achieve simplicity (Lindqvist, 1989).

Lindqvist was the first to propose a method that incorporates the geometry of the bow, including stem, flare, and waterline. Bow form is critical when developing a model adaptable to various hull forms. The methods were validated using a series of full-scale data from three ice-breaking hulls. The only major issue with Lindqvist's model is that all trials were taken from the Baltic Sea. As such, the validation did not appropriately accommodate changes in the ice parameters, and its accuracy in Arctic regions is not guaranteed (Erceg & Ehlers, 2017). Also, the simplified nature of this method adds an element of error to the prediction result that may undervalue the ice resistance estimate. The predictions are known to be reasonably accurate for larger ships, with some uncertainty for smaller ships and for ice parameters that differ from those of the Baltic Sea (Erceg & Ehlers, 2017).

2.1.5 Keinonen

Keinonen's method is known to be one of the most comprehensive empirical models because it was developed using full-scale trials and operator expertise for 18 of the world's

most relevant icebreakers. This allowed Keinonen to incorporate the bow shape factors, dimensional ship parameters, and ice properties in the greatest detail compared to its predecessors (Erceg & Ehlers, 2017). This semi-empirical model consists of three components: open water, resistance under 1m/s, and resistance over 1m/s. This is to account for the typical speed-dependent variable found in the other methods (Keinonen, Browne, Revill, & Reynolds, 1996).

Keinonen's method also accounts for hull condition correction based on coating and age and for environmental and ice parameters. Bow form is also a large contributor to a ship's ice-breaking capability, which is accounted for by using the bow waterline and flare angle. Keinonen goes so far as to also divide the semi-empirical equations into two hull categories, round and chined (Keinonen, Browne, Revill, & Reynolds, Icebreaker characteristics synthesis, 1996).

Keinonen's method has proven to be accurate within the following constraints (Keinonen, Browne, Revill, & Reynolds, 1996). Keinonen's method was validated against ships and conditions that fall within these ranges, and they are reflective of most hull form shapes that operating regularly in ice:

- $H_i = 0.5 \sim 1.7\text{m}$ (Ice thickness)
- $\sigma_f = 150 \sim 700\text{kPa}$ (Flexural strength of ice)
- $\psi = 40^\circ \sim 80^\circ$ (Average bow flare angle at waterline)
- $\beta = 12^\circ \sim 40^\circ$ (Average buttock angle at waterline)

This range of input variables result in a robust prediction method applicable to a broad scope of ships. This range incorporates the majority of hull types used for modern ice-breaking.

2.1.6 Riska

The most recent model considered in this analysis is the one developed by Riska. It is a derivation of the Lindqvist method by incorporation of other relevant research. It was validated using full-scale data, however, it only considered Baltic Sea conditions (Erceg & Ehlers, 2017). The Riska method uses two terms, one for speed-independent resistance and another for speed dependent. Riska assumes many of the ice parameters as constant for simplicity and only relies on the ice thickness to describe the ice (Riska, Wilhelmson, Englund, & Leiviska, 1998). This method incorporates three variables: external conditions, ship size, and hull shape. Since many ice parameters were assumed constant and higher than usually measured in full-scale trials, Riska’s method typically slightly overestimates measured resistance.

2.1.7 Semi-Empirical Summary

(Vance, 1980)

$$R_{ice} = 55.8583(\rho_w - \rho_i)gBh^2 + 0.0188\sigma_f vB \sqrt{\frac{h}{g}}$$

(Lewis, Debord, & Bulat, 1982)

$$R_{ice} = \left(3.8989 + 0.0123 \frac{\sigma_f}{\rho_w g h} + 0.223 \left(\frac{v}{\sqrt{gB}} \cdot \frac{L}{h} \right) \right) \cdot \rho_w g B h^2$$

(Zahn & Philips, 1987)

$$R_{ice} = \left(4.254 + 3.963 \cdot 10^{-5} \left(\frac{v}{\sqrt{gB}} \right)^2 \left(\frac{L}{h} \right)^3 \right) \cdot \rho_w g B h^2$$

(Lindqvist, 1989)

$$R_{ice} = (R_c + R_b) \left(1 + \frac{1.4v}{\sqrt{gh}} \right) + R_s \left(1 + \frac{9.4v}{\sqrt{gL}} \right)$$

$$R_c = \frac{F_v (\tan \varphi + (\mu \cdot \cos \varphi / \cos \psi))}{1 - (\mu \cdot \cos \varphi / \cos \psi)}$$

$$R_b = \frac{27}{64} \sigma_f \left(\frac{h^{1.5}}{\sqrt{\frac{E}{12(1-v^2)\rho_w g}}} \right) \left(\tan \varphi + \frac{\mu \cdot \cos \varphi}{\sin \alpha \cdot \cos \psi} \right) \left(1 + \frac{1}{\cos \psi} \right)$$

$$R_s = \Delta \rho g h B \left(T \frac{B+T}{B+2T} + \mu (0.7L - \frac{T}{\tan \varphi} - \frac{B}{4 \tan \alpha} + T \cos \varphi \cos \psi \sqrt{\frac{1}{\sin^2 \varphi} + \frac{1}{\tan^2 \alpha}} \right)$$

(Keinonen, Browne, Revill, & Reynolds, 1996)

$$R(V)_{total} = R(V)_{ow} + R(1ms^{-1})_{ice} + R(> 1ms^{-1})_{ice}$$

Ships With Round Hulls

$$R(1ms^{-1}) = 0.015 \cdot h_e^{1.5} \cdot C_s \cdot B^{0.7} \cdot L^{0.2} \cdot T^{0.1} \cdot (1 - 0.0083(t + 30)) \cdot C_h \cdot (0.63 + 0.00074 \cdot \sigma_f) \cdot (1 + 0.0018(90 - \psi)^{1.6}) \cdot (1 + 0.003(\beta - 5)^{1.5})$$

$$R(> 1ms^{-1})_{ice} = 0.009 \cdot (V_{increase} / \sqrt{gL}) \cdot B^{1.5} \cdot L^{0.5} \cdot h_e \cdot (1 - 0.0083(t + 30)) \cdot C_h \cdot (1 + 0.0018(90 - \psi)^{1.6}) \cdot (1 + 0.004(\beta - 5)^{1.5})$$

Ships with Chined Shoulders

$$R(1ms^{-1}) = 0.08 + 0.017 \cdot h_e^{1.25} \cdot C_s \cdot B^{0.7} \cdot L^{0.2} \cdot T^{0.1} \cdot (1 - 0.0083(t + 30)) \cdot C_h \cdot (0.63 + 0.00074 \cdot \sigma_f) \cdot (1 + 0.0018(90 - \psi)^{1.6}) \cdot (1 + 0.004(\beta - 5)^{1.5})$$

$R(> 1ms^{-1})_{ice} = 0.009 \cdot (V_{increase}/\sqrt{gL}) \cdot B^{1.5} \cdot L^{0.5} \cdot h_e \cdot (1 - 0.0083(t + 30)) \cdot C_h$ $\cdot (1 + 0.0018(90 - \psi)^{1.4}) \cdot (1 + 0.003(\beta - 5)^{1.5})$
<p>(Riska, Wilhelmson, Englund, & Leiviska, 1998)</p> $R_{ice} = C_1 + C_2$ $C_1 = f_1 \frac{1}{2\frac{T}{B} + 1} BL_{par}h + (1 + 0.021\varphi)(f_2Bh^2 + f_3L_{bow}h^2 + f_4BL_{bow}h)$ $C_2 = (1 + 0.063\varphi)(g_1h^{1.5} + g_2Bh) + g_3h \left(1 + 1.2\frac{T}{B}\right) \frac{B^2}{\sqrt{L}}$

2.2 Ship Propulsion

Connecting a ship's resistance to its emissions profile requires analyzing its propulsion system. This calculation presents one of the most significant challenges in creating a generalized emissions profile because many propulsion values are specific to a hull and its installed powerplant system. However, the relevant literature does provide some insight into methods for predicting the necessary losses in efficiency. This section will focus on the efficiency losses and the propeller geometry effects.

Several transmission losses must be understood to determine the brake power from the resistance of a ship. These include the thrust deduction factor (t), equation (1) and the total propulsive efficiency (η_p), equation (2). Propulsive efficiency directly relates the effective power to the shaft power by combining three other efficiencies: hull efficiency, behind hull efficiency, and shaft efficiency (Zubaly, 1996).

Thrust deduction is effectively the added resistance due to the propeller effects, which gives the relation between ship resistance and thrust. Equation (1) defines the relationship between total resistance and thrust using the thrust deduction.

In typical cases, the thrust deduction can be analyzed using a series of towed and self-propelled model tests or by using computational fluid dynamics (CFD). However, these methods are costly and therefore not a feasible solution for a general emissions model. Zubaly (1996) suggests a range of Harvald (1983) thrust deduction values of 0.15-0.20 for single screw ships and 0.10-0.18 for twin screws. (Harvald, 1983) provides additional plots for estimating the trust deduction based on the ship parameters, form, and propeller size.

$$T = \frac{R_T}{1 - t} \quad (1)$$

where:

T	-	Total Thrust
R _T	-	Total Resistance
t	-	Thrust Deduction

The NRC has also provided thrust deduction equations for the CCGS Henry Larsen model tests, described further in Section 2.4.1. This analysis determines the thrust deduction at various speeds and ice thicknesses. The calculated values are also compared against the range provided by (Zubaly, 1996).

Propulsive efficiency is equally difficult to define for a generalized model. Determining these efficiency values would require a detailed analysis of a ship hull and its propeller. In most cases, the ships for which the emissions model will be subjected will not have the level of specification available to calculate these values accurately. Therefore, the propulsive efficiency must be estimated. The components that make up the overall propulsive efficiency are described by equation (2).

$$\eta_P = \frac{P_E}{P_S} \quad (2)$$

$$= \frac{P_E}{P_T} \times \frac{P_T}{P_D} \times \frac{P_D}{P_S}$$

$$= \eta_H \times \eta_B \times \eta_S$$

where:

P_E	-	Effective Power
P_T	-	Thrust Power
P_D	-	Delivered Power
P_S	-	Shaft Power
η_P	-	Propulsive Efficiency
η_H	-	Hull Efficiency
η_B	-	Behind Hull Efficiency
η_S	-	Shaft Transmission Efficiency

2.3 Marine Emissions Regulations

Regulations surrounding permissible ship emissions and future targets for ships transiting open water already exist. The regulations considered are those adopted by the IMO. These regulations will serve exclusively as a basis for developing the generalized emissions model; however, additions must be made to adapt emission calculations to ships in ice. Most notably, according to the International Convention for the Safety of Life at Sea (SOLAS), ships are not required to report their emissions as part of the carbon intensity index (CII) when operating in ice (International Maritime Organization, 2022). This regulation specifically emphasizes cargo ships and ferries with a quantified economic value as opposed to service vessels such as offshore supply boats. Additional research was conducted to capture methods for adapting the CII methodology to other service vessels.

2.3.1 Marine Fuel Consumption

Ship emissions are based on several fuel consumption considerations. Once the required power is determined, fuel consumption and carbon dioxide emissions are calculated by factoring in the installed powerplant of a vessel. The most basic setup for consideration would be a direct drive or geared transmission where the propeller shaft is mechanically connected to the main engines. The shaft and engine power are most closely related in this arrangement. This would contrast with a diesel-electric or separated drivetrain where the power is transferred electrically from the main engines to individual propulsion motors. Direct drive systems are common in bulk carriers with large slow-speed diesels that often transit at consistent operating conditions. Icebreakers, in contrast, often have a separated propulsion system to allow for added power when needed for heavy ice conditions. Therefore, the model must be adaptable to various powering systems.

To translate power into fuel consumption, one must know the specific fuel consumption (SFC) of a ship's installed powerplant. Specific fuel consumption will differ based on the engines installed and usually sits between 155-225 [g/kWh] for marine diesel engines (Sustainable Ships, 2022). However, this value is not constant for each engine. Instead, engines are most fuel-efficient when operating near 85%-90% of their maximum continuous rating and experience decreased efficiency with decreased power. Therefore, the benefit of a separated drivetrain over a direct drive is maintaining all running engines in their most efficient operating condition. Engine manufacturers typically provide the SFC, however, this data is not always available for specific ships and would need to be estimated within the provided range.

Carbon emissions are based on fuel types and the amount consumed. The emissions can be calculated once the fuel consumption and fuel type are known. The IMO provides a table of carbon dioxide production rates in tons of carbon per ton of fuel (C_F) for various common marine fuel types, summarized in Table 1 (International Maritime Organization, 2018). As defined by the IMO, special considerations are required for dual fuel applications and gas turbines.

Table 1 - Conversion factors between fuel consumption and CO₂ emissions (International Maritime Organization, 2018).

Type of Fuel	Carbon Content	C_F (t-CO₂/t-Fuel)
Diesel/Gas Oil	0.8744	3.206
Light Fuel Oil (LFO)	0.8594	3.151
Heavy Fuel Oil (HFO)	0.8493	3.114
Liquefied Petroleum Gas (LPG)	0.8182	3.000
Liquefied Natural Gas (LNG)	0.7500	2.750
Methanol	0.3750	1.375
Ethanol	0.5217	1.913

2.3.2 IMO EEDI & CII

The IMO also has a specific set of regulations for emissions reduction and monitoring for existing vessels. These regulations are described as the carbon intensity index (CII) and the energy efficiency design index (EEDI). They have become an integral part of modern commercial cargo transport by sea. The EEDI is considered a design metric, and the CII is a quantitative assessment of a ship's economic benefit to environmental impact ratio. Despite neither of these terms being directly required to calculate a ship's live fuel consumption, a modern emissions model must consider their relevance.

The EEDI is a design metric for evaluating a ship's emissions profile. It remains a constant value and is changed by modifying a ship's operating parameters, main machinery, or cargo capacity. The units of EEDI are the grams of carbon dioxide production over the deadweight tonnage times ship speed (International Maritime Organization, 2018). There are special considerations for ships transiting ice. However, the EEDI regulations focus on deadweight as a metric for evaluating economic capacity and are only mandatory for cargo and passenger-type vessels. This metric aims to develop a baseline for ship design and lifecycle tracking for greenhouse gas emissions. This regulation does not address a large portion of service-based vessels that operate in Arctic regions. Most notably, these regulations do not account for scientific research, icebreakers, and supply boats.

Additional research has reformed how service-based and non-cargo vessels can consider the EEDI value. This research looked at ways to evaluate service-based work, including tasks like anchor handling, towing and scientific research. Gasper & Erikstand (2009) developed a basic formula for assessing EEDI as presented in equation (3) and their focus was defining the mission parameter for various service tasks. One example they used was for an offshore supply vessel (OSV). They defined six operating profiles and nine operating states for this type of vessel. These operating conditions were weighed by time, and their emissions profile was defined by the specific fuel consumption of each task. Although they focused the research on OSVs, the method of creating customized mission profiles for specific specialized ships can be applied.

$$Energy\ Emissions = \frac{Emission}{Mission \cdot Time} \quad (3)$$

The authors of this research admit that there are several limitations and that additional work is needed to define accurate operating profiles for specific ships. Most notably, they highlight the inaccuracy of estimating the time allotted to each operating profile and how that can differ drastically from a ship's actual use. Also, accurately assessing the SFC of service-based vessels can be challenging because much of their tasks can be tactical, leading to fluctuations in SFC (Gasper & Erikstand, 2009).

The CII is another method that the IMO uses to regulate ship emissions. The CII measures the carbon a ship produces compared to its gross carrying capacity and distance traveled. It is mandatory for cargo-carrying vessels over 5000 GT to report (International Maritime Organization, 2022). The CII does not consider actual cargo transported; this is only considered in the alternate voluntary Energy Efficiency Operational Indicator (EEOI). The EEOI requires actual cargo when calculating the emissions per tonne-mile (Det Norske Veritas, 2022).

Much like the EEDI, the CII is a method for providing emissions assessment rather than prediction. To predict the attained CII value for a given vessel and operation, it is first necessary to predict the fuel consumption and emissions. Accurately predicting fuel consumption and emissions for ships in ice represents a gap in the body of knowledge. The current research proposes a general method for estimating fuel consumption and emissions for ships in ice.

2.3.3 CIS Ice Charts

The Canadian Ice Service (CIS), which is part of Environment and Climate Change Canada (ECCC), supplies daily ice charts. The ice charts are generated for waterways surrounding Canada's coasts and describe the ice coverage of a particular region. Historical ice charts were used as a source of validation for the research (Canadian Ice Service, 2022).

The ice charts use a system of zones identified by egg codes. These codes describe the ice coverage of each specified zone in terms of the concentration in tenths, the stage of development with associated thickness, and the general floe size (Milakovic, Schutz, Piehl, & Ehlers, 2018). There are typically up to three defined ice stages for each egg code. Each ice type identified in an ice regime denotes a different stage of development within a range of thicknesses. The partial concentrations of each ice type indicate the potential of encounter and can be used to assess risk. The zones or ice regimes are determined by detailed analysis of satellite imagery which is used to determine the thickness and drift patterns of sea ice (Canadian Ice Service, 2022).

Several methods exist to determine a ship's capability to safely operate in ice conditions in the Canadian Arctic. The first and oldest is known as the Zone Date System (Transport Canada, 2010). This method is based on historical ice data in the Canadian Arctic and does not consider current ice charts. It provides a date range of accessibility to specific areas based on historical ice conditions and the ice class of a given ship. This method is dated because it does not allow the operator to evaluate their risk and consider

current ice conditions. It also does not account for climate change; therefore, ice predictions are based on dated ice probability models.

The second method developed for the Canadian Arctic was AIRSS. This method influenced the more recent IMO's Polar Operational Limit Assessment Risk Indexing System (POLARIS). Both systems allow the operator to perform a quantitative risk assessment for their ship's Polar classification in a specific zone. In POLARIS, this risk calculation is called the Risk Index Outcome (RIO) (International Maritime Organization, 2016). The RIO is calculated by equation (4), where the risk index values (RIV) are determined based on the ship's Polar classification and ice types.

RIVs are whole number integers where positive values indicate lower risk and increasing negative values indicate higher risk (International Maritime Organization, 2016). The RIO considers partial concentration as a probability of ice type encounter. As such the RIV values are weighted based on concentration levels. This allows the calculations to consider concentrations of open water. RIVs are determined in the IMO regulations depending on the ships ice class and the ice type.

RIO's are used as an operational parameter to determine the risk of transit. Any positive values constitute normal operation for the specific class of vessel while negative values present elevated operational risk (International Maritime Organization, 2016). When the RIO is less than negative ten, the ship may only transit under special considerations and under extreme risk.

$$RIO = \sum_{i=1}^n C_i \times RIV_i \quad (4)$$

where:

RIO	-	Risk index outcome
RIV	-	Risk index value
C _i	-	Concentration of partial ice thickness

2.3.3.1 Equivalent-level Ice

The most common way of defining the thickness of a zone is to define its equivalent ice thickness (H_v). This method takes the average thickness for each defined stage and the total weighted average by concentration according to Equation (5) (Milakovic, Li, Polach, & Ehlers, 2020). The problem with this method is that it averages the entire zone and may not accurately describe the location the ship passes through. The interest in the equivalent ice thickness lies in understanding the average trend of ice chart ice regime data into a single value to support the ability to make performance predictions.

$$H_v = \frac{\sum_{i=1}^n h_i \cdot c_i}{c_{tot}} \quad (5)$$

where:

H _v	-	Equivalent ice thickness
H _i	-	ice thickness
c _i	-	partial concentration
c _{tot}	-	total concentration

2.4 CCGS Henry Larsen

The CCGS Henry Larsen forms the basis for all research on sea ice estimation in this study. Launched in 1987, this ship is an Arctic class 4 medium icebreaker operated by the CCG to carry out missions in the Arctic and along Canada's East Coast. The primary missions of this ship include Arctic Ocean research, hydrographic surveys, and program

icebreaking. The program's icebreaking tasks include seasonal icebreaking along the northwestern coast of the island of Newfoundland. This primarily comprises harbor breakouts, escorts, and northern resupply missions. Figure 1 shows the CCGS Henry Larsen in Deception Bay, Quebec, on October 31, 2022, during one of its Arctic resupply missions.



Figure 1 - CCGS Henry Larsen in Deception Bay, QC, on October 31, 2022.

The vessel's specifications include an overall length of 99.8 m with an installed power of 16,080 kW split across three (3) Wärtsilä Vasa – 16V32 main engines. This powerplant drives two (2) fixed-pitch shafted propellers through a diesel-electric arrangement. The CCGS Henry Larsen also has a bubbler system designed to lubricate the hull with air when transiting through particularly heavy ice. The bubbler is operated by ejecting pressurized air from the mid-body below the waterline. The bubbler operation was not considered in this analysis.

The CCGS Henry Larsen was used for this analysis because of the extensive testing completed by the NRC at both the model and full scales. The operational parameters of the CCGS Henry Larsen are presented through several publications from the NRC, which provide the tools that enable extensive statistical analysis.

2.4.1 Type 1200 Model Tests

Model tests were completed on the CCGS Henry Larsen model hull form throughout the year 2019 to define the open water and ice-covered performance capabilities of the ship (Wang, 2023).

The model ship was built at 1:20 scale. The overall length of the model was 4.06 m. Some slight modifications were made in consultation with the CCG to adapt the hull for the installed test equipment, including propellers and rudder (Wang, 2023).

The thrust deduction factor was also determined using a regression analysis of the model scale results on the hull form. The resulting regression equation is shown in Equation (6) and are derived from the model tests (Wang, 2023).

Open water tests were conducted in a 200 m towing tank, and the power prediction method used was based on the International Towing Tank Conference (ITTC) 57 procedures (ITTC Resistance Committee, 2011). The correlation allowance for the ITTC procedures was 0.0004, which mirrors the approach of the NRC model analysis (Wang, 2023). There is some concern regarding using the correlation allowance at slow speeds because the value is validated against full-scale trials conducted at higher ship speeds.

However, the open water component makes up a small portion of ice resistance, and high variability exists in the measured full-scale data.

The open water resistance curve is necessary for statistically estimating sea ice thickness because it is a significant component of the net measured thrust. The open water curve for the full-scale ship (based on the model test measured values) is shown in Figure 2. A trend line was used to define the lower speed range because the operational speed in all considered ice cases was low, and the fit was acceptable. The equation for open water resistance at speeds up to 12 knots is shown in Equation (7).

$$t = 0.23J^2 + 0.04J + 0.07 \quad (6)$$

where:

$$J = \frac{V_A}{nD}$$

where:

J	-	Advance Coefficient
V_A	-	Total Resistance
n	-	Thrust Deduction
D	-	Propeller Diameter
t	-	thrust deduction

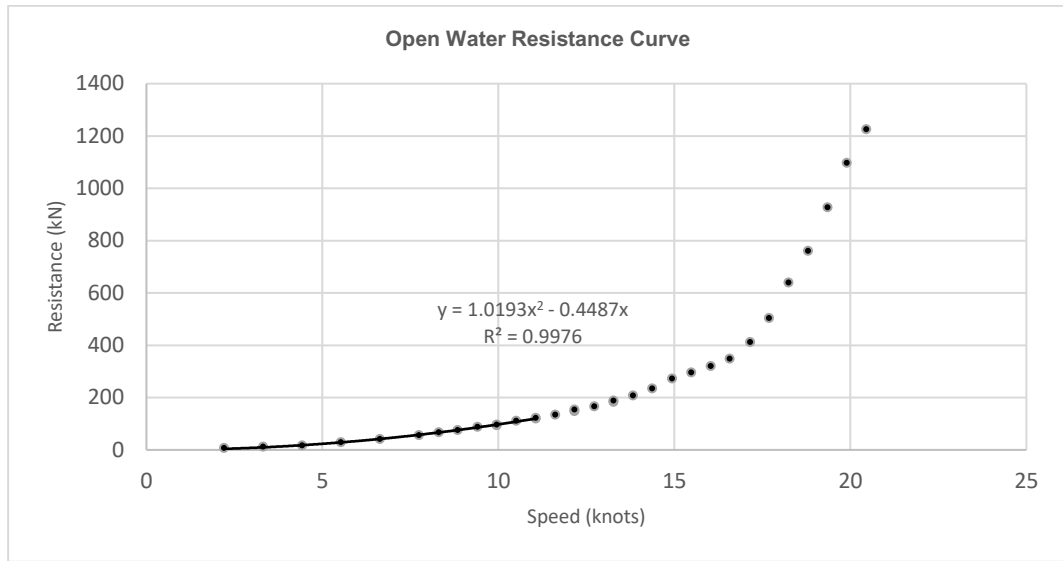


Figure 2 - Open water resistance curve for full-scale ship, ITTC 57.

$$R_{OW} = 1.0193V_S^2 - 0.4487V_S \quad (7)$$

where:

- R_{OW} - Open Water Resistance
- V_S - Ship Speed

The model was tested in ice at the National Research Council of Canada's Ocean, Coastal and River Engineering Research Centre (NRC-OCRE) for both open water and ice performance (Wang, 2023). These tests were conducted between November and December of 2020. Several tests were completed to capture the individual components of icebreaking resistance, including level ice, pre-sawn ice, creep tests, and open water tests (Wang, 2023). This approach allowed the analysis of specific components of icebreaking: breaking, clearing, buoyancy, and open water.

The ice resistance model tests were analyzed using a regression analysis approach. The analysis was subdivided into individual components corresponding to icebreaking, ice-crushing, buoyancy, and open water. Equation (8) illustrates the summation of forces contributing to total ice resistance. Equation (9) outlines the regression results for the

icebreaking component and includes the ice strength number. Equation (10) shows the ice buoyancy component of total resistance. Equation (11) shows the ice clearing equation and includes the ice thickness Froude number (ITTC Resistance Committee, 2011).

$$R_{IT} = R_{BR} + R_C + R_B + R_{OW} \quad (8)$$

where:

R_{IT}	-	Total Ice Resistance
R_{BR}	-	Icebreaking Resistance
R_C	-	Ice Crushing Resistance
R_B	-	Ice Buoyancy Resistance
R_{OW}	-	Open Water Resistance

$$R_{BR} = 1.896(S_N)^{-1.66} \rho_i B h_i V_S^2 \quad (9)$$

where:

S_N	-	Ice Strength Number
ρ_i	-	Ice Density
B	-	Beam
h_i	-	Ice Thickness
V_S	-	Ship Speed

where:

$$S_N = \frac{V_S}{\sqrt{\frac{\sigma_f h_i}{\rho_i B}}}$$

where:

σ_f	-	Ice Flexural Strength
------------	---	-----------------------

$$R_B = 1.71(\rho_s - \rho_i) g h_i B T \quad (10)$$

where:

T	-	Draft
-----	---	-------

$$R_C = 1.448(F_h)^{-1.11} \rho_i B h_i V_S^2 \quad (11)$$

where:

F_h - Ice Froude Number

where:

$$F_h = V_s / \sqrt{gh_i}$$

The primary purpose of the total ice resistance equation is to determine the ice resistance for any given ship speed and ice thickness. However, in the current research the equation was solved for ice thickness for a given ship speed and thrust to determine statistical ice thickness, described in section 3.1.

2.4.2 Full-scale Data

The NRC has led a full-scale data acquisition campaign on the CCGS Henry Larsen in cooperation with the CCG and Memorial University (Wang, et al., 2023). The data used for the research presented here spans from February 2, 2022 – March 4, 2022. The navigation area is in the coastal regions on the west coast of Newfoundland, particularly the Strait of Belle Isle. The segments considered in this paper stretch as far south as Pakuashipi, Quebec. This period was selected as it presented the highest number of steady operating segments to analyze.

The NRC also tested the bubbler system on the CCGS Henry Larsen during March 2022 (Wang, et al., 2023); therefore, additional information regarding ice parameters is

available. Tests were conducted on ice samples: the measured average ice density (ρ_i) was 900 kg/m³, and the average ice strength (σ_f) was 500 kPa. These parameters were used to calculate statistical ice thickness (Wang, et al., 2023).

A VAF TT-Sence® was installed on each propulsion shaft to measure the propulsion data: Thrust, Torque, RPM, and Power (Wang, et al., 2023). The digital Data Acquisition System recorded ground and water speeds, rudder command and angle, and position data, among other metrics (Wang, et al., 2023). The data used for this analysis was recorded at 1 Hz. Figure 3 shows the TT Sense ® as mounted on the port shaft. The primary strain gauges for measuring torque and thrust are within the casing surrounding the shaft on the left of the photo.



Figure 3 - TT Sense ® mounted on CCGS Henry Larsen port shaft.

3 Methodology

In this section, the experimental procedure is outlined in detail. The first area of research discussed is the process for statistically estimating sea ice using a ship performance model and live captured full-scale field data. Secondly, the process for analyzing and comparing semi empirical models is emphasized. The approach to estimating general propulsive efficiency is outlined and finally, the method for modelling ship emissions is presented.

3.1 Statistical Approach for Estimation Sea Ice Thickness

To ensure data segments were consistent, each day was reviewed to identify segments with the highest degree of steady operation. This was achieved by reviewing both the RPM and speed through water (STW) outputs. Segments were chosen at times where both these metrics were deemed to be constant. Also, only conditions where the ship was moving forward were considered. Tactical ice maneuvers, including harbor breakouts, were excluded.

As an example, Figure 4 illustrates the path travelled by the CCGS Henry Larsen on February 24, 2022, from which two data segments were derived. The corresponding measured RPM and STW for this duration are shown in Figure 5. It is observed that there are several durations of constant RPM during this time. The periods from hour markers 2-3.5 and 4.5-5 were chosen as segments 11 and 12 respectively. During both segments the CCGS Henry Larsen is observed to be travelling with a constant heading and with an

average speed of 7-8knots. The respective CIS ice chart for February 24 confirms that the CCGS Henry Larsen was travelling through an ice field for both segments. This process was used to evaluate all data segments used for analysis. Since the rpm remains constant the speed oscillations observed from time 4.5-5 are indicative of variations in the ice composition and floe size.



Figure 4 - Route plot for segments #11 and #12.

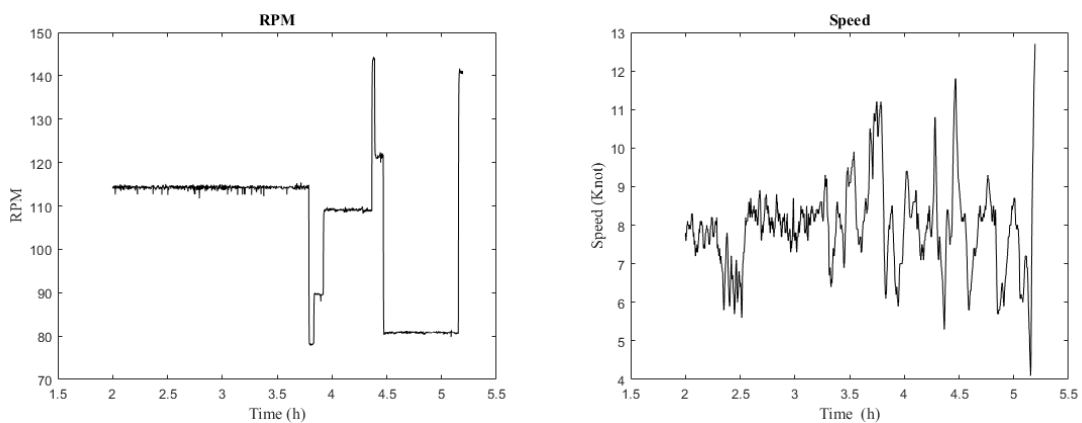


Figure 5 - Full-scale RPM (Left) and Speed (Right) for duration of segments #11 and #12.

Twenty-Two segments were selected with durations ranging from 17 minutes to 174 minutes. In total, 19.84 hours of data was considered for the statistical analysis of sea ice thickness. The details of each segment are summarized in Table 2.

Table 2 - Table of data segments used for statistical estimation of sea ice thickness.

Run #	Date	Duration [h]
1	2-Feb-22	2.02
2	2-Feb-22	0.60
3	3-Feb-22	0.19
4	3-Feb-22	1.02
5	20-Feb-22	0.77
6	21-Feb-22	1.53
7	21-Feb-22	0.28
8	21-Feb-22	1.05
9	21-Feb-22	0.35
10	23-Feb-22	0.50
11	24-Feb-22	1.63
12	24-Feb-22	0.50
13	27-Feb-22	0.40
14	3-Mar-22	0.40
15	3-Mar-22	0.73
16	3-Mar-22	0.33
17	4-Mar-22	0.77
18	4-Mar-22	0.93
19	4-Mar-22	1.42
20	4-Mar-22	1.07
21	4-Mar-22	0.45
22	4-Mar-22	2.90
	Total Time:	19.84

The data segments were selected based on identifying steady running conditions, meaning that the RPM and speed remained at the same magnitude for the duration of the data set. These segments typically resulted in estimated thickness values that also remained constant within the confines of each segment. Only segments that remained in a single zone on the CIS ice chart for their entire duration were selected. This process ensured the highest probability that the ice conditions corresponding to the segment were constant.

Each data set was first identified by plotting the speed over water against time, RPM for each propeller against time, and the combined port and starboard thrust over time. The advance coefficient (J) was calculated at each time interval using the speed over water and the propeller rate of rotation by equation (6) (Wang, 2023). The thrust deduction was then determined using the advance coefficient as per Equation (12). The thrust deduction factor identifies change in thrust, relative to the resistance of the ship, caused by hydrodynamic effects of the rotating propeller in close proximity to the hull. The component of ice resistance is defined by Equation (13). The thrust deduction is first applied to the measured thrust value and then the Open water resistance is calculated for the measured speed and subtracted from the effective thrust.

Thickness is then calculated using the regression equation developed in the model tests. Due to the implicit nature of the regression equation, it is not possible to solve directly for ice thickness. Therefore, bilinear interpolation is used in conjunction with a table of values to determine ice thickness by Equation (14) as a way to interpolate between two variables, those being speed and ice thickness. The table of values was developed using ice thicknesses ranging from 0 m to 5 m and speeds ranging from 0 knots to 15 knots. Intervals

of calculation were set to 0.1 m and 0.1 knots respectively. Bilinear interpolation was achieved by first interpolating the thickness at both the higher and lower bounds of speed. The actual thickness was then interpolated between the upper and lower bounds of speed.

$$J = \frac{V_A}{nD} \quad (12)$$

$$R_{i(measured)} = T_E(1 - t) - R_{OW} \quad (13)$$

$$R = \frac{1}{(V_2 - V_1)(H_{i_2} - H_{i_1})} [V_2 - V \quad V - V_1] \begin{bmatrix} R_{11} & R_{12} \\ R_{21} & R_{22} \end{bmatrix} \begin{bmatrix} H_{i_2} - H_i \\ H_i - H_{i_1} \end{bmatrix} \quad (14)$$

where:

R	-	Ship Resistance
H _i	-	Ice Thickness
V	-	Ship Speed
V _A	-	Speed of Advance
J	-	Advance Coefficient
n	-	Rotations Per Second
D	-	Propeller Diameter

There is a degree of error when using bilinear interpolation on a nonlinear equation. It was identified that there was a 2% error or ± 0.002 m in the ice thickness calculated using this method because of the assumption of linearity between interpolation points. This level of error in the thickness was acceptable given the variability in the ice coverage. It also satisfied the desired level of precision like that of the CIS ice charts, ± 0.005 m.

The thickness was analyzed by calculating the average thickness over each segment including the variance and standard deviation. Having a low standard deviation would indicate high consistency in the ice cover throughout each segment. Higher standard

deviation would indicate that the ice coverage is either inconsistent or the stage of ice encountered changes during the selected segment. High standard deviation could also indicate ridge encounters, however the selection process was meant to eliminate segments with ridges.

The CIS ice charts were reviewed for each data segment on their respective day. The corresponding global positioning system (GPS) coordinates for each segment were plotted using a keyhole markup language (KML) file. Comparing the plots with the ice charts indicated the zones through which the CCGS Henry Larsen travelled. Using this comparison, the equivalent ice thickness and thickness for each development stage could be extracted from the chart egg codes.

The final analysis was to compare the statistically estimated ice thickness from performance models to the equivalent thickness from ice charts. The first method was to compare the equivalent ice thickness to identify if a correlation exists between estimated thickness and calculated equivalent thickness. The second analysis was to identify the stage of development indicated by the comparison of estimated ice thickness and ice chart egg codes to verify that the charts accurately account for the encountered ice type identified by each segment.

3.2 Empirical Ice Resistance Comparison

The model test performance equation that the NRC developed for the CCGS Henry Larsen is its own prediction method for ice resistance. However, unlike the semi-empirical methods highlighted in Section 2.1.7, the NRC CCGS Henry Larsen model is specific to

only the one ship tested. As it is known that the NRC model has a high degree of prediction accuracy for the CCGS Henry Larsen through full scale trials, it can be used to tune a chosen empirical model to improve its accuracy. The benefits of this approach include maintaining the generalization of these models to adapt to any ship while tuning their magnitude.

The experimental method chosen to analyze the empirical models was a 2^k factorial design (Montgomery, 2013). The factorial design approach is beneficial for this application because of its ability to evaluate the significance of several factors simultaneously with minimal analysis. The objective of the factorial design would be to determine the function that is the difference between the NRC model equation and a chosen empirical method. To achieve this result while maintaining the empirical model's integrity, only those variables which are similar between the two models are considered in the factorial design. Since this is an analytical problem any number of factors can be considered, and no limitations or replications are required to achieve statistical significance. The experiment will need to consider variables pertaining to the ice properties, the ship scale, and operational parameters.

The chosen empirical model is drawn from the ones outlined in Section 2.1. The models must be compared to assess their validity and this is achieved by expanding on the semi-empirical analysis of Erceg and Ehlers (2017). With the availability of model test data from the CCGS Henry Larsen, the methods can be compared against the NRC model across a range of both ship speed and ice thickness. This provides a more comprehensive assessment of the empirical models than the few field data points that were used in the research of Erceg and Ehlers (2017). The objective is to identify which empirical models

have the highest prediction accuracy across a range of ice thicknesses. These models will form the basis for a modified empirical method. Erceg and Ehlers (2017) concluded that no one empirical method was accurate for all the ships tested in his research. However, a lack of experimental data limited the scope of that project. It is anticipated that with a more thorough analysis of differing ice thicknesses the comparison of empirical models will be more conclusive.

The end goal of this analysis is to define a function of significant terms that is the difference between the chosen empirical model and the NRC equation. The objective is to achieve a function with the least terms to maintain simplicity of the model while tuning the empirical method. Since ice conditions are often generalized for a given area, including strength and density, it can be assumed that actual encounters will often not follow a prescribed function. These prediction methods are simply a method for quantifying the average encounters and therefore it is not necessary to obtain a perfect fit in this analysis.

3.3 Estimating Propulsive Efficiency

As indicated through the literature review in Section 2.2, the propulsion coefficients are not easily predictable for general ships since they are dependent on hull, propeller and shafting geometry. This presents a challenge in designing an overall emissions model as these values must be defined to predict a ship's fuel consumption in ice with an acceptable degree of accuracy. Literature does provide a scope of propulsive values that apply to the majority of ships, however they pertain to ships in open water. There is a significant gap in understanding of general performance in ice.

The most appropriate approach to this scenario is to determine the specific propulsion efficiencies for each ship to which the emissions model is applied. However, this would significantly increase the complexity of the model and require access to data and specifications not readily available in all cases. The CCGS Henry Larsen is a unique case in that both the live propulsive data and the machinery specifications are available for study in this research. Therefore, CCGS Henry Larsen is used as an example for a detailed analysis of propulsive efficiencies. This includes a regressive analysis of the measured torque and thrust values at the shaft and considering the propeller efficiency curves. This is used to determine an estimate of the total propulsive efficiency from the effective power to the shaft power. This regressive value can be compared against the general open water values to validate the literature and propose values to use for the emissions model.

The thrust deduction can also be analyzed through a regression analysis. The NRC model tests resulted in a thrust deduction equation which is used to determine the operating thrust deduction at full-scale. The regression analysis of this variable focusses on the influence of ice thickness on thrust deduction. Similar to the propulsive efficiency, the regression analysis of thrust deduction can be used to advise values for use in the general emissions model.

4 Results

The results are subdivided into three main categories: the statistical estimation of sea ice thickness, estimating resistance in ice using modified empirical methods, and estimating emissions from regression of propulsion efficiencies. The subdivision treats this analysis as three independent studies culminating in the final emissions model. One data segment is tracked across all sections to highlight the progression of the research calculations. Where necessary, anomalies of other data segments are emphasized. The complete dataset for all segments considered is presented in the appendices.

4.1 Ice Thickness Estimates

Ice thickness was estimated for all 22 data segments using a combination of software packages that included MATLAB, Microsoft Excel, and Google Earth Pro. All data from the CCGS Henry Larsen was provided in spreadsheets and comma-separated value (CSV) format and therefore was manipulated and sorted using Microsoft Excel. MATLAB was used to expedite the analysis of segment data and to produce the plots of measured ship values and ice thickness. Google Earth Pro was used to plot the CCGS Henry Larsen's transit and to compare CIS ice chart data to identify ice presence visually. Figure 6 shows a plot of all the data segments considered for analysis. Route #14 is emphasized as it will be the primary route for discussion and detailed analysis.



Figure 6 - Plot of all 22 data segments located around the northwest peninsula of Newfoundland.

4.1.1 Validating Method in Open Water Transit

One form of validation for the statistical method was to test its capacity against open water conditions. As there is no ice thickness during this operation, the model would be expected to predict as such. Any predicted thickness in open water would suggest an error within the model test or some form of additional resistance. Figure 7 shows the map of a known open water transit along the southern coast of Newfoundland, where the CCGS Henry Larsen was traveling to the south. This is a quasi-steady-state segment adequate for validating the methodology.

The resultant estimated ice thickness during this segment is presented in Figure 8. The thickness was calculated at one-second intervals, and the mean thickness predicted was 1.4cm with a standard deviation of 1cm. It is expected that some value of estimated ice thickness would be observed when dealing with full-scale trial data as the ship is not running in a genuinely steady condition.

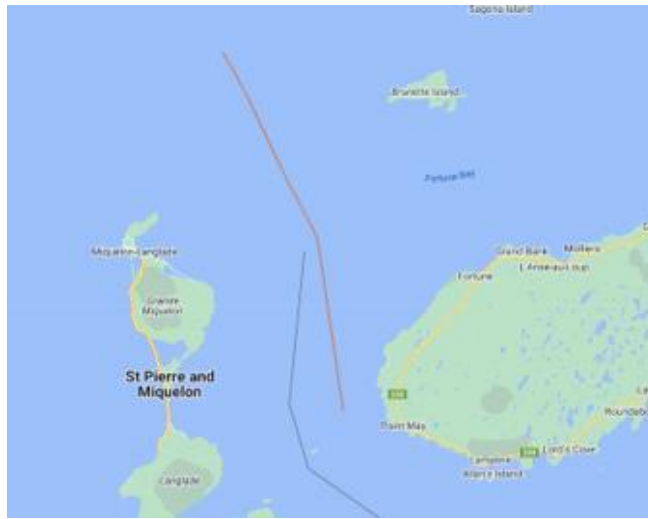


Figure 7 - Map of open water segment.

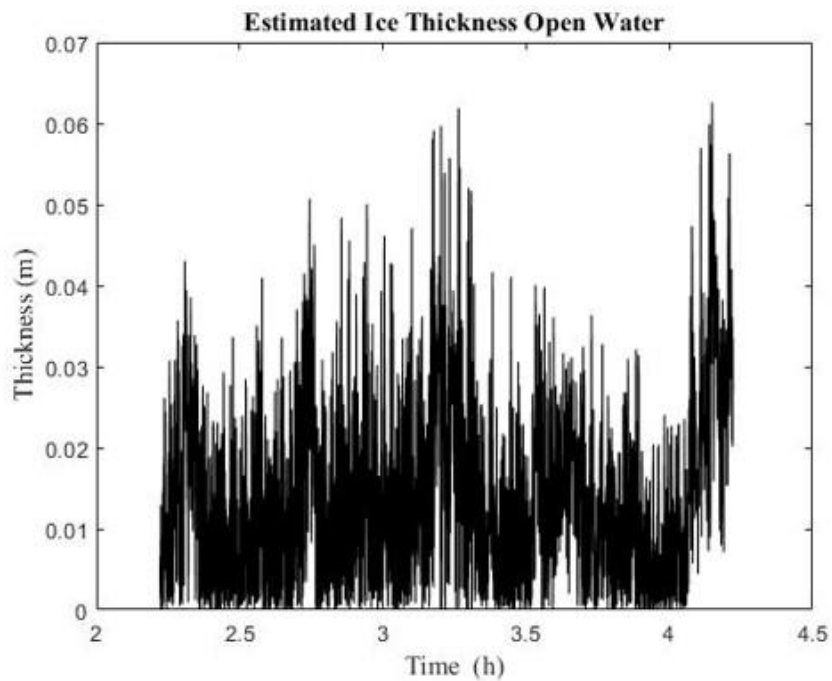


Figure 8 - Open water estimated ice thickness for model validation.

It was also noted that at a sample rate of 1Hz, there is a lot of noise in the data, more than 6 cm thick during some peaks. This result was compared to the known ice prediction segments, which did not indicate the same degree of noise at the same sample rate. It was

concluded that this noise is most likely due to the sea state. It was deemed acceptable to ignore this added resistance because it is not present in ice-covered conditions.

Several open water segments showed a consistently higher ice thickness with an average thickness of around 4cm. These sudden changes were observed to occur when the CCGS Henry Larsen changed headings or transited between inshore and offshore locations. Therefore, it is most likely that the CCGS Henry Larsen is experiencing added wind and wave resistance between the head seas and the following seas as it changes heading. As the model is designed to estimate sea ice thickness, it associates all added resistance as equivalent ice thickness. The wind resistance is also present in ice-covered conditions; however, it is difficult to quantify its value without robust wind measurements. If meteorological data was collected, the component of wind resistance could be incorporated, given that the vessel's profile is known. However, the component of wind resistance becomes proportionally smaller as the ice resistance increases. Therefore, its contribution to the level ice calculation is reduced as the total ice thickness increases. There are also no negative values because the lookup table used for calculating ice thickness in the model was incapable of predicting negative thickness.

4.1.2 Statistical Ice Estimate Results

Ice thickness was estimated at a frequency of 1 Hz throughout each data segment considered. One of the segments, identified by number 14, is shown in greater detail to illustrate the complete result profile. Segment 14 was recorded between 6:38 am and 7:02 am on March 3rd, 2022. During this time, the CCGS Henry Larsen transited west of

Flowers Cove on the Northern Peninsula of Newfoundland for approximately 3.76 nautical miles.

The ice chart for March 3rd, 2022, was accessed through the CIS archives and is presented in Figure 10 (Canadian Ice Service, 2022). The general area of operations is circled and is identified as the Strait of Belle Isle, and the specific path is shown in Figure 9. The zone through which the CCGS Henry Larsen transits for this data segment is identified by the letter F which identifies the ice code describing the ice in the region. The egg code indicates over 90% concentration divided between two stages of development. The first stage is identified as 30% concentration of thin-first year ice with thickness ranging from 0.3 m to 0.7 m. The second stage is identified as 70% concentration of grey-white ice with a 0.15 m to 0.3 m thickness. Both stages are identified as big floes with floe sizes ranging from 500 m to 2000 m. The equivalent ice thickness is calculated at 0.31 m for this zone using equation (5).

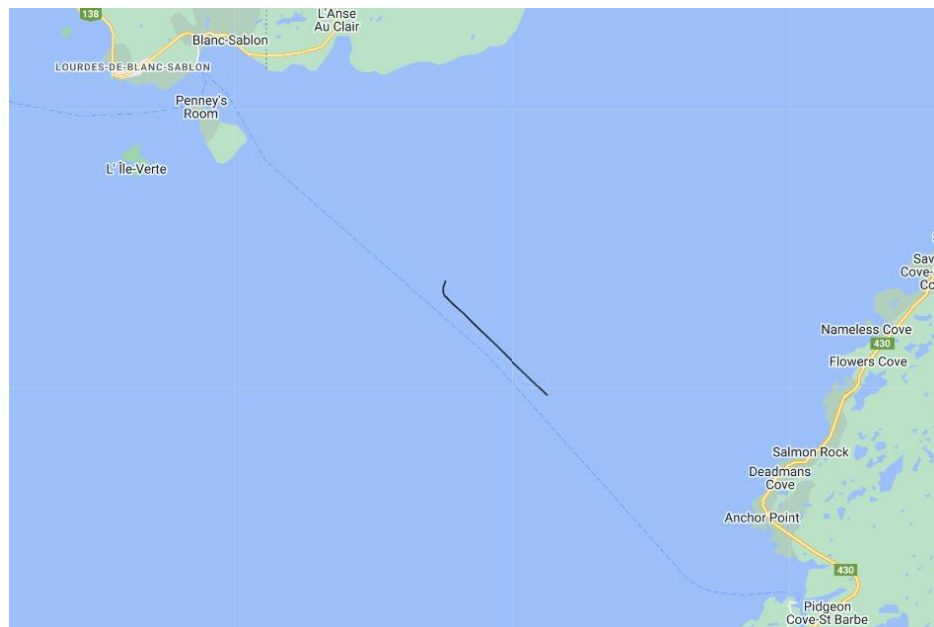


Figure 9 - Plot of segment #14 route in the Strait of Belle Isle.

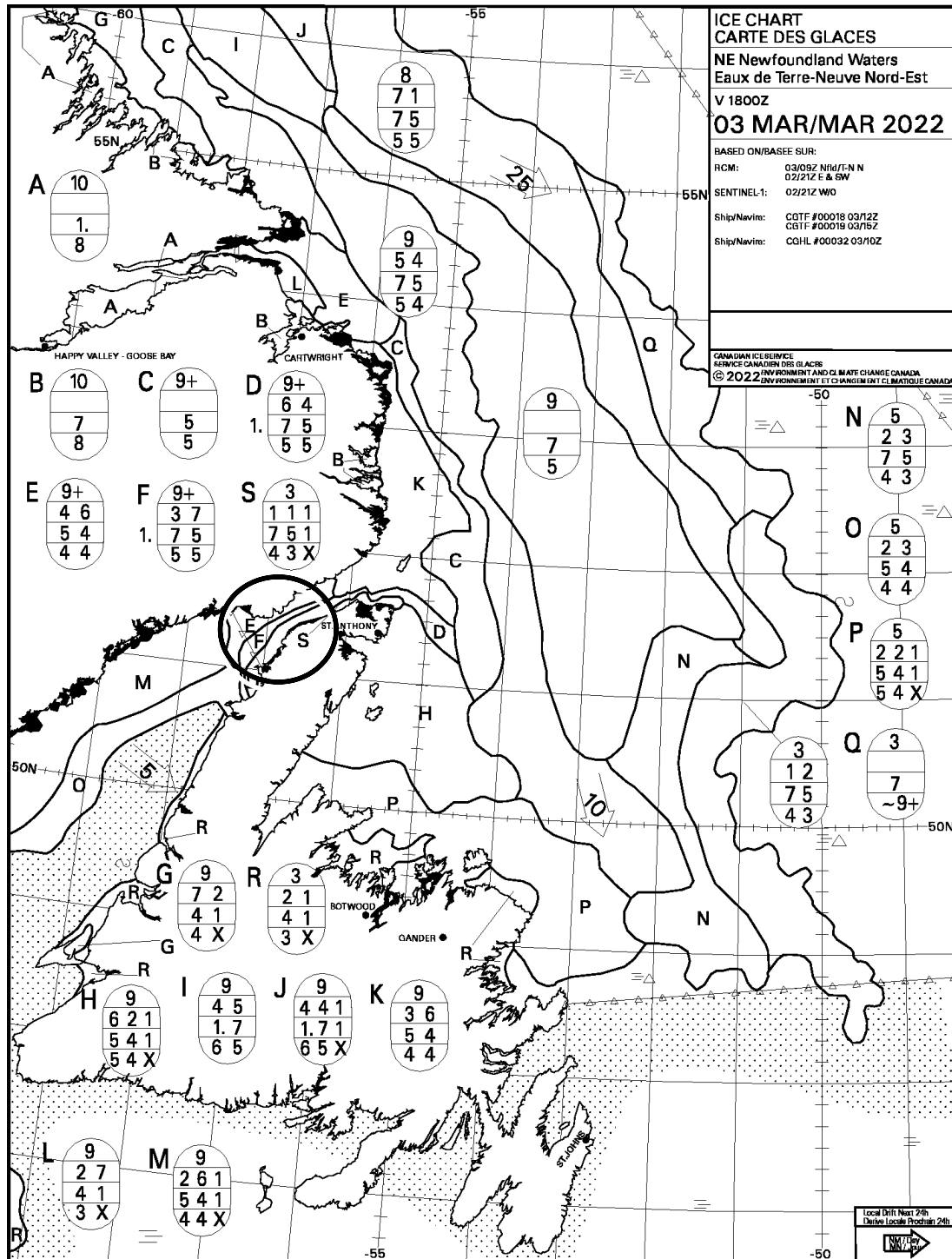


Figure 10 - CIS Ice Chart for NE Newfoundland Waters March 3rd, 2022 (Canadian Ice Service, 2022) © Her Majesty the Queen in Right of Canada, as represented by the Minister of Environment Canada, [2022].

The statistical ice thickness was estimated using the model test regression models for ice resistance, and the plot of thickness over time is presented in Figure 11. The average thickness over this segment was 0.314 m, with a standard deviation of 0.054 m. In this case, the average thickness is very close to the equivalent ice thickness determined from the ice chart, indicating that the ship has transited an even distribution of the stages of development indicated by the egg code. Upon inspection of the thickness, it trends towards thinner ice. The first half is identified as thin-first-year ice because the thickness remains above 0.3m. However, it is deduced that the CCGS Henry Larsen begins to transition to an area with grey-white ice towards the end of the segment.

The rough floe size can also be identified from this graph in Figure 11. The ice chart indicated floe sizes ranging from 500m to 2000m. The total distance traveled was 3.76 nautical miles or 6900m. Therefore, the CCGS Henry Larsen should have encountered between 4-13 major floes. The data shows five distinct prolonged spikes in ice thickness that could infer the size of each floe. This is inferred because the estimated thickness is directly proportional to the measured thrust based on the statistical model employed. For each segment considered, the CCGS Henry Larsen was transiting in a constant direction. This result contrasts with the scenario where the ship would navigate along leads in the ice cover. Therefore, the ship would encounter complete ice floes rather than transiting between them. Most notably, the spike from time stamp 9.7 hr to 9.8 hr would infer a floe size of approximately 1700 m, within the predicted range. Similar conclusions were derived from all other segments in ice to validate this inference. The NRC identified during trials that the thrust was reduced between ice floes as the resistance would shift from a predominance of icebreaking resistance to ice clearing (Wang, et al., 2023).

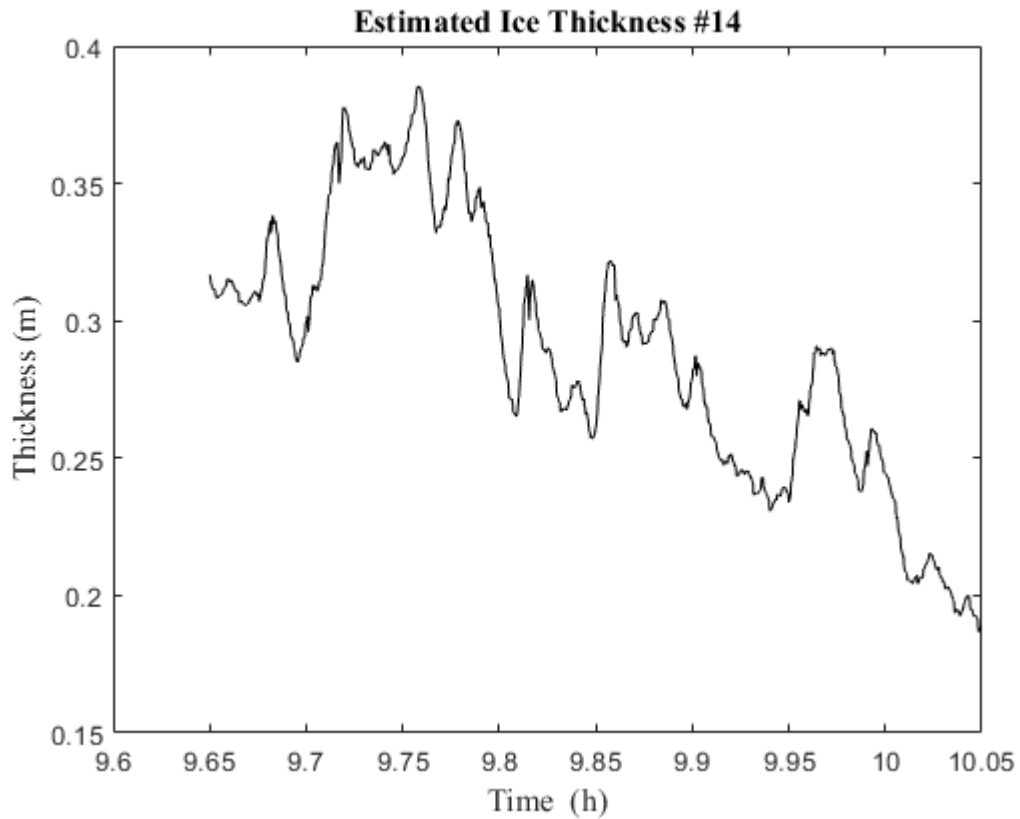


Figure 11 - Ice thickness estimate for segment #14.

Each data segment was analyzed the same way as segment 14. Table 3 shows a summary of the results, including the most probable stage of development encountered based on the comparison of estimates and ice chart data. Each segment was verified using the identical method outlined in segment 14, including comparing ice thickness and evaluating floe sizes. It should be noted that not all the data provided a definitive result within 20% of the equivalent thickness. For one-third of cases, the estimated thickness was comparable to equivalent ice thickness, suggesting an encounter with several stages of development. This was identified by a higher variability in thickness and distinct steps in thickness. However, most cases did not relate to equivalent ice thickness and were closely related to a specific stage of development. Additional details presented in Appendix A.

Table 3 - Summary of statistical ice thickness estimates and ice chart comparison. Additional Details provided in Appendix A – CCGS Henry Larsen Data Segment Analysis.

# of segment	Statistical Ice Thickness [m]	Std Dev. [m]	EQ Ice Thickness equation (5) [m]	First Conc. Thickness [m]	Second Conc. Thickness [m]	Third Conc. Thickness [m]	Stage of Development
1	0.010	0.008	0.1	0.225	0.125	0.050	Open Water
2	0.116	0.023	0.1	0.225	0.125	0.050	Grey Ice
3	0.087	0.012	0.15	0.225	0.125	0.050	New Ice
4	0.103	0.016	0.15	0.225	0.125	0.050	Grey Ice
5	0.329	0.087	0.17	0.225	0.125	~	Grey-White Ice
6	0.198	0.041	0.26	0.500	0.225	0.125	Grey-White Ice
7	0.307	0.075	0.26	0.500	0.225	0.125	Thin First Year
8	0.305	0.049	0.26	0.500	0.225	0.125	Thin First Year
9	0.272	0.020	0.26	0.500	0.225	0.125	Grey-White Ice
10	0.207	0.026	0.26	0.500	0.225	0.125	Grey-White Ice
11	0.404	0.046	0.13	0.225	0.125	0.050	Outside Chart Range
12	0.327	0.062	0.28	0.500	0.225	~	Thin First Year
13	0.184	0.028	0.36	0.500	0.225	~	Grey-White Ice
14	0.314	0.054	0.31	0.500	0.225	~	Thin First Year
15	0.357	0.059	0.31	0.500	0.225	~	Thin First Year
16	0.284	0.052	0.31	0.500	0.225	~	Grey-White Ice

17	0.178	0.092	0.17	0.225	0.125	~	Grey-White Ice
18	0.066	0.034	0.17	0.225	0.125	~	Limited Grey-White Ice
19	0.061	0.044	0.17	0.225	0.125	~	Limited Grey-White Ice
20	0.070	0.009	0.09	0.225	0.125	0.050	New Ice
21	0.089	0.009	0.18	0.225	0.125	0.050	New Ice
22	0.076	0.020	0.18	0.225	0.125	0.050	New Ice

4.1.3 Special Cases

4.1.3.1 Segment 1 – Open Water

A few special cases indicated no initial obvious correlation to the ice chart predictions and therefore required further investigation. Additional analysis was required to identify these anomalies.

The analysis of case number one (1) indicated that the ice thickness was near zero for the entire duration of the data segment. This indicated that the ship was likely traveling through open water. However, as the ice chart indicated otherwise, this needed to be verified by other means. Firstly, the advance coefficient (J) was considered across the entire segment and remained constant at 0.24. Based on the NRC model test data, advance coefficients of 0.24 coincided with open water, and lower values indicated ice encounters (Wang, 2023). Also, while consulting the ice chart, it was clear that the CCGS Henry Larsen

was transiting a zone that bordered open water. Figure 12 shows the estimated thickness for data segment #1.

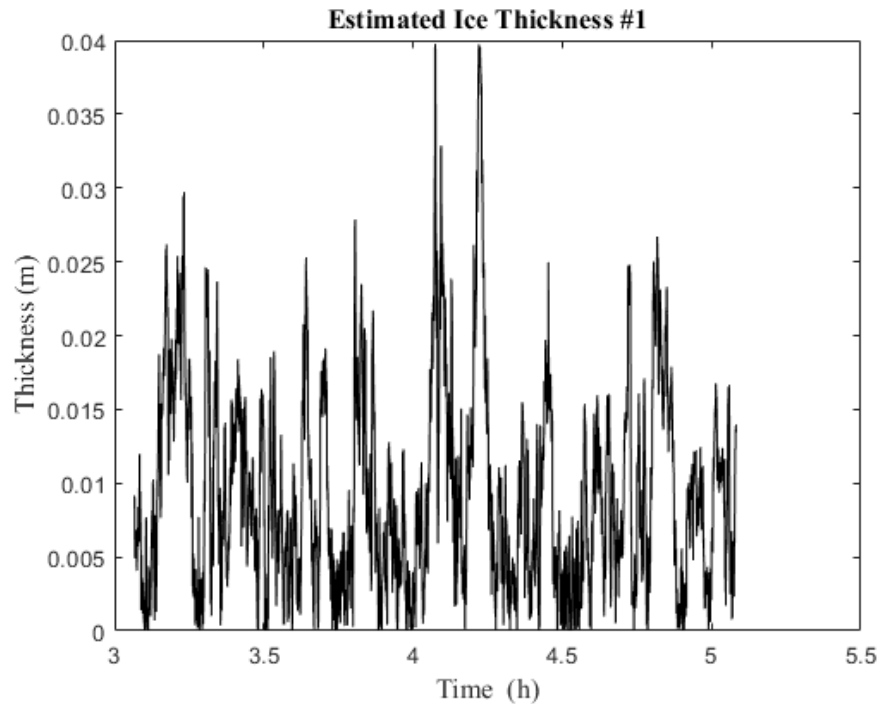


Figure 12 - Segment #1 ice thickness estimate resembling open water.

The conclusion for this data segment was that the ship was transiting in open water along the border of the ice, which is common practice to maximize fuel efficiency in transit. The benefit of this data segment is that it demonstrates a low degree of error from the statistical estimation method for ice thickness within 1 cm. This segment also resembles the analysis of open water in Section 4.1.1 in that there is a high degree of noise correlating to added wave resistance. This data was further analyzed to capture the thickness before the chosen segment. Evidently, the CCGS Henry Larsen encountered ice as it left Tête-à-la-Baleine, QC, until it reached open water and changed heading northeast.

4.1.3.2 Segment 11 – Zone Boundary Shift

It was evident that the statistical thickness was beyond the ice thickness described by the ice chart for case 11. Upon further inspection of the ice chart for this day, it was evident that the CCGS Henry Larsen transited near a border between two identified ice zones. The adjoining zone indicated thicker ice than the one in which the CCGS Henry Larsen was transiting, which correlated better. When comparing the ice charts between consecutive days, it was evident that the zone boundary shifted. Therefore, it is possible the CCGS Henry Larsen was transiting the adjoining zone due to boundary shift with time since the current chart was dated by 12 hours at the time of encounter. This is an apparent disadvantage of the ice chart system in that they become outdated as ice shifts, particularly in narrow passages with high currents, such as the Strait of Belle Isle. In these cases, it isn't easy to accurately describe the ice conditions at the ship's location. This behavior is expected in areas with fast-moving ice conditions.

4.1.3.3 Segment 19 – Mixed open water and ice encounters

For cases 18 and 19, the estimated average ice thickness falls below the minimum ice thickness suggested in the ice chart of 0.1m. Upon inspecting the estimated thickness shown in Figure 13, half of this data is operated in an ice-free zone with segments of near zero thickness and advance coefficients near 0.24. However, the latter half indicates an encounter with grey-white ice. When consulting the CIS ice chart, the total concentration

is only 9/10th, which indicates the presence of 1/10th open water. Therefore, the ice chart does reflect the estimated thickness.

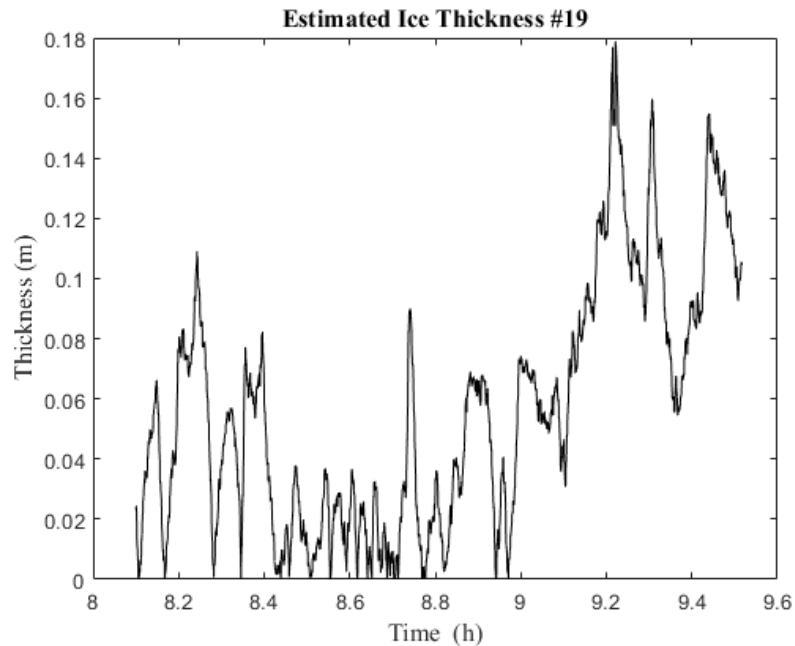


Figure 13 - Estimated Ice Thickness for Dataset 19.

4.2 Modified Empirical Ice Prediction Model

The next part of the research and the first component of estimating ship emissions was to develop a method for predicting the resistance of ships. It is acknowledged that a complete model would consider open water and ice performance. However, this research focuses on methods for predicting ice resistance. The literature is consistent that the Holtrop method is adequate for open water predictions, particularly of displacement-type ships (Holtrop & Mennen, 1982). Therefore, it is recommended that Holtrop's method be employed for open-water portions of the emissions prediction model. In the case of the

CCGS Henry Larsen, the open water test results scaled using ITTC procedures are used for greater accuracy (ITTC Resistance Committee, 2011).

Like open water, several empirical methods for predicting ice resistance are described in Section 2.1. However, the literature is undecided on which method is the most appropriate for a given ship. The empirical methods are compared against the NRC regression equation to evaluate their validity at varying ice thicknesses and ship speeds, given the presence of model test data for the CCGS Henry Larsen. A similar approach is taken to the empirical review conducted by (Erceg & Ehlers, 2017) while expanding on the analysis by looking at a larger spectrum of ice conditions.

4.2.1 Analysis of Existing Empirical Models

Figure 14 through Figure 16 show the comparison of six empirical prediction methods with the NRC regression model. The three oldest methods, including Vance, Lewis, and Zahn & Philips, are discarded due to their simplicity compared to the more recent models. These models consistently overestimate the resistance with high inconsistency, especially at thinner ice thickness levels. The older methods are included to demonstrate the progression of prediction methods over time.

Figure 14 shows the ice resistance predictions at an ice thickness of 0.5m. This graph indicates that all three modern models, including Riska, Lindqvist, and Keinonen, predict close results to the NRC model, while Riska and Lindqvist have the best fit. Figure 15 shows the same prediction at 1m of ice thickness. Compared with the thinner ice, the

Riska and Lindqvist models are now proportionally lower than the NRC model. Figure 16 shows the predictions at 1.5m; the results are similar to the medium thickness.

Of the three newer methods, Keinonen was the most consistent model compared to the NRC results. Riska and Lindqvist were identified as having a higher degree of variability compared with the NRC model at different ice thicknesses. Particularly in thinner ice, these two models predicted higher resistance compared to the NRC model. This would become an issue since the prior ice thickness predictions in Section 4.1 are below 0.5m. In contrast, Keinonen's model consistently predicts about 20% less resistance than the NRC model across all thicknesses. As this model is consistently proportional to the NRC model, it is the best candidate for making simple modifications to affect its predicted magnitude.

These results are consistent with the relevant semi-empirical research (Erceg & Ehlers, 2017). That research concluded that none of the six prediction methods could accurately predict resistance. However, a lack of data points did not allow them to assess different changing environmental parameters. They analyzed data from three different ships, and upon additional inspection, the Keinonen method also predicts resistance about 20% lower than measured values for each of those ships. This confirms that the Keinonen model is most appropriate as it can be applied to various hull forms with similar prediction results.

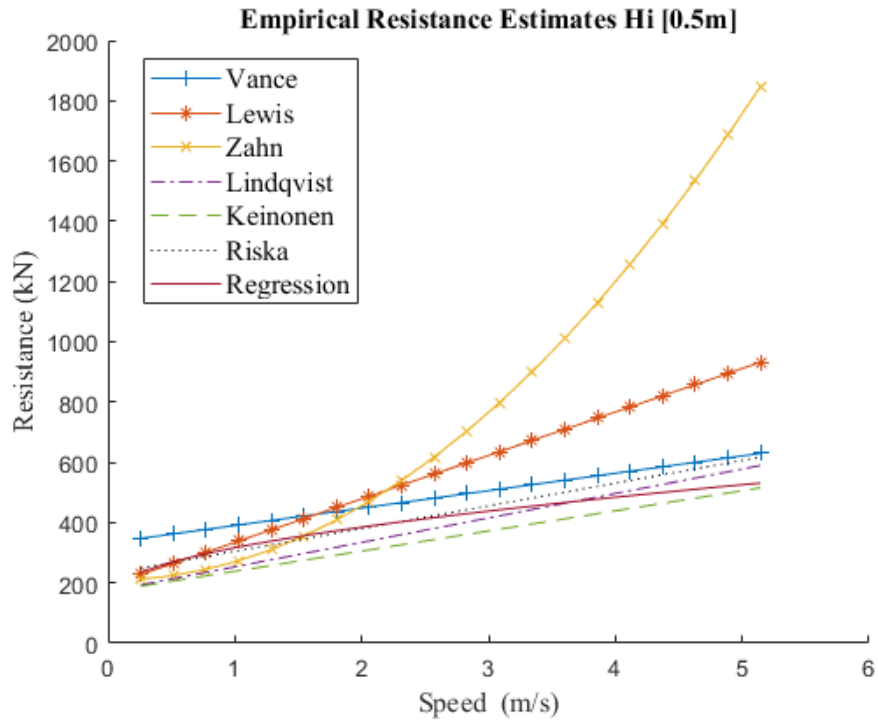


Figure 14 - Empirical resistance estimates for CCGS Henry Larsen at an ice thickness of 0.5m.

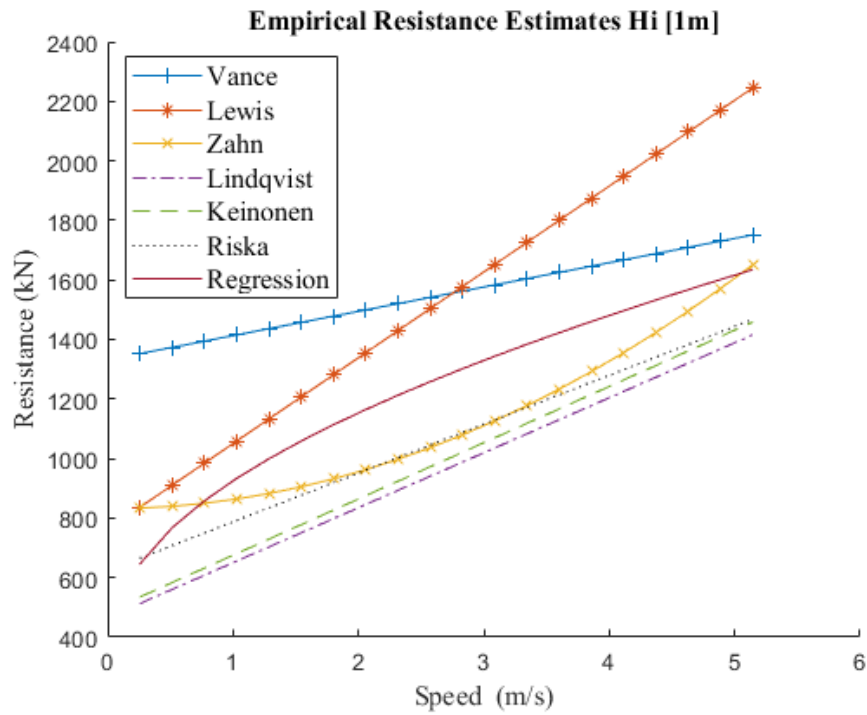


Figure 15 - Empirical resistance estimates for CCGS Henry Larsen at an ice thickness of 1m

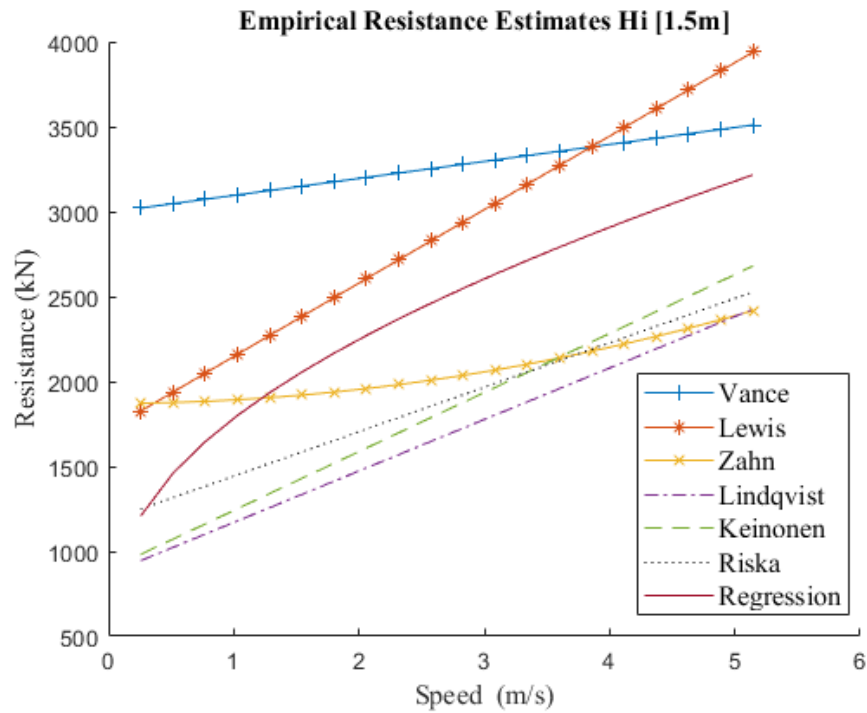


Figure 16 - Empirical resistance estimates for CCGS Henry Larsen at an ice thickness of 1.5m

4.2.2 Factorial Design Experiment

The chosen method for predicting ice resistance was Keinonen’s based on its consistency when tested against differing ships, ice thickness and ice flexural strength. However, it underpredicts the resistance in all cases. Therefore, a method is proposed by which a modifying equation be applied to tune the model using a validated performance mode. As previously stated, the NRC model for the CCGS Henry Larsen is a reliable prediction method. However, it is specific only to one hull, making it inappropriate to apply to other vessel types; this would align its accuracy with the older prediction models based on singular ship performance. However, because the NRC model is accurate to the CCGS Henry Larsen, it can be used as a datum to tune the Keinonen model if the Keinonen model

can be modified to fit the NRC model for the CCGS Henry Larsen while retaining its capacity for various hull types. In that case, it can be considered a more appropriate prediction method.

Table 4 - Parameters for chosen empirical methods.

			Keinonen et al. (1996)	NRC Regression (2023)	Common Variables
Operational Parameter	V	Ship speed	V	V	V
Ship Size	L	Ship length	L	L	L
	B	Ship breadth	B	B	B
	T	Ship draft	T	T	T
Bow Shape	β	Average buttock angle at waterline	β		
	ψ	Average bow flare angle at waterline	ψ		
Ice-Related	h	Ice thickness	h	h	h
	σ_f	Ice strength	σ_f	σ_f	σ_f
	ρ_i	Ice Density		ρ_i	
	ρ_w	Water Density	ρ_w	ρ_w	ρ_w
	μ	Hull ice friction	μ		
	hs	Snow thickness	hs		
	t	Ice surface temperature	t		
	C_h	Hull condition factor	C_h		
	C_s	Factor of salinity of water	C_s		
	g	Speed of Gravity		g	

To develop the modified equation, the relevant variables that could be significant must be determined. Retaining the benefits of the Keinonen model, such as bow shape, requires modifying only the common variables between this model and the NRC model. Table 4 defines the variables required for the Keinonen and NRC models and highlights seven common parameters. All the common variables except for the water density are considered possibly significant for the analysis. Water density is not included because it

typically remains constant between predictions relative to the other variables. The chosen variables can be written as a potential functional expression shown in equation (15). The 2^k factorial design experiment was used to determine the significant variables and the necessary function.

$$\frac{R_{i(NRC)}}{R_{i(Keinonen)}} = f(V, L, B, T, h_i, \sigma_f) \quad (15)$$

As six factors were considered, this was a 2^6 factorial design. Stat-Ease® Design Expert was used to conduct the factorial experiment. A 2-level six-factor design experiment requires 64 runs for a complete experiment. There was no restriction on the calculations and no need to modify the experiment to a fractional factorial design because this was an analytical experiment. Likewise, there was no need for replications. Four center points were also included to test for curvature. Table 5 defines the six factors and their levels. The maximum level of ship-based parameters is based on the CCGS Henry Larsen specifications, while the low level is based on a concept Coast Guard light icebreaker basic dimensions. The ice thickness and speed levels were chosen based on the range of values identified during the analysis in Section 4.1.2. The ice strength was based on NRC tested values ranging from 300kPa to 700 kPa (Wang, et al., 2023).

Table 5 - Design of experiments factors.

Factor	Name	Units	Type	SubType	Min	Max	Mean	Std. Dev.
A	Ice Thickness	m	Numeric	Continuous	0.2	1	0.6	0.3909
B	Speed	m/s	Numeric	Continuous	0.5	5	2.75	2.2
C	Length	m	Numeric	Continuous	40	100	70	29.32
D	Beam	m	Numeric	Continuous	10	20	15	4.89
E	Draft	m	Numeric	Continuous	4	7	5.5	1.47
F	Ice Strength	MPa	Numeric	Continuous	0.3	0.7	0.5	0.1955

The values for each run were calculated by finding the difference between the Keinonen and NRC prediction results for each required factor level. A square root transformation was chosen since the Keinonen method has a linear fit while the NRC model has a second-order polynomial fit. Figure 17 shows the half-normal plot of significant terms, indicating a high degree of significant terms and allied terms, meaning a p-value of less than 0.05. The Pareto chart in Figure 18 shows the terms sorted by their significance. This chart indicates that an excess of 20 terms and allies are significant to satisfy the t-limit of 2. It is unreasonable to accommodate many terms in the desired modified equation. The goal is not to replicate the NRC model in its exactness but instead to tune the Keinonen model to predict closer results to expected values.

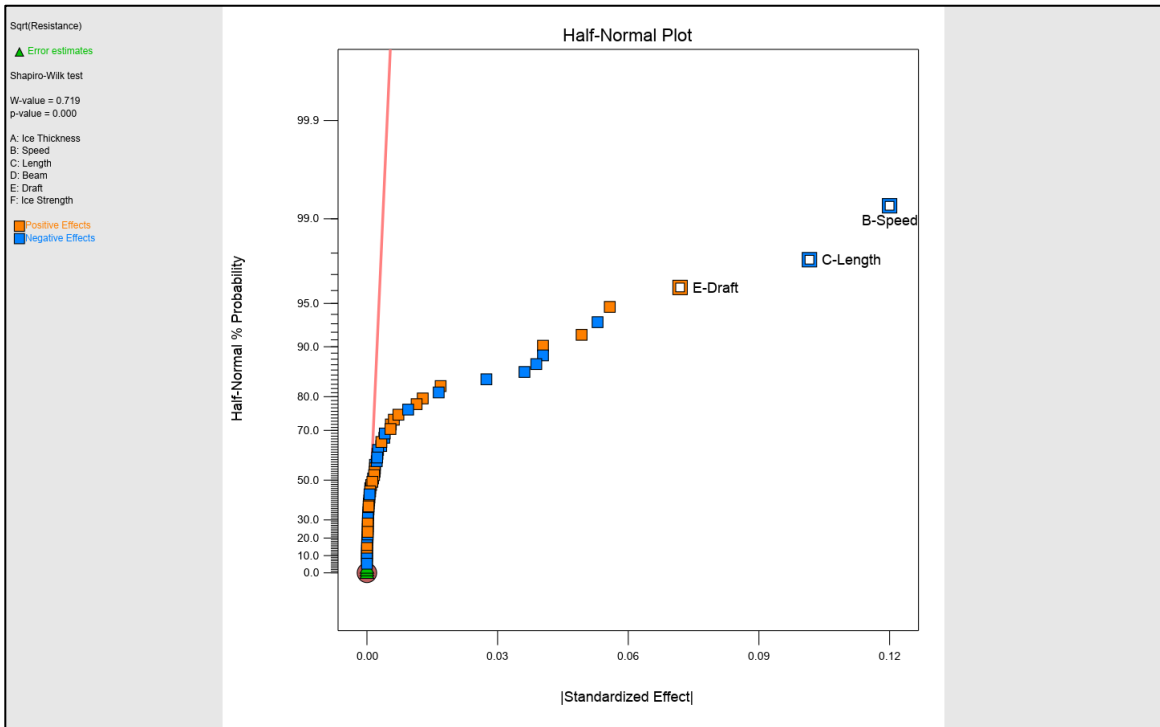


Figure 17 - Half-normal plot to identify statistically significant terms StatEase®

Based on the Pareto chart, satisfying the Bonferroni limit would allow for a reasonable fit for the desired purpose. The Bonferroni correction modifies the threshold by dividing the desired threshold by the number of tests. Three significant terms were identified to satisfy this limit of 3.523 t-value: Ship speed, length, and draft. Interestingly, none of the ice parameters were of high significance between the NRC and Keinonen models. This is significant to note because it indicates that the differences between these models lie with the ship's scale and not the ice parameters. The analysis of variance showed a clear indication of significance with these three variables because their p-values are all less than 0.0001.

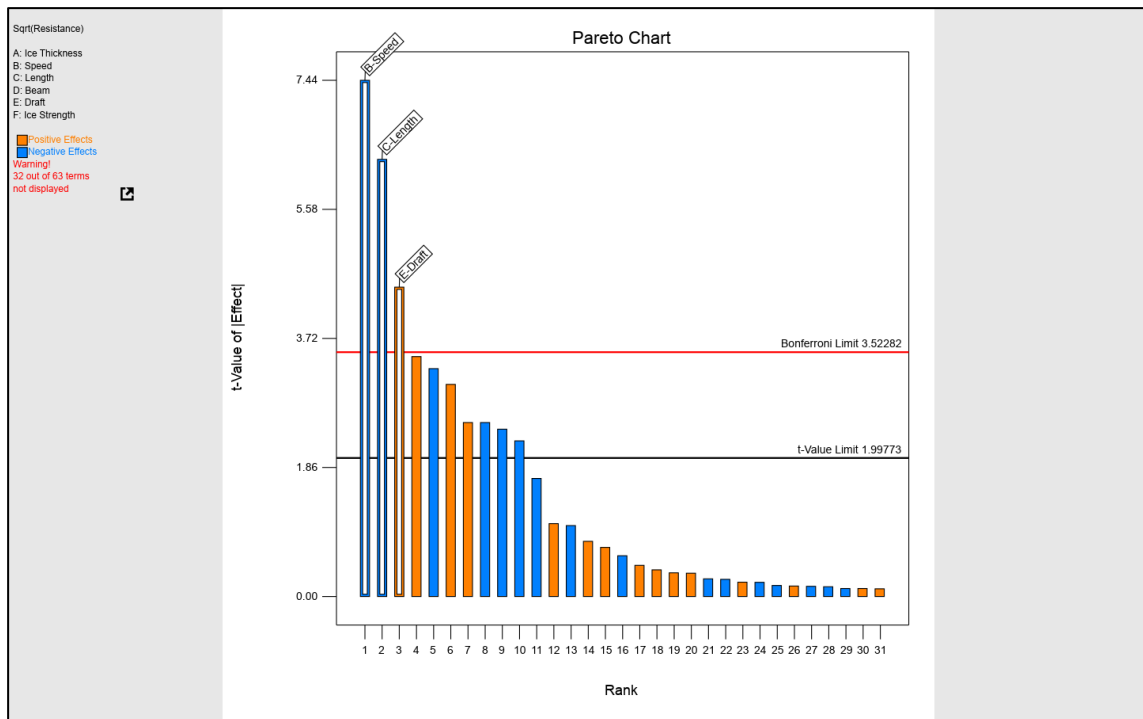


Figure 18 - Pareto graph showing the t-value of most significant terms StatEase®

The R^2 value for this analysis was 0.6456, which could be identified as low. However, as previously mentioned, a perfect fit of the NRC model was not desired to

maintain simplicity. StateEase® indicated that this value agreed with the predicted R^2 value and that the model has adequate precision with little interference from noise.

The results must first be validated by analyzing residuals using the Design Expert software to complete the analysis. Firstly, the results must be normally distributed for the analysis to be a full factorial experiment. For this to hold true, the residuals should all be distributed close to the normal line when arranged on a normal plot. Figure 19 shows this normal distribution and validates that the data can be considered normal because the residuals lie close to the line.

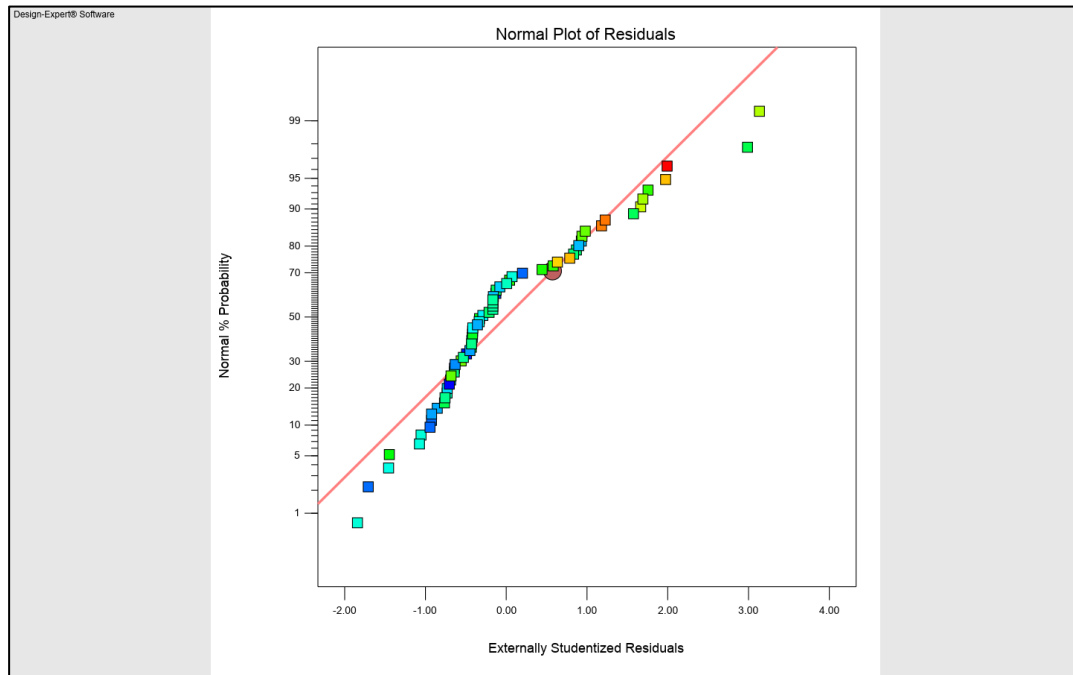


Figure 19 - Normal plot of residuals. The assumption of normality is valid.

The residual vs. predicted plot in Figure 20 verifies the second assumption. This shows that the data points are within the desired limits, denoted by the horizontal lines, and that the data is evenly distributed about zero. The order of the test runs was randomized; however, this is unnecessary for an analytical experiment and therefore did not need to be

tested. Regardless of the order, the responses are always the same in an analytical experiment.

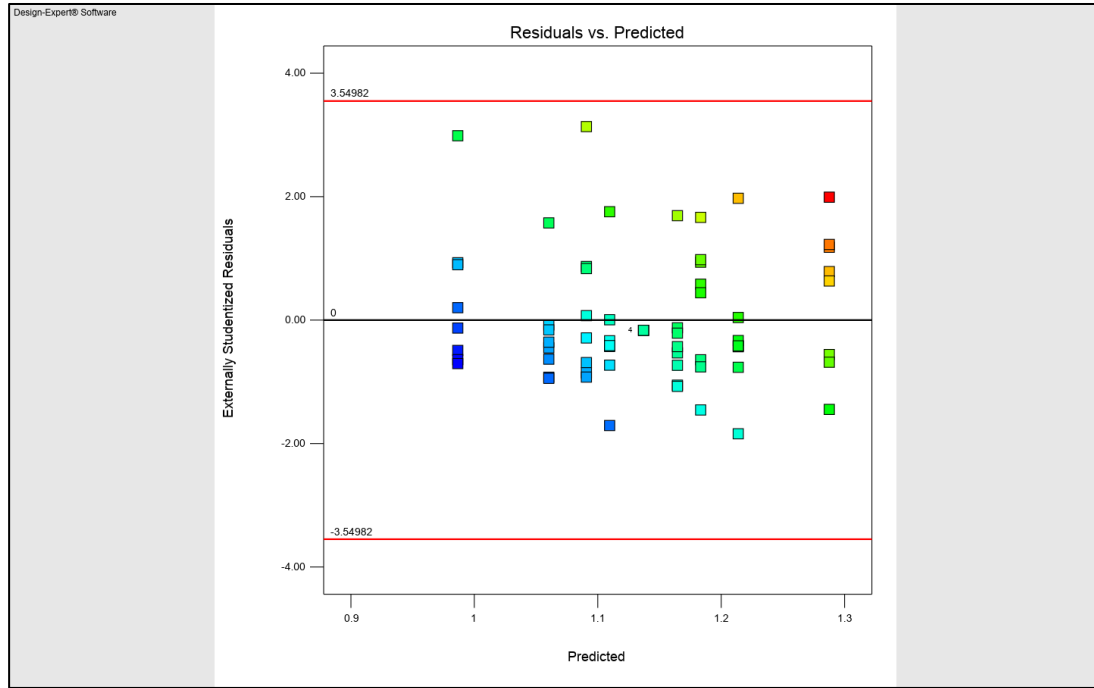


Figure 20 - Residual vs predicted plot. Residuals are evenly distributed and within limits.

Once the analysis of residuals was completed to validate the model, the equation in terms of actual factors could be used to generate the modified equation for ship ice resistance based on Keinonen’s model. Equation (16) shows the complete modified model that is implemented into the emissions model for predicting ship performance in ice. As previously determined by the full factorial design, three parameters are used to keep the model simple: ship speed, length, and draft. These are applied as a quadratic multiplier to the Keinonen model. The first term in the modified equation of 1.199 correlates to the 20% error observed in the base Keinonen equation.

$$R_i = R_{i(Keinonen)}(1.199 - 0.0273V - 0.0017L + 0.0246T)^2 \quad (16)$$

4.2.3 Validating Modified Keinonen Model

The modified Keinonen method must be validated against existing ship performance observations to ensure that it will accurately predict ship performance in ice. This was first applied to the CCGS Henry Larsen; the plot is shown in Figure 21. As predicted, the new model does not fit the NRC prediction with high precision. However, it does predict resistance at the same magnitude. This indicates that the model, based on Keinonen's method, is accurately tuned to predict ice resistance observations on the CCGS Henry Larsen. A similar observation was made across a spectrum of ice thicknesses from 0.2m to 1.5m with minimal variance from the NRC model.

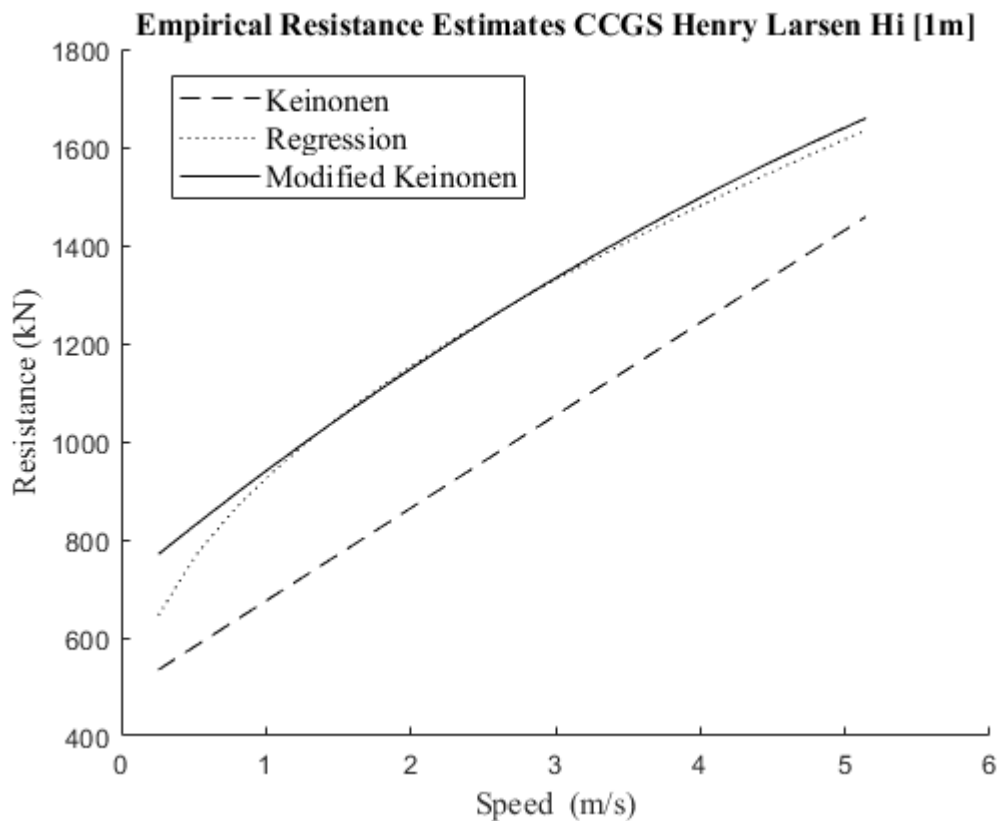


Figure 21 - Modified Keinonen model used to predict the resistance of CCGS Henry Larsen in 1m level ice at speeds from 0.5-5m/s.

However, validating the model only against the CCGS Henry Larsen does not address the concern for generalization. This does not verify if the model is appropriate for other vessel types. Testing this model on other ship types requires additional vessel performance data. In the research conducted by Erceg and Ehlers (2017), they compared the regression resistance curves of four ice-going vessels. One of these vessels was the MT Sotka which has a length of 150m and a beam of 21.5m. These dimensions make the MT Sotka almost one and a half times the size of the CCGS Henry Larsen. It also has different bow angles and is based on slightly different ice conditions from that of the CCGS Henry Larsen. Table 6 presents a complete summary of the ship parameters used to predict the MT Sotka ice resistance.

Table 6 - Empirical prediction parameters for the MT Sotka (Erceg & Ehlers, 2017).

		MT Sotka
L	Ship length	150m
B	Ship breadth	21.5m
T	Ship draft	9.5m
β	Average buttock angle at waterline	29 ⁰
ψ	Average bow flare angle at waterline	43.9 ⁰
h	Ice thickness	0.54m
σ_f	Ice strength	500kPa
μ	Hull ice friction	0.15
hs	Snow thickness	0m
t	Ice surface temperature	-2C
C_h	Hull condition factor	1.0
C_s	Factor of salinity of water	0.90

Figure 22 shows the plot of predicted resistance using the Keinonen and modified Keinonen models. The regression equation was generated using only five operational

measurements between the speeds of 3-4 m/s. The Modified model intersects the regression curve at 4m/s, suggesting high precision. This result indicates that the proposed modified equation is valid for use across differing ship types. It has achieved the purpose of adjusting the prediction magnitude of Keinonen’s model while retaining the components of ice parameters and hull shape.

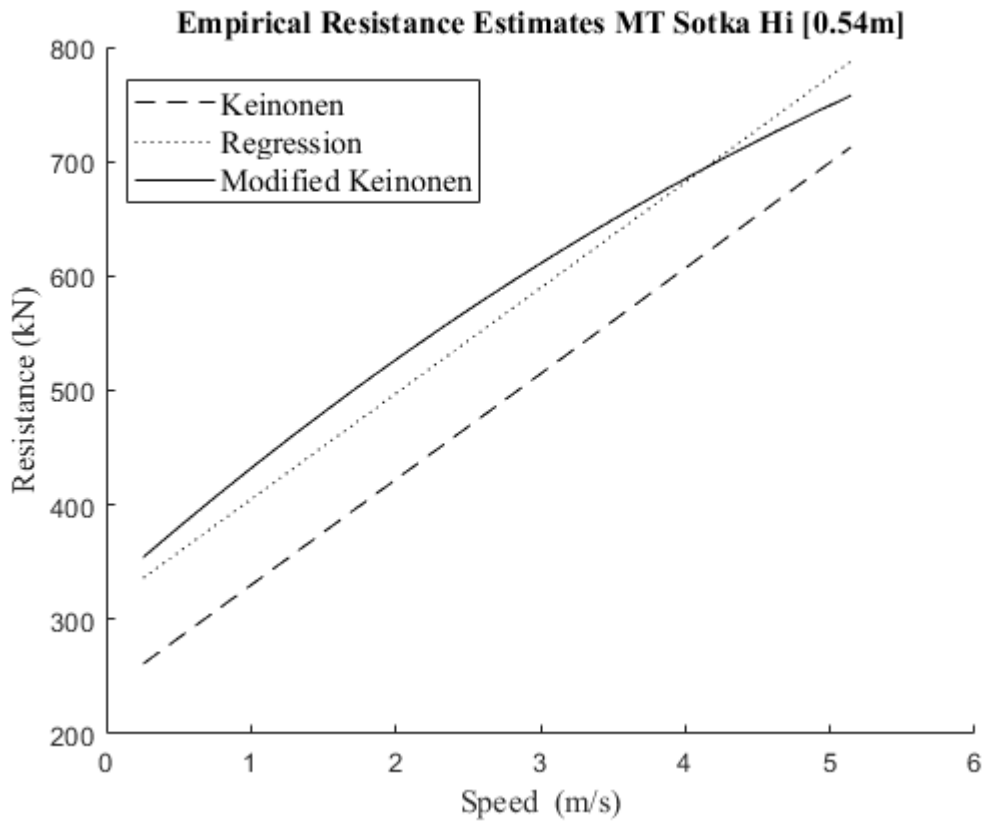


Figure 22 - Modified Keinonen model used to predict the resistance of MT Sotka in 0.54m level ice at speeds from 0.5-5m/s.

4.3 Regression Ship Propulsion Efficiencies

Estimating a ship's propulsion efficiencies is a critical link between its performance characteristics and the emissions profile, which is necessary for predicting fuel

consumption and carbon output. The specific parameters of the hull and propeller must be known to define the propulsion losses properly. With such data for the CCGS Henry Larsen, these values can be discussed in more detail. This section provides a detailed method for determining the losses in cases where the necessary data is available. The results also serve to advise on how to estimate propulsion efficiency in the absence of ship monitoring data. The goal of this section is to determine an adequate generalization of propulsive efficiencies for use in the emission estimator.

4.3.1 Thrust Estimates

4.3.1.1 Thrust Deduction

Section 2.2 defines the thrust deduction as the portion of resistance caused by the propeller operating behind a hull. It is caused by the lower pressure created ahead of the propeller and determines the relationship between bare hull resistance and required thrust as per equation (1). The NRC model test of the CCGS Henry Larsen included the definition of a regression-based thrust deduction curve as shown in equation (17), where the thrust deduction is a function of the advance coefficient. This equation was used to determine the thrust deduction for the CCGS Henry Larsen emissions analysis, and it is recommended for best accuracy to use existing model test data where possible.

$$t = 0.23J^2 + 0.04J + 0.07 \quad (17)$$

where:

t	-	Thrust Deduction
J	-	Advance Coefficient

An equation for thrust deduction based on the advance coefficient is impractical for general use cases because it is necessary to know the shaft RPM. This is not always being measured, and when predicting ship routes, one cannot assume the shaft speed. Therefore, a secondary regression analysis can be completed to relate the thrust deduction to known variables such as speed and ice thickness. Figure 23 shows a plot of the model test thrust deduction values plotted against the values generated from a modified thrust deduction equation (18). Although not a perfect fit for the data, the thrust deduction based on speed and ice thickness is adequate.

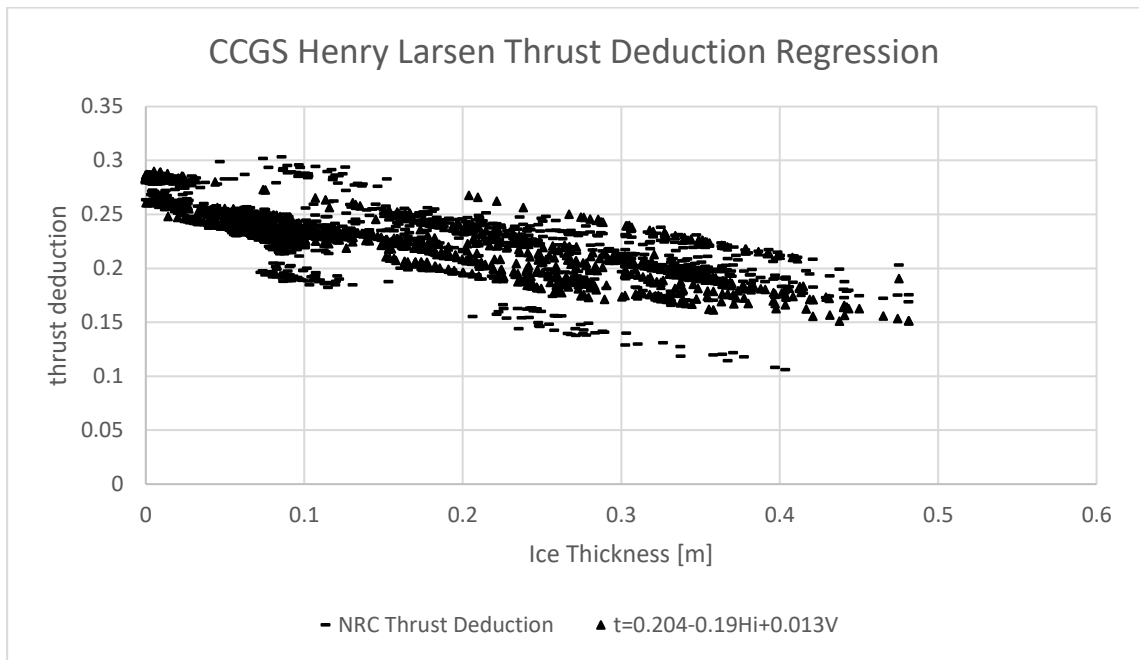


Figure 23 - Regression analysis of CCGS Henry Larsen thrust deduction for all 22 data segments. Thrust deduction as a function of ship speed and ice thickness.

$$t' = 0.204 - 0.19H_i + 0.013V_s \quad (18)$$

where:

- t' - Estimated Thrust Deduction
- H_i - Ice Thickness
- V_s - Ship Speed

As expected, the thrust deduction increases with increased speed. This increase happens because the propeller induces a greater low pressure with increased shaft speed. The ice thickness has an interesting effect on the thrust deduction as it reduces with increased thickness. This decrease is evident in Figure 24, which shows the function of thrust deduction at 1m/s speed intervals and thicknesses up to 1m. It can be explained by the ice passing through the propeller disk. Ice in the propeller disk and ahead of the propeller reduces the low pressure from the propeller due to interactions and changes of the fluid properties. The existence of ice can create a blockage effect, which reduces the inflow speed and consequently induces a near bollard condition with lower thrust deduction. Also, the relative thrust to speed at increasing ice thicknesses would reduce the thrust deduction.

There are limitations to this conclusion because the analysis of the 22 data segments did not include ice thicknesses greater than 0.5m. At the same time, the CCGS Henry Larsen can break up to about 1m of level ice (Government of Canada, 2015). It is assumed that the function is valid up to 1m based on the regression analysis. It is also known that the open water thrust deduction is around 0.24, which correlates well with the regression model.

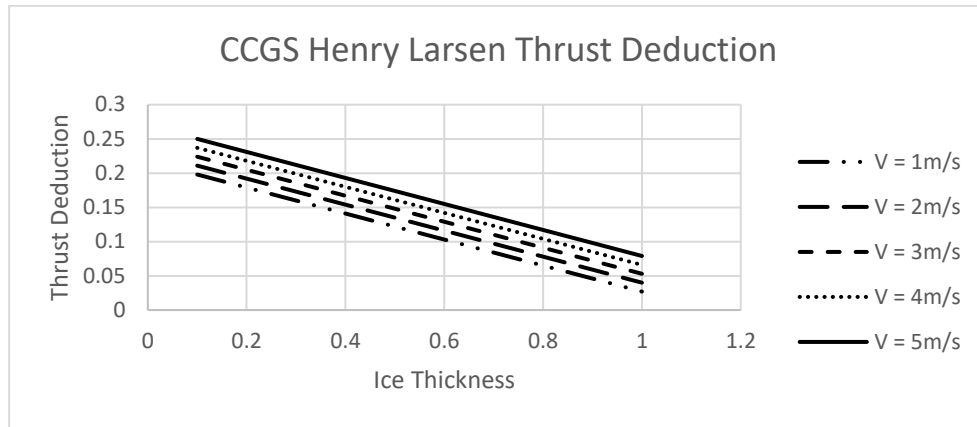


Figure 24 - CCGS Henry Larsen thrust deduction curves based on regression equation of speed and ice thickness. Curves are shown at speeds ranging from 1m/s to 5m.s in thicknesses up to 1m.

The regression approach is still specific to the CCGS Henry Larsen; however, it provides insight into the behavior of thrust deduction with ice thickness. The ice thickness also affects the thrust deduction more than the ship speed. Relevant literature suggests that thrust deductions range from 0.1 to 0.2 (Zubaly, 1996). Based on the CCGS Henry Larsen model, the open water thrust deduction can be assumed at the highest value of 0.2 and decreasing to 0.1 by max designed thickness. This is modeled by equation (19).

$$t' = 0.2 - \left(\frac{0.1}{Hi_{design}} \right) Hi \quad (19)$$

where:

- t' - Estimated Thrust Deduction
- Hi - Ice Thickness
- Vi_{Design} - Maximum level ice for given ship

4.3.1.2 Thrust Prediction

As stated, the thrust deduction calculated for the CCGS Henry Larsen data segments was based on the NRC model equation (17). This was applied to the resistance values calculated with the Keinonen model and the proposed modified Keinonen models. Figure

25 shows the plot of CCGS Henry Larsen thrust predictions against the measured data at the shaft.

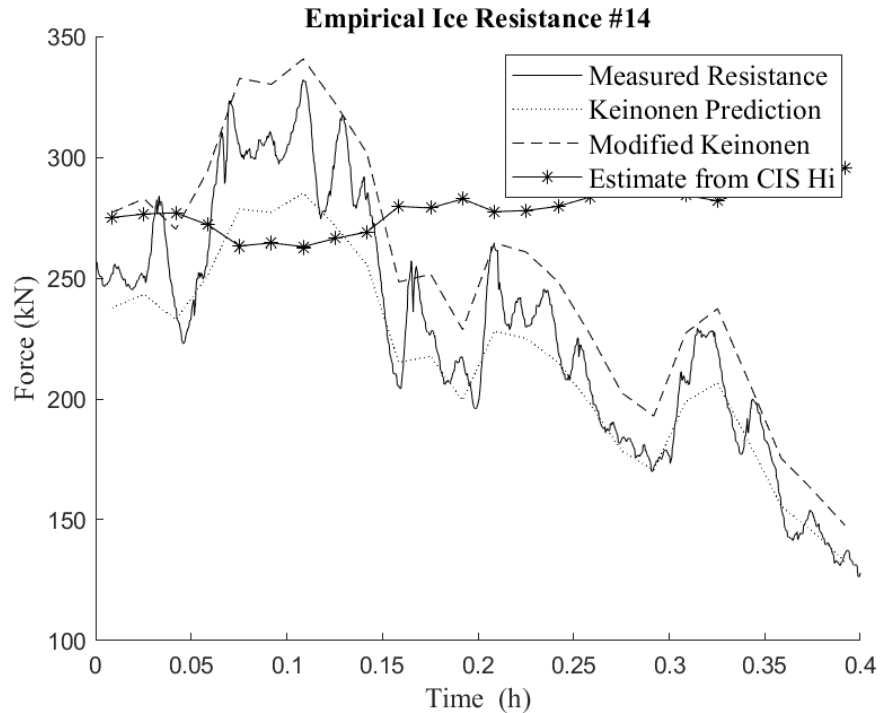


Figure 25 - Plot of CCGS Henry Larsen thrust measured and predicted for data segment #14.

In Figure 25, the solid line represents the measured thrust values from the TT Sense® sensor, the dotted line is the straight Keinonen prediction, and the dashed line shows the modified Keinonen prediction. These predictions used the measured speed and estimated thickness to predict thrust. These predictions show a high degree of accuracy compared to the measured thrust values.

A third estimate is shown in Figure 25 with a solid starred line which appears to differ greatly from the other models. This is because it is based on the measured ship speed and the equivalent-level thickness from the CIS ice charts. It appears that the thrust predictions are inverted, and this occurs because the model is speed dependent. As the

model assumes constant level ice, it expects speed increases to correlate with increased thickness. However, the speed increases are often indicative of leads with thinner ice and lower thrust. This observation is an issue identified with the equivalent-level ice prediction accuracy. However, it will be evident that longer transits with an average thickness near the equivalent thickness will result in similar emissions predictions.

The greatest problem arises when the encountered ice differs significantly from the equivalent-level ice thickness from CIS charts. For example, the thrust plots for data segment #3 are shown in Figure 26. The average ice thickness during this transit was 0.087m, while the equivalent thickness was 0.15m, almost twice as thick. This results in a predicted thrust for equivalent ice that is three times the actual measured thrust. The result is the creation of an inaccurate emission profile. However, no current methods exist for predicting the location of individual ice types reported in an ice chart.

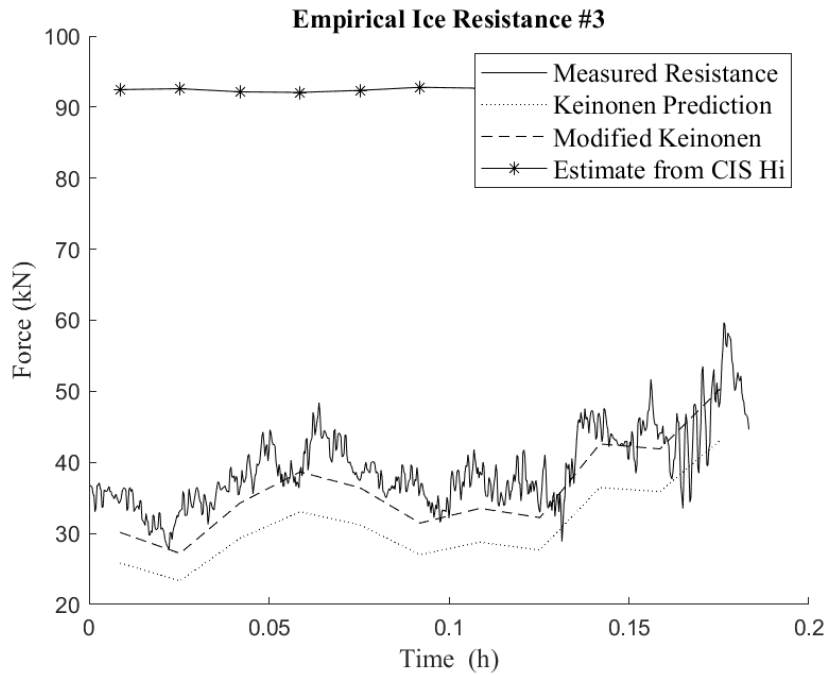


Figure 26 - Thrust predictions for data segment #3.

4.3.2 Propeller Efficiency

4.3.2.1 Behind Hull Efficiency

The propulsion efficiencies must be estimated for the CCGS Henry Larsen and general ship models, similar to the thrust deduction. Since these losses exist between the thrust and engine power, they are considered entirely dependent on the installed propeller, hull form wake fraction, and shafting system. As defined in Section 2.2, the primary propulsion efficiencies are the behind hull efficiency (η_B) and the shaft efficiency (η_s). The shaft efficiency is caused by friction in the stern tube and shaft bearings. It typically has a value of 0.98 (Zubaly, 1996). The behind hull efficiency, if defined by equation (20), is the ratio of thrust power at the propeller to delivered power at the shaft. The thrust power requires the use of advance speed; however, this value would rarely be known for general vessels.

$$\eta_B = \frac{P_T}{P_D} = \frac{TV_A}{2\pi n Q_D} \quad (20)$$

where:

η_B	-	Behind Hull Efficiency
P_T	-	Thrust Power
P_D	-	Delivered Power
T	-	Thrust
V_A	-	Speed of Advance
n	-	rotations per second (rps)
Q_D	-	Torque

The TT Sense® sensor on the CCGS Henry Larsen is used to measure thrust and torque from the shaft using optical sensors. This allows for the regression analysis of behind-hull efficiency. Since the advance speed would not be known for most general ships, the ship speed through water was used for thrust power instead of a wake analysis. Note it

would be possible to use the advance speed for the CCGS Henry Larsen because the advance coefficient can be estimated, and shaft rotations per minute was collected.

Figure 27 shows a plot of the measured thrust power denoted by small dots and the motor power indicated by plus markers. These data points are drawn from all 22 data segments. The average difference between these values gives a behind-hull efficiency of 0.7225 with a standard deviation of 0.3046. Motor power was then estimated for all data points using the behind hull efficiency of 0.7225 and plotted with circle markers. The high standard deviation in this value does distort the results. However, this occurs to a greater degree at lower powers. As most data is below 1MW, this dramatically distorts the standard deviation. The average ship typically has a behind-hull efficiency of around 0.8 (Zubaly, 1996); however, since the CCGS Henry Larsen is an icebreaking hull form, it is expected that the losses due to the behind-hull efficiency would be greater. For ships transiting ice, assuming behind hull efficiency between 0.72-0.8 would be acceptable, depending on the design of the hull form.

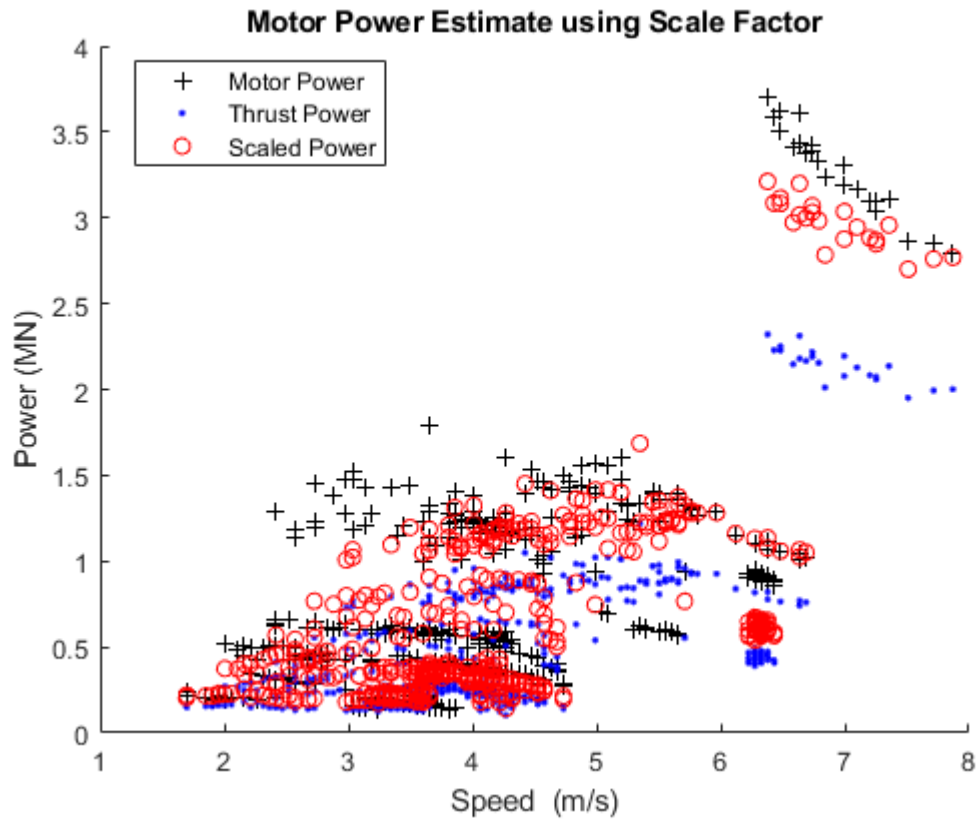


Figure 27 - Motor power estimated using a regression scaling factor.

Since propeller and shafting data are available for the CCGS Henry Larsen, there is a more accurate and detailed method for deriving the motor power. This can be achieved through detailed analysis of the propeller performance curves in open water. The propeller geometry must be used to generate the propeller efficiency curves to conduct this analysis. The specifications are listed in Table 7, and the efficiency curves are shown in Figure 1.

Table 7 - CCGS Henry Larsen propeller specifications (Wang, 2023)

	CCGS Henry Larsen
Diameter	4120 mm
Pitch Ratio at 0.7R	0.844
Blade Area Ratio	0.723
Number of Blades	4

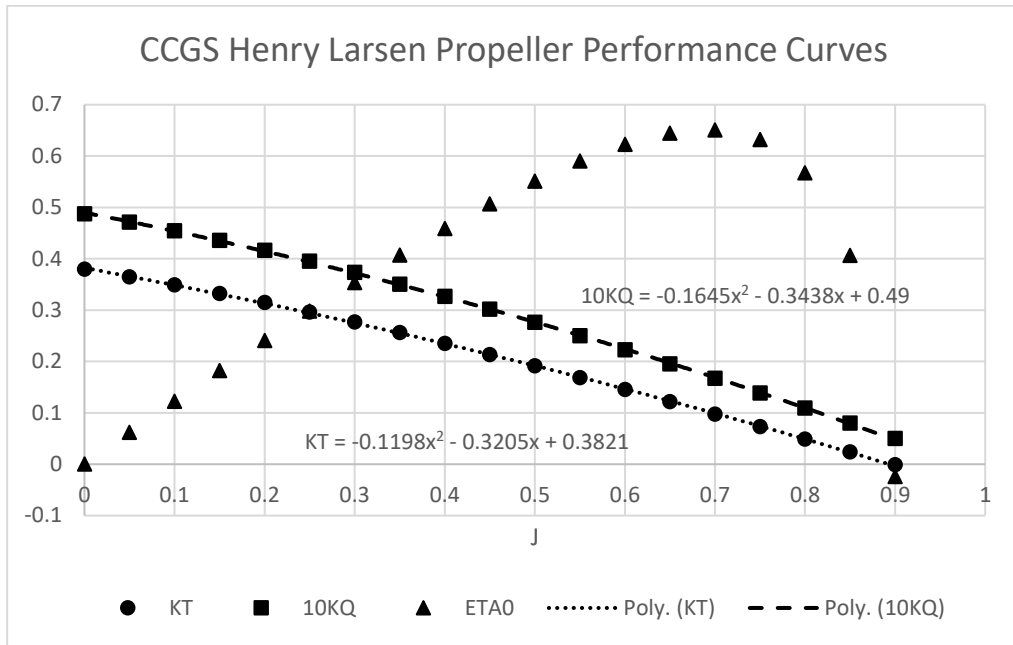


Figure 28 - Propeller performance curves in open water, CCGS Henry Larsen full scale propellers.

The efficiency curves are used to translate from measured thrust to predicted torque. This estimated torque can then be compared against the measured values to evaluate the method's effectiveness in calculating motor power from thrust. The thrust, shaft speed, and propeller diameter can be used to calculate the thrust coefficient using equation (21). The corresponding advance coefficient is determined from the thrust coefficient trendline in Figure 28. The corresponding torque coefficient is determined from the same plot using the advance coefficient. Finally, the shaft torque can be calculated using equation (22). The delivered power is by equation (23) using the shaft speed and inferred torque values from the propeller efficiency curves.

The inferred power values were calculated for all data points and plotted against the measured values and thrust power in Figure 29. The thrust power is shown with small dot

markers, plus markers identify the measured values, and the inferred values are identified by circles.

$$KT = f_1(J) = \frac{T}{\rho n^2 D^4} \quad (21)$$

$$KQ = f_2(J) = \frac{Q}{\rho n^3 D^5} \quad (22)$$

$$P_D = 2\pi n Q \quad (23)$$

where:

- KT - Thrust Coefficient
- KQ - Torque Coefficient
- P_D - Delivered Power
- T - Thrust
- ρ - Water Density
- n - Rotations Per Second (rps)
- Q - Speed of Advance
- D - Propeller Diameter

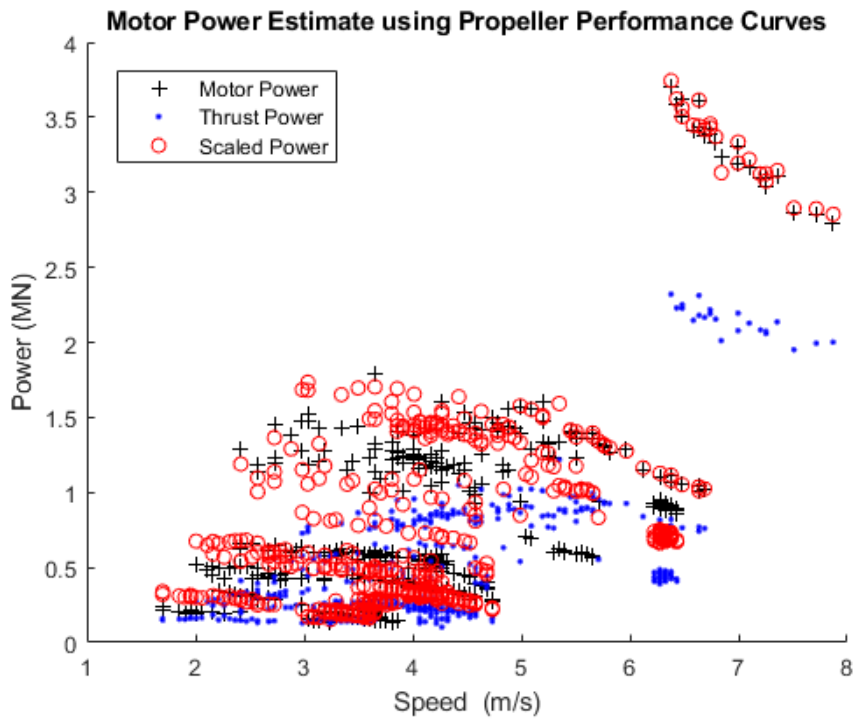


Figure 29 - Motor power estimated using propeller efficiency curves.

The average prediction error was within 5%, which is acceptable given the high variability in the operating conditions. The standard deviation in the difference of estimated power to measured power was 0.272, which is a better result than the single value behind hull efficiency. The high density of low power values skews the result like the scaled efficiency approach. However, the low calculation error and accuracy at higher operating powers indicated that the method of estimating power using propeller efficiency curves is superior. Despite this, the scaled behind hull efficiency of 0.7225 is sufficient in the probable case where thrust and shaft speed data is unavailable. In the case of the CCGS Henry Larsen, live data could be used to predict motor power on demand.

4.3.2.2 Live Power Predictions

The previous methods for calculating power can be used to estimate the live power demands from all 22 data segments. Figure 30 shows the plot of required shaft power throughout segment #14. Two curves are shown, the solid curve is the predicted shaft power using the propeller performance curves, and the dotted curve is based on the constant behind hull efficiency of 0.7225. Due to the improved accuracy of the propeller performance method and availability of live data, further analysis of CCGS Henry Larsen emissions is based on this method. However, the similar prediction results of the constant hull efficiency suggests it would be an equally appropriate model for the overall emissions predictions.

These predictions also consider hotel loads. Hotel loads are not a primary consideration of this research; however, they present a measurable impact on the emissions

profile. In the case of the CCGS Henry Larsen, the hotel loads are known to be approximately 600kW. This value is applied to both prediction methods. Hotel loads will vary for different ship types. A typical range would be 6%-12% of the total installed power. However, this will change drastically based on the type of vessel. For example, the hotel load of a passenger vessel would be a significant component of total power when compared to a bulk carrier or icebreaker. A database of ship hotel loads would be required to build a generalized hotel load prediction model. Such a model could potentially relate ship scale and deadweight or other parameters to estimate hotel loads.

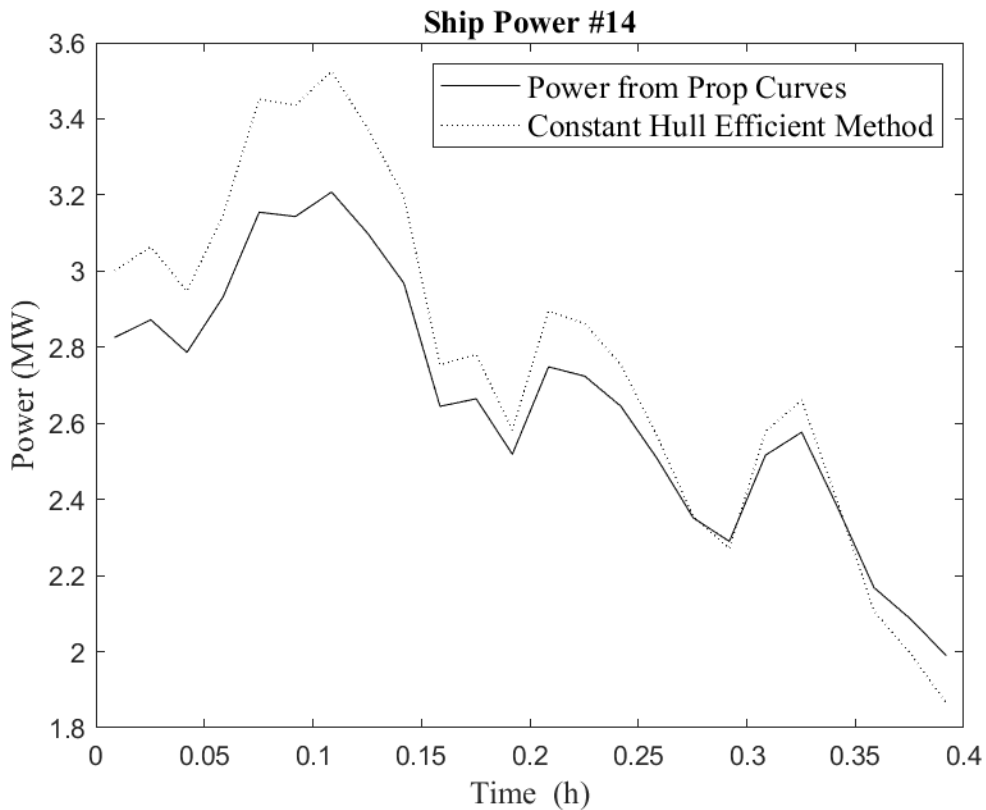


Figure 30 - CCGS Henry Larsen Power Predictions using scaled behind hull efficiency and propeller curves for segment #14.

4.4 Emissions Predictions

4.4.1 Fuel Consumption

Fuel consumption is determined using the given ship's power requirement and Specific Fuel Consumption (SFC). The plot of SFC for the main engines on the CCGS Henry Larsen is unknown and not available publicly from the manufacturer. Therefore, the SFC must be estimated for the CCGS Henry Larsen, and an average value of 200g/kWh was chosen. The fuel consumption can be estimated using the function in equation (24), where fuel consumed is the integral of the motor power over time divided by the SFC. The carbon dioxide production rate can be estimated by multiplying the fuel consumption by the non-dimensional conversion factor between fuel and emissions as per equation (25). The fuel type on the CCGS Henry Larsen is heavy fuel oil; therefore, the non-dimensional factor (C_F) is 3.114, as taken from Table 1 in Section 2.3.1.

$$Fuel\ Consumed(t) = \frac{1}{SFC} \int_0^{t_2} P_M(t) dt \quad (24)$$

$$CO_2(t) = C_F \cdot Fuel\ Consumed(t) \quad (25)$$

where:

SFC	-	Specific Fuel Consumption
P_M	-	Motor Power
C_F	-	tons of carbon/ton of fuel

The fuel consumption and carbon production for data segment 14 are presented in Figure 31 based on the above calculations. The solid line shows the fuel consumed over time based on the modified Keinonen resistance prediction and propeller coefficient calculated delivered power. This plot indicates an estimated fuel consumption of 0.266 t of Heavy Fuel Oil (HFO) for 23.5 minutes of travel through the ice with an average thickness

of 31.4cm. The dashed line shows the emission production for the segment. A total of 0.828t of carbon dioxide is estimated to have been produced during this segment.

The dotted line is a secondary fuel consumption estimate based on the CIS ice chart equivalent-level ice prediction. This result shows a similar estimate of 0.284 t of consumed fuel. The CIS and statistical ice thickness processes yield similar results for most segments if the average estimated thickness is close to the equivalent thickness. The CIS chart predictions were extremely different for a couple of segments when the statistical and equivalent thickness drastically differed.

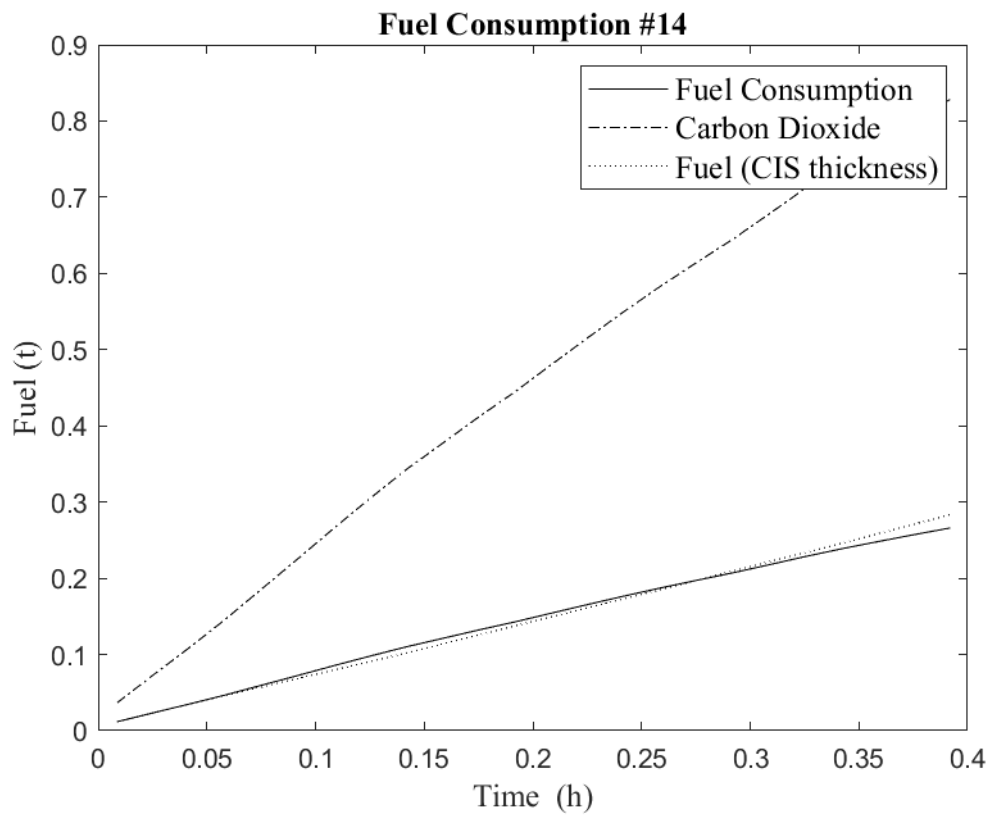


Figure 31 - Fuel Consumption and carbon emissions for CCGS Henry Larsen segment #14

4.4.2 Complete emissions prediction model

The results and analysis can be combined into a single emissions model equation, as shown in equation (26). The critical value in this model lies with total resistance predictions calculated using the proposed modified Keinonen empirical model. This is most important because its simplicity can be applied to any ice-going ship without detailed ship specifications. In rare or specific cases where a ship is instrumented with sensing equipment like the CCGS Henry Larsen, the more extensive techniques detailed throughout this research can be employed. This case includes using model test data to predict the thrust deduction and a detailed propeller analysis to define the bare hull efficiency.

$$Fuel\ Consumed(t) = \frac{1}{SFC} \left(\frac{1}{\eta_S \eta_B} \int_0^{t_2} R_T(t) \cdot \frac{V(t)}{1 - t'(t)} dt + P_{hotel} \right) \quad (26)$$

where:

Total Resistance:

$$R_T(t) = (R_{i(Keinonen)}(1.199 - 0.0273V - 0.0017L + 0.0246T)^2 + R_{ow})(t)$$

Thrust Deduction:

$$t'(t) = 0.2 - \left(\frac{0.1}{Hi_{design}} \right) Hi(t)$$

Assumptions:

$$\eta_S = 0.98$$

$$\eta_B = 0.7225$$

$$SFC = 200g/kWh$$

$$P_{hotel} = \frac{P_{installed}}{10}$$

5 Discussions

5.1 Practical Application of Equivalent-level Ice

This research investigated a method for statistically estimating sea ice thickness from measured ship performance. The approach aimed to capture the encountered ice thickness during full-scale operation as a basis for developing an emissions model for ships transiting in ice. Despite concerns about the accuracy of the TT Sense® measuring equipment, this method proved to be adequate at predicting encountered ice thickness during quasi-steady state operating conditions with a low degree of error. Therefore, the stand-alone estimation model has been proposed to be adapted into the NRC data acquisition system.

There are several practical applications for using such an estimating model. Firstly, it can be cost-effective for instrumented ships to capture the ice thickness they are transiting in. For ships instrumented with the TT Sense® technology, they can be provided real-time feedback about the environment that they are traveling in when the thrust and torque data is paired with a detailed performance model. This could allow the operators to inform navigational decisions and assist in maintaining operational safety.

Alternative methods for evaluating ice thickness primarily focus on image processing using forward-looking cameras. The main benefit of image processing is identifying concentrations and leads ahead of the ship, which is advantageous for navigation. However, forward-looking cameras have significant limitations in that they are computationally demanding and require clear visibility. Significant precipitation, fog,

darkness, and large ship motions can distort or render the process inoperable. Forward-looking cameras are also incapable of determining ice thickness.

The NRC has also used over-the-side cameras to measure ice thickness during their full-scale trials (Wang, et al., 2023). This method focused on measuring the thickness of ice pieces that passed along the side of the hull. The imaging system was calibrated by capturing an object with known dimensions and then calibrating the image pixel dimensions. Similar to forward-looking cameras, this method has several disadvantages, including needing to manually process the images. There would also be some degree of depth distortion in the image's edges, and accurate measurements would require that the measured ice is planar and not rotated relative to the camera. Also, over-the-side cameras only capture individual pieces and do not account for the global ice thickness encountered by the hull. Therefore, the proposed estimation method using scaled model test results and full-scale data is more reliable when compared with current image processing.

5.2 Limitations

There remain some limitations to the current research. All analysis was conducted in quasi-steady state running conditions to estimate sea ice thickness. Therefore, the current model does not consider the effects of drastic changes in heading and speed necessary for special maneuvers required when operating in ice. To calibrate its predictions, the model must be subjected to controlled maneuver cases and compared with measured ice thicknesses. This could not be completed with existing CCGS Henry Larsen datasets because of a lack of knowledge about the encountered ice.

The analysis also highlights significant limitations of the emissions model where a ship is used with insufficient specification of available data. Many performance characteristics, including propeller and hull efficiencies, heavily depend on comprehensive knowledge of a ship's open water and ice performance. This is usually determined through model tests and full-scale trials or regression analysis. In some cases, such as the behind hull efficiency, this can be calculated if the propeller specification is known and the shaft speed is assumed. This limits the application of the model as such data are often not published.

Model test data is also not readily available for many existing ships. Especially with aging fleets, many vessel designs did not include model testing, limiting the possibility for detailed application of this research. However, with modern shipping, there is a high degree of interest in emissions reduction and digital twin applications. Therefore, model testing and full-scale instrumentation are becoming common on new specialized ships, opening up real-time monitoring and performance predicting possibilities.

Regarding the fuel predictions presented in this research, the limit of data and available engine monitoring on the CCGS Henry Larsen did not allow for proper validation. Due to a lack of instrumentation, the model could not be validated by full-scale data beyond the calculation of propulsion motor power. It is not anticipated that there would be significant losses in transmission, and therefore the motor and engine power were considered equal. However, future instrumentation to monitor engine power output and fuel consumption would be advantageous for comparing real-time performance and fuel consumption.

This correlation between motor and engine power is interesting on the CCGS Henry Larsen because it operates on a diesel-electric system where the main engines operate as generators to power the electric propulsion motors. The operational benefits of this system include reduced shafting requirements and engine placement freedom to improve the center of gravity. However, there is no clear correlation of motor to engine power is unknown because they are not mechanically connected. This could have significant implications on the fuel economy. Further research is, therefore, necessary to analyze the differences in emissions profiles between various propulsion systems.

5.3 Future Applications

There are several applications for this research in the marine industry for predicting and forecasting. The first application was presented in Section 5.1, which uses emissions and ice thickness estimates for real-time ship operating performance evaluation. More specifically, the detailed method of emissions prediction can be employed directly onboard for live feedback that can be used to inform navigation decisions on the bridge. The emissions model can track the carbon production rate for specific voyages and provide vital information about the impacts of certain operations on the emission profile. This can inform innovative ways of using the ship to reduce emissions.

There are also several ways the model can be expanded upon through additional research endeavors. One such way is to apply the model in training simulators, and another is to use it to inform route planning decisions.

5.3.1 Simulator Training

Ship simulators are a regular tool for training new seafarers. The benefits of such technology primarily include the reduced cost associated with operating and simulated ships over a real one. It allows navigators in training to accumulate virtual sea time without the risks of operating a real ship with little experience. Another less common use of simulators is replicating dangerous operations in risk-free environments. This approach has been used for many years in other industries, such as aerospace and industrial mining, to mitigate risks through prior simulation. This technique has expanded offshore to the marine industry through large industrial applications such as offshore energy projects and, more recently, ice navigation.

Over the past few years, a research team at Memorial University has conducted novel tests on operator behavior in ice using ship simulators. The early research tested the experience level of navigators on their ability to clear pack ice by comparing the performance of experienced navigators and cadets (Veitch, et al., 2019). A second research project assessed the effects of targeted training on cadet navigation (Thistle & Veitch, 2019). This theory was expanded through additional research by assessing the value of a primitive decision support system for inexperienced navigators in ice (Soper, et al., 2022). Despite a limited test group and isolated scenario, the combined research indicated that experience drastically improves ice management and that targeted ice navigation advice improves how new operators manage prescribed ice fields. However, it is important to note that targeted training does not account for all possible scenarios due to the variability in ice

conditions. It was discovered through this research that experience through trial and error had a significant influence on navigator success (Thistle & Veitch, 2019).

The main problem with trial and error through success is the safety risk it imposes on the marine asset and crew. More recent research was aimed at targeting performance-based feedback as a means of educating inexperienced navigators to address this issue. The most recent research along this line evaluated operator behavior in a simulator when given real-time ice load conditions on the hull (Miller, et al., 2023). This addition gave participants measurable feedback on the ships' performance by informing them if they were within operational limits.

A similar approach could be used to evaluate operator behavior when presented with live emission rates. A proposed simulator trial could include testing emissions production in different ice navigation scenarios to minimize emissions. This could be compared against emergency scenarios to identify navigator decision influence on emissions.

A simulator could also be used to investigate the emissions profile of various tactical maneuvers typical of ice navigation. The benefit of simulator use over full-scale ship in this application includes maintaining a constant ice condition, lower experiment cost, and the ability to conduct more tests. These tests are an important consideration because tactical maneuvers in ice are a higher emissions producer when compared with steady-state operations. Tactical maneuvers include turning, harbor breakouts, and ramming to pass through ice ridges.

5.3.2 Route Planning Optimization

The route a ship takes is a vital factor in the emissions produced. Therefore, route optimization is a critical component when planning a voyage. This is usually straightforward in open water cases because the optimized route is typically the shortest distance. From a corporate perspective, route optimization reduces fuel consumption, cost, and time.

Route planning in the Arctic is significantly more challenging because the sea conditions and ice cover are inconsistent. Also, some ships may not be classed appropriately to navigate all areas of a given ice field. Therefore, route optimization in ice is a multivariable problem. A recent research study at Memorial University developed a digital route optimizer for ships transiting in ice (Browne, et al., 2022). This goal-based agent evaluates a series of operating parameters by assigning weights to determine the optimal path. These goals include the distance, speed, and emissions with the ice class and installed power as hard limits. The agent can determine optimal routes by weighing each goal separately.

The emissions goal in this route planning agent could be improved to provide more robust predictions, and the agent could be used to optimize routes through ice based on fuel consumption. The agent could also be used to replicate planned routes in ice and develop a potential emissions profile. When compared, the agent could advise on how to modify one's chosen route to improve the rate of fuel consumption.

The route optimizing agent can also be used to identify potential ways operators could game emissions regulations, such as the CII calculations from the IMO. These

findings could be used to inform regulatory bodies on the robustness of their regulations and potentially advise methods for improvement.

5.4 Future Improvements

There are a few emissions model limitations and areas that could be improved through additional research. They include further analysis of propulsion equipment efficiency and improved adaptation to tactical ice operations.

The current researched emissions model was validated by comparing estimates against measured data from the CCGS Henry Larsen. However, data collection was limited to the power measured at the motor because the NRC instrumentation does not currently include engine power or fuel consumption. Therefore, fuel consumption and emissions predictions were based solely on the IMO regulations.

There are two ways in which the fuel calculation could be improved. The first method would be to add instrumentation such as an engine power monitor or fuel meter to collect fuel consumption data. A regression analysis could be used to determine the relationship between motor power and engine power. Alternatively, an electric load analysis could be used to determine the transmission losses of the diesel-electric system on the CCGS Henry Larsen. Either analysis would need to be conducted on a series of ice-going vessels to capture the efficiency of different propulsion systems.

As previously stated, the current model is specific to steady ice-breaking conditions and does not consider tactical scenarios where the ship changes directions and accelerates regularly. Further testing is required to capture the emissions profile of such maneuvers.

One proposed method would be to record operating data for prescribed tactical maneuvers in different ice conditions. To properly conduct such an analysis, additional metrics would need to be considered, including throttle inputs, accelerations, and ship heading. The ice condition, including thickness and concentration, would need to be recorded as they cannot be estimated using the current statistical approach, and CIS ice charts do not provide enough granularity. This information would be used to develop the emissions response in transient operating states.

One of the concerns in tactical maneuvers is the influence of human factors on emissions outputs. Simulator trials would be advantageous in this area as they provide a low-cost method of evaluating human factors once the tactical emissions profile is developed.

6 Conclusions

Given basic hull specifications and operating conditions, this research provides a novel method for predicting complete consumption for general ships transiting ice-covered waters. Various methods are suggested based on the degree of data available for emissions calculation to ensure a high prediction accuracy. The complete model amalgamates existing performance methods with new considerations supported by regression analysis and rigorous validation.

The developed method uses a modified empirical model approach to predict the hull performance in ice using basic parameters of the hull and a chosen ice thickness, flexural strength, and ship speed. This resistance predicts the thrust and power through regression analysis of a ship's propulsion efficiencies or estimated values. The emissions are determined by applying the specific fuel consumption rate of the installed machinery to the power requirement, and IMO regulations are used to determine emissions based on fuel type.

Through validation of the model with data from the CCGS Henry Larsen, it proved to predict ship performance and emissions in known ice fields accurately. However, when ice thickness is not known, there was a tendency to have skewed emission results based on assumed equivalent thickness from CIS ice charts. This is generally avoided by analyzing longer routes where the average ice thickness encountered would be probabilistically close to the equivalent thickness. With improvements gained through tactical validation, the model can potentially advise route planners and operators of the emissions implications of navigational decisions.

7 References

- Browne, T., Tran, T. T., Veitch, B., Smith, D., Khan, F., & Taylor, R. (2022). A method for evaluating operational implications of regulatory constraints on Arctic shipping. *Marine Policy*, 135, 104839.
- Canadian Ice Service. (2022, 11 29). *Ice archive*. (Government of Canada) Retrieved 8 16, 2022, from <https://iceweb1.cis.ec.gc.ca/Archive/page1.xhtml>
- Daley, C., & Riska, K. (1990). *Review of Ship-Ice Interaction Mechanics*. Helsinki: Teknillinen korkeakoulu.
- Det Norske Veritas. (2022). *CII – Carbon Intensity Indicator*. Retrieved from DNV: <https://www.dnv.com/maritime/insights/topics/CII-carbon-intensity-indicator/answers-to-frequent-questions.html#:~:text=How%20is%20the%20CII%20calculated,carrying%20capacity%20and%20nautical%20mile>.
- Erceg, S., & Ehlers, S. (2017). Semi-empirical level ice resistance prediction methods. *Ship Technology Research*, 64(1), 1-14.
- Frederking, R. (2003). A model for ship routing in ice. *Proceedings 17th International Conference on Port and Ocean Engineering under Arctic Conditions* (pp. 16-19). Trondheim, Norway: POAC 03.
- Gasper, H. M., & Erikstand, S. O. (2009). Extending the Energy Efficiency Design Index to Handle Non-Transport Vessels. *International Conference on Computer and IT Applications in Shipbuilding*, 525-536.
- Government of Canada. (2015). *CCG Fleet: Vessel Details*. Retrieved from CCGS HENRY LARSEN: <https://inter-j01.dfo-mpo.gc.ca/fdat/vessels/70>
- Harvald, A. F. (1983). *Resistance and propulsion of ships*. John Wiley & Sons.
- Holtrop, J., & Mennen, G. (1982). An approximate power prediction method. *International Shipbuilding Progress*, 29(335), 166-170.
- International Maritime Organization. (2016). *Guidance on Methodologies for Assessing Operational Capabilities and Limitations in Ice*.
- International Maritime Organization. (2018, October 26). *Guidelines on the Method of Calculation of the Attained Energy Efficiency Design Index (EEDI) for New Ships*. IMO Publications and Documents.
- International Maritime Organization. (2022, June 10). *Interim Guidelines on Correction Factors and Voyage Adjustments for CII Calculations (CII Guidelines, G5)*. IMO Publications and Documents.

- ITTC Resistance Committee. (2011). Recommended procedures and guidelines: resistance test. *International Towing Tank Conference*.
- Keinonen, A. J., Browne, R. P., & Revill, C. R. (1989). *Icebreaker design synthesis - analysis of contemporary icebreaker performance*. AKAR Inc. Report for Transport Canada, Transport Development Centre, TP 10923E.
- Keinonen, A. J., Browne, R. P., Revill, C. R., & Reynolds, A. (1996). *Icebreaker characteristics synthesis*. AKAC Inc. report for Transport Canada, Transportation Development Center, TP 12812E.
- Lewis, J. W., Debord, F. W., & Bulat, V. A. (1982). Resistance and propulsion of iceworthy ships. *Trans Soc Nav Archit Mar Eng (SNAME)*, (pp. 90:249-276).
- Lindqvist, G. (1989). A straightforward method for calculation of ice resistance of ships. *Proceedings of 10th International Conference on Port and Ocean Engineering under Arctic Conditions (POAC)*. Lulea, Sweden.
- Milakovic, A.-S., Li, F., Polach, R. U., & Ehlers, S. (2020). Equivalent ice thickness in ship ice transit simulations; overview of existing definitions and proposition of an improved one. *Ship Technonlogy Research*, 67(2), 84-100.
- Milakovic, A.-S., Schutz, P., Piehl, H., & Ehlers, S. (2018). A method for estimation of equivalent-volume ice thickness based on WMO egg code in absence of ridging parameters. *Cold Regions Science and Technology*, 155, 381-395.
- Miller, L. P., Quinton, B., Soper, J., & Veitch, B. (2023). Development of Ice-Load Algorithm for Real-Time Feedback During Simulator Training. *Offshore Ocean and Arctic Engineering Conference*. Melbourne: ASME.
- Montgomery, D. C. (2013). *Design and Analysis of Experiments*. Hoboken: John Wiley & Sons Inc.
- Riska, K., Wilhelmson, M., Englund, K., & Leiviska, T. (1998). *Performance of merchant vessels in ice in the Baltic*. Helsinki, Finland: Research Report No. 52, Winter Navigation Research Board.
- Soper, J., Smith, J., Power, J., & Veitch, B. (2022). An evaluation of decision support technology in simulated offshore ice management. *OMAE2022-78097*. Hamburg.
- Sustainable Ships. (2022). *Specific Fuel Consumption [g/kWh] for Marine Engines*. Retrieved from Sustainable Ships: [https://www.sustainable-ships.org/stories/2022/sfc#:~:text=Specific%20Fuel%20Consumption%20\(SFC\)%20of,stroke%20or%20four%2Dstroke](https://www.sustainable-ships.org/stories/2022/sfc#:~:text=Specific%20Fuel%20Consumption%20(SFC)%20of,stroke%20or%20four%2Dstroke).

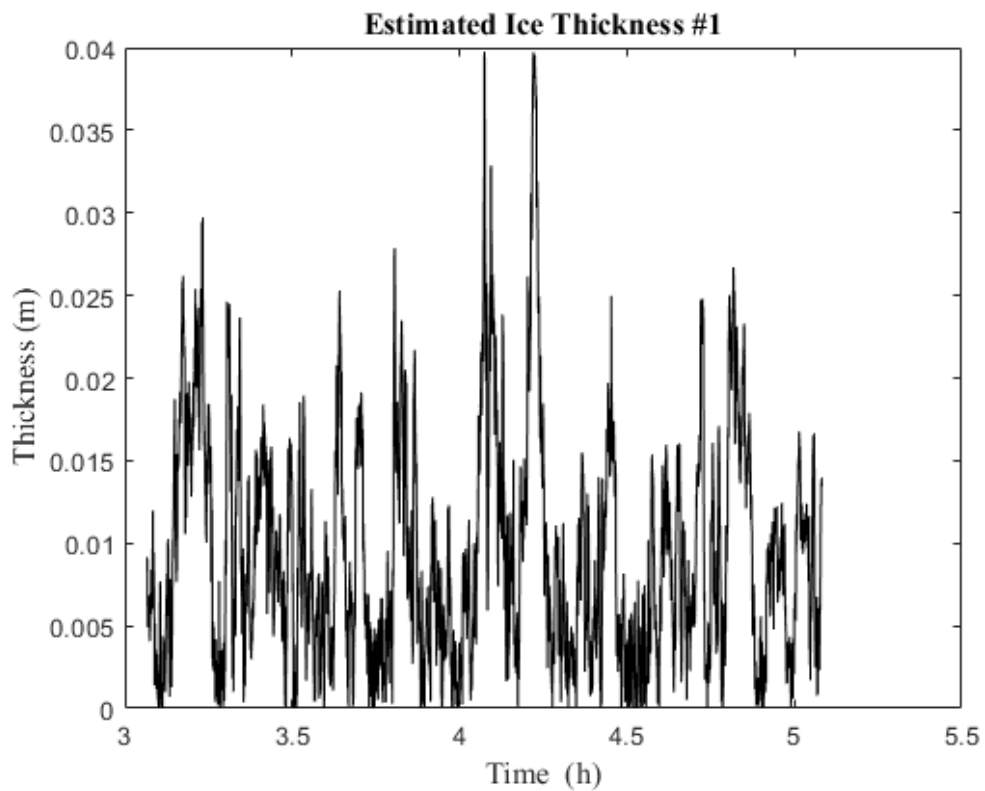
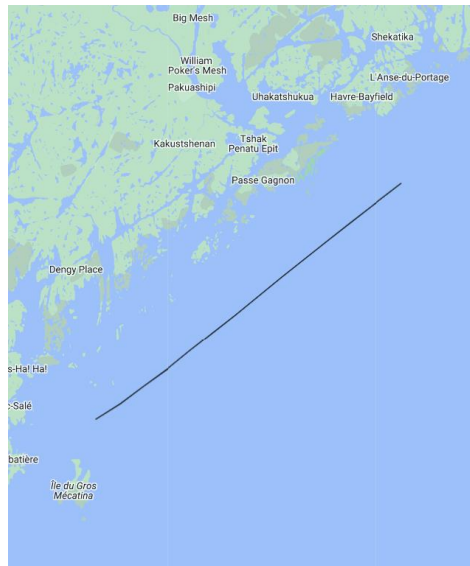
- Thistle, R., & Veitch, B. (2019). An Evidence-Based Method of Training to Targeted Levels of Performance. *Proceedings, Annual Meeting, Society of Naval Architects and Marine Engineers*. Tacoma.
- Transport Canada. (2010, January 14). *Zone/Date System (Z/DS)*. Retrieved from Government of Canada: <https://tc.canada.ca/en/marine-transportation/Arctic-shipping/zone-date-system-z-ds>
- Vance, G. P. (1980). *Analysis of the performance of a 140-ft Great Lakes icebreaker: USCGC Katmai Bay. Report No. 80-8*. U.S. Army CRREL.
- Veitch, E., Molyneux, D., Smith, J., & Veitch, B. (2019). Investigating the influence of bridge officer experience on ice management effectiveness using a marine simulator experiment. *Journal of Offshore Mechanics and Arctic Engineering*, *141*(4), 1-12.
- Wang, J. (2023). Development of an improved ice model test method to evaluate vessel's ice performance using CCG's Henry Larsen icebreaker model. *ISOPE*. Ottawa.
- Wang, J., Brown, J., Meadus, C., Hickey, G., Ennis, T., Mews, K., . . . Baggs, J. (2023). Performance evaluation of CCG's icebreaker henry larsen with air bubbler system in ice. *ISOPE*. Ottawa.
- Zahn, P. B., & Philips, L. (1987). *Towed resistance trials in ice of the USCGC Mobile Bay (WTGB103)*. Montreal, Canada: Transport Canada, Transportation Development Centre.
- Zubaly, R. B. (1996). *Applied Naval Architecture*. Cornell Maritime Press.

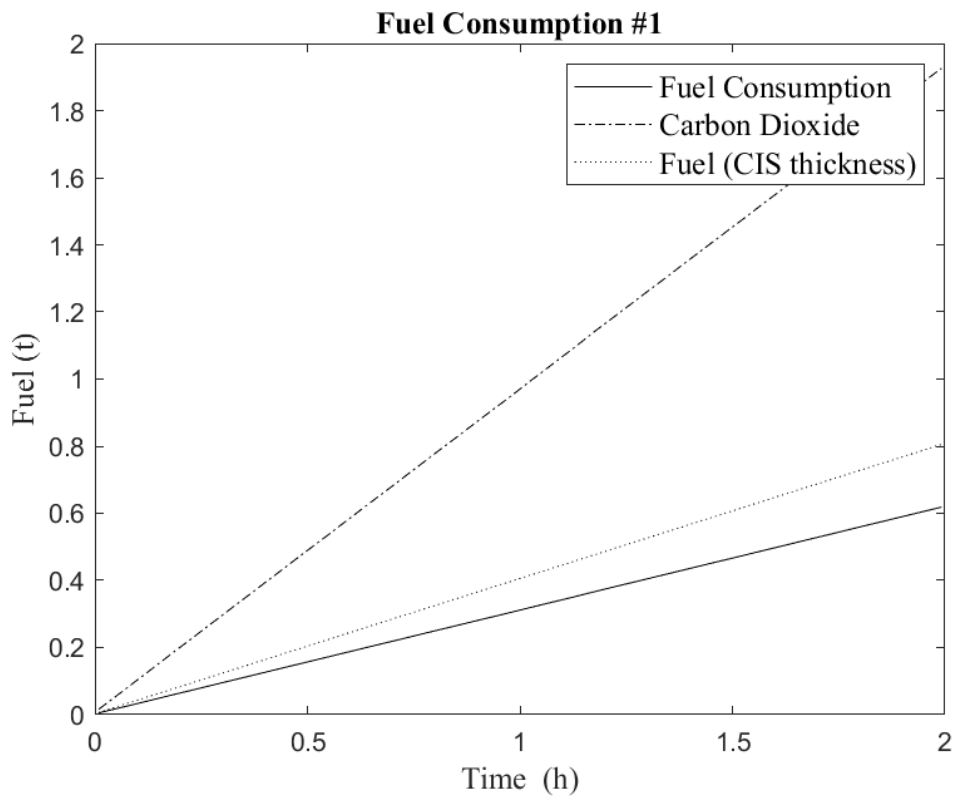
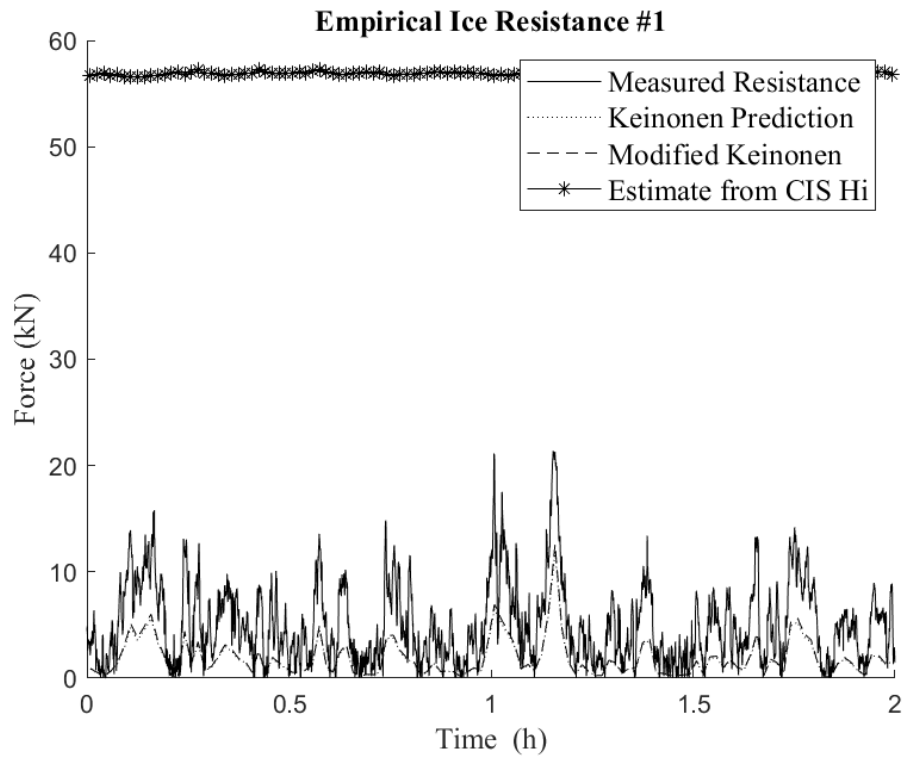
8 Appendix A – CCGS Henry Larsen Data Segment Analysis

This Appendix contains detailed analysis of all twenty-two data segments that were analyzed in the research work. Each data segment includes the following summarizing information:

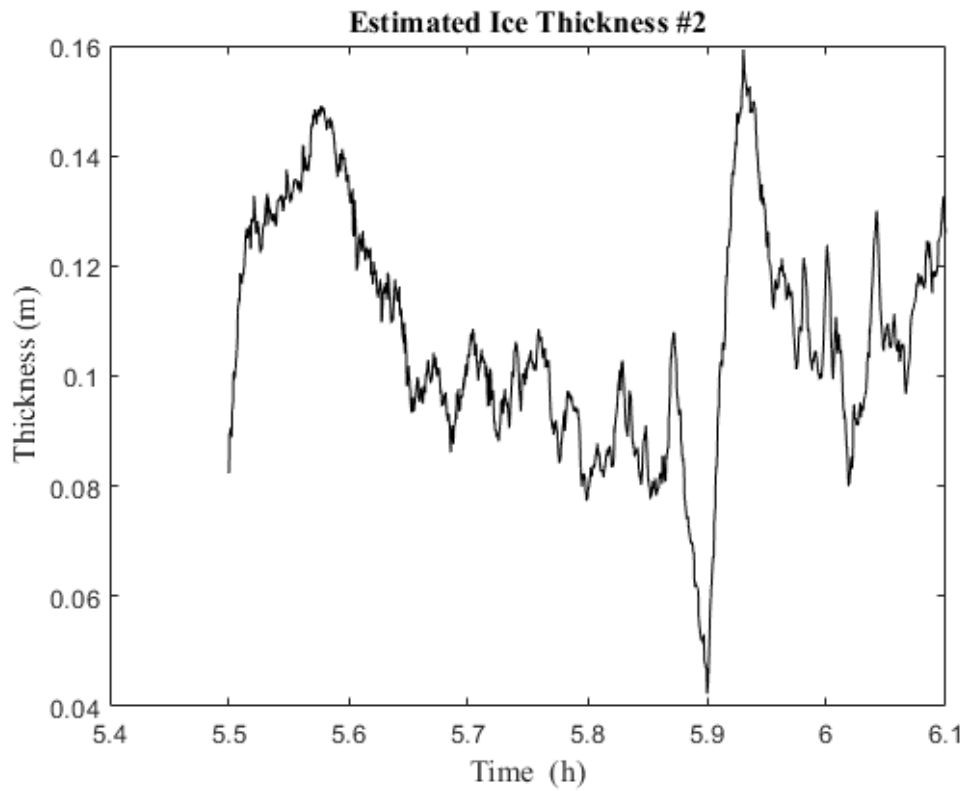
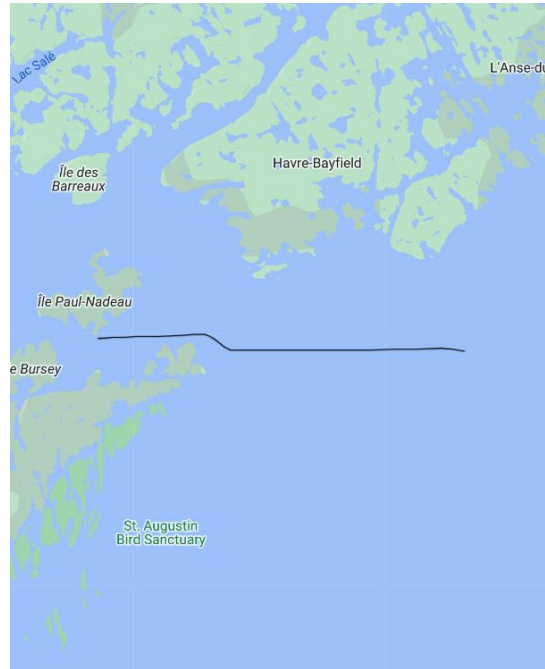
1. Numerical data describing CIS ice chart regimes and segment date.
2. Map plotting the location and transit for each segment.
3. Ice thickness estimated through performance estimation.
4. Plot of empirical ice resistance estimate including Modified Keinonen Method.
5. Plot of cumulative fuel consumption and carbon dioxide produced.

Data Segment #1	
Date	February 2, 2022
Statistical Thickness	0.01m
CIS equivalent thickness	0.1m
First Concentration/ Thickness	1% - 0.225m
Second Concentration/ Thickness	4% - 0.125m
Third Concentration/ Thickness	5% - 0.05m
Ice Type	Open Water

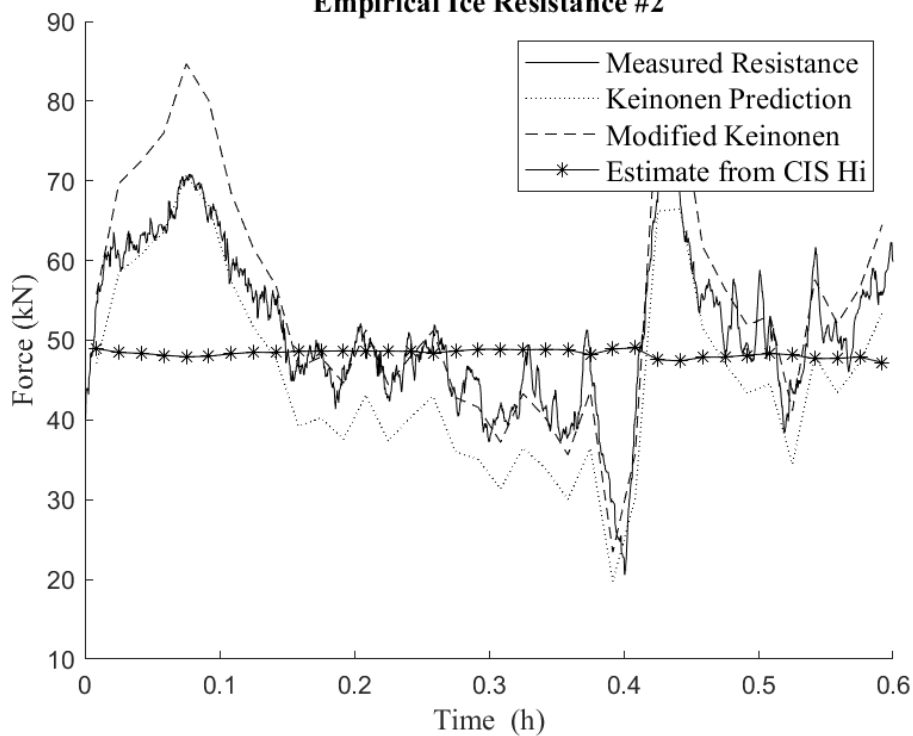




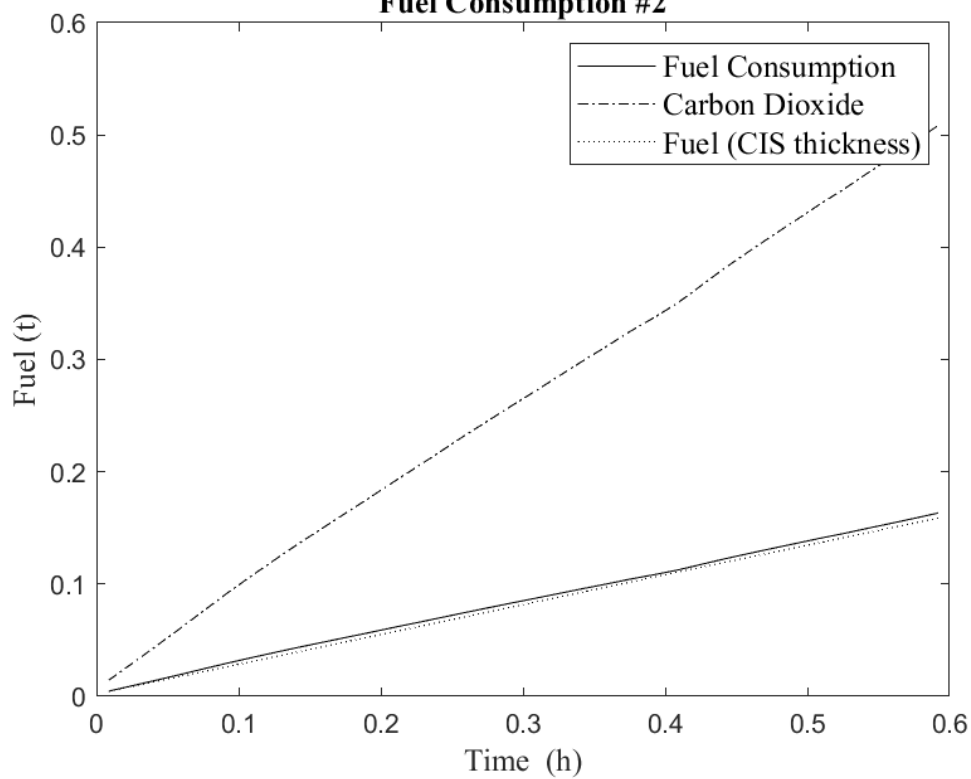
Data Segment #2	
Date	February 2, 2022
Statistical Thickness	0.116m
CIS equivalent thickness	0.1m
First Concentration/ Thickness	1% - 0.225m
Second Concentration/ Thickness	4% - 0.125m
Third Concentration/ Thickness	5% - 0.05m
Ice Type	Grey Ice



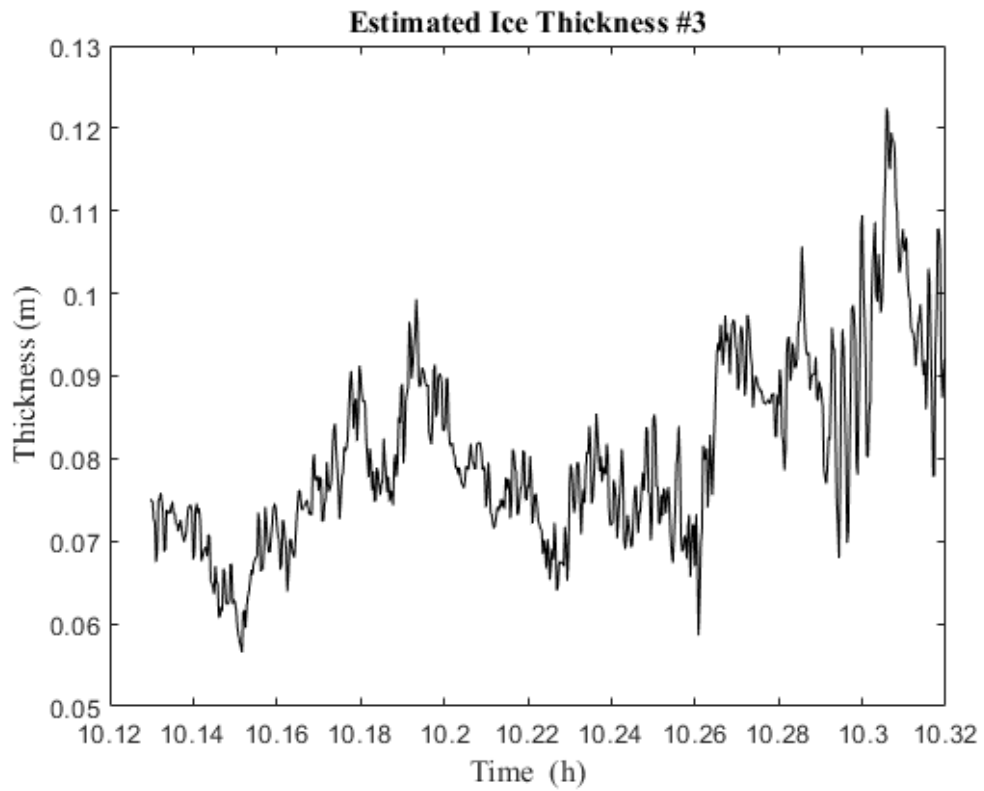
Empirical Ice Resistance #2

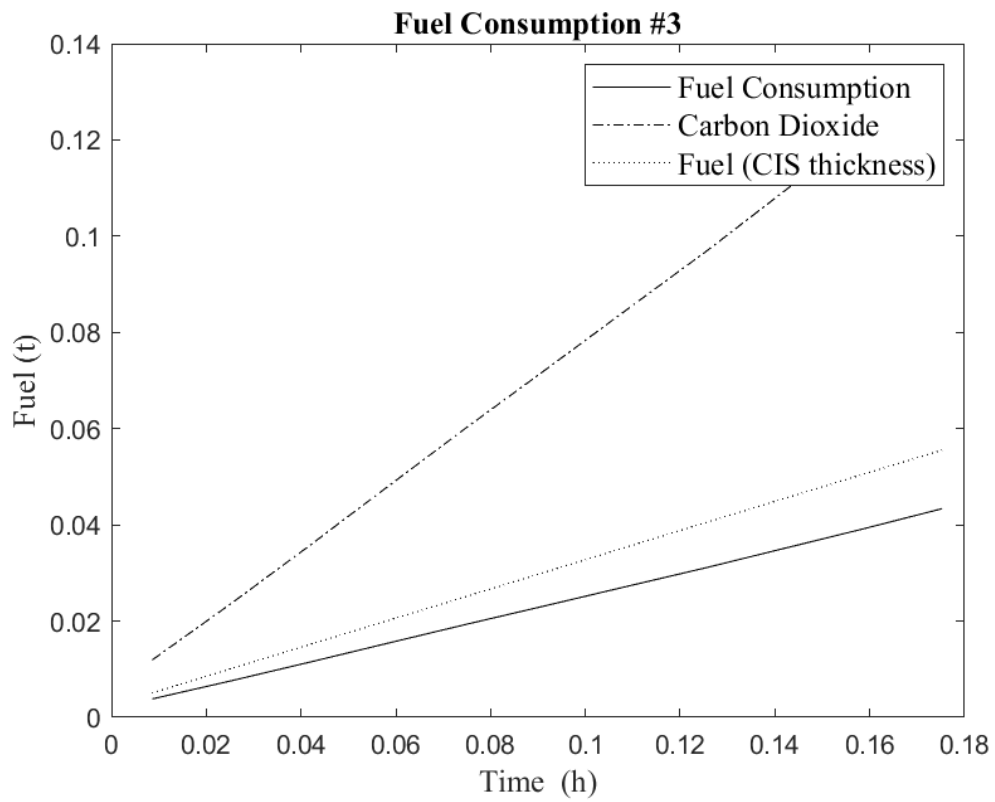
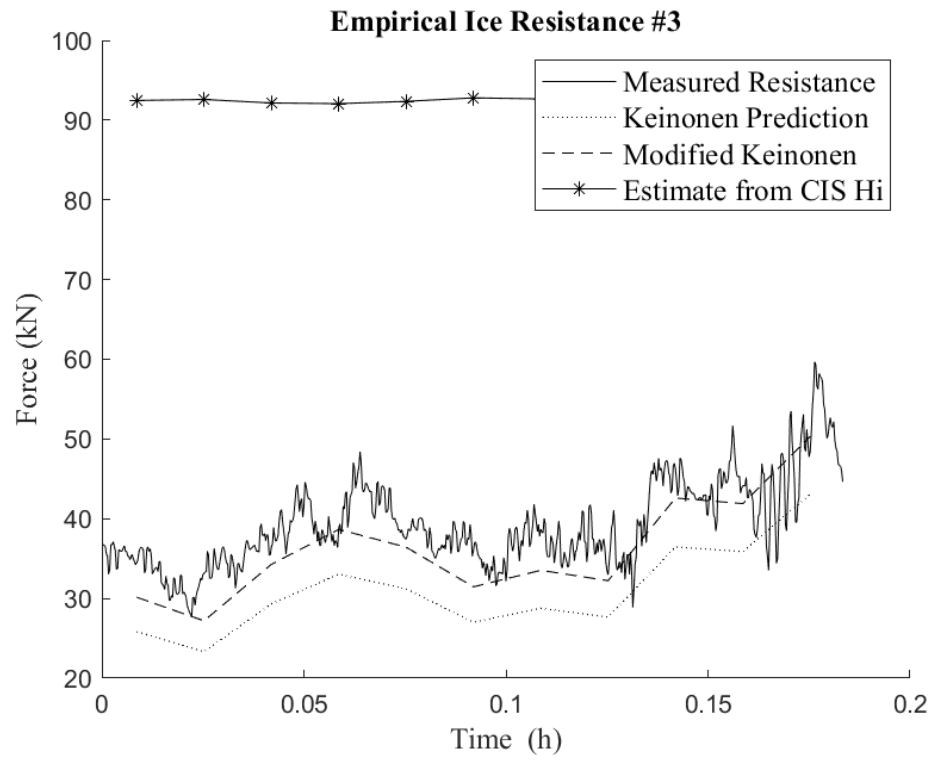


Fuel Consumption #2

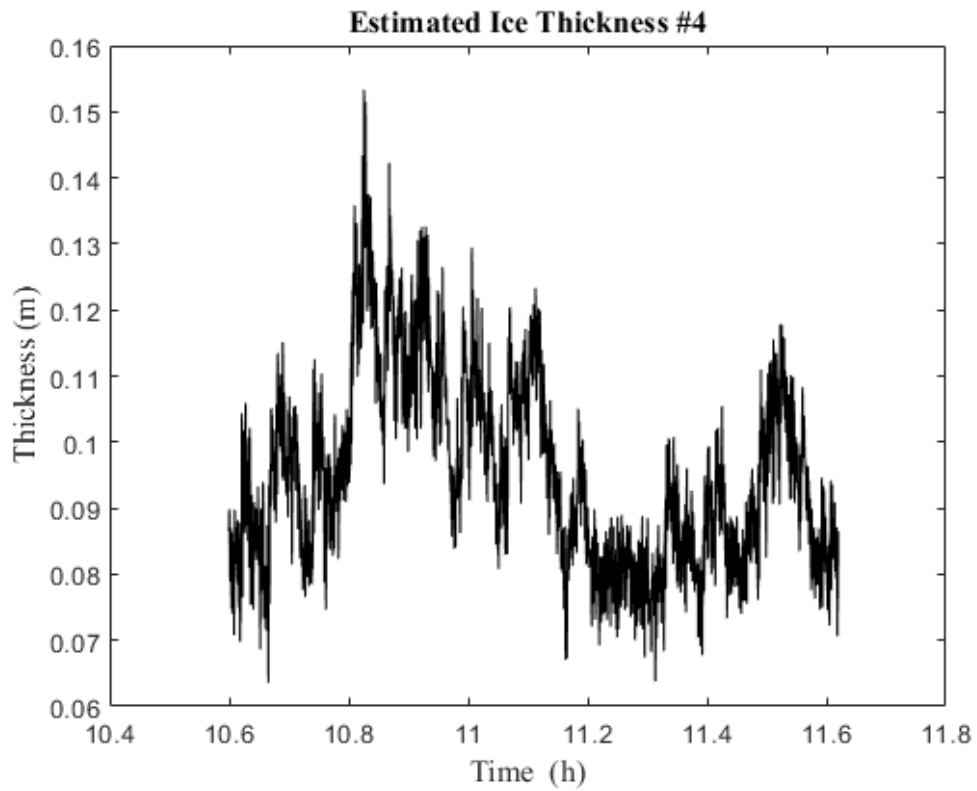


Data Segment #3	
Date	February 3, 2022
Statistical Thickness	0.087m
CIS equivalent thickness	0.15m
First Concentration/ Thickness	3% - 0.225m
Second Concentration/ Thickness	4% - 0.125m
Third Concentration/ Thickness	1% - 0.05m
Ice Type	New Ice

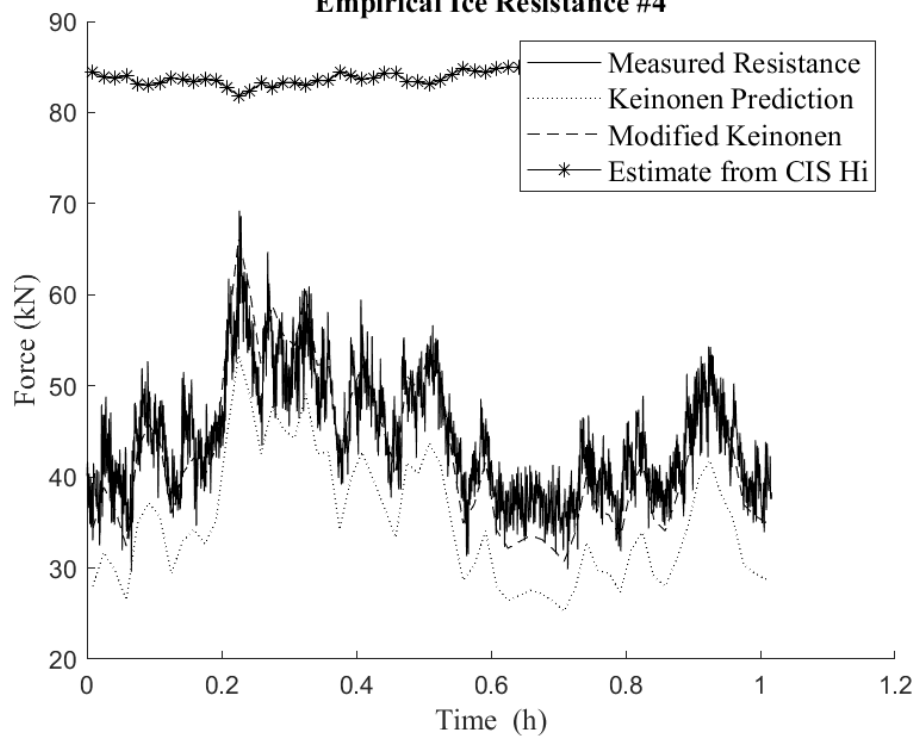




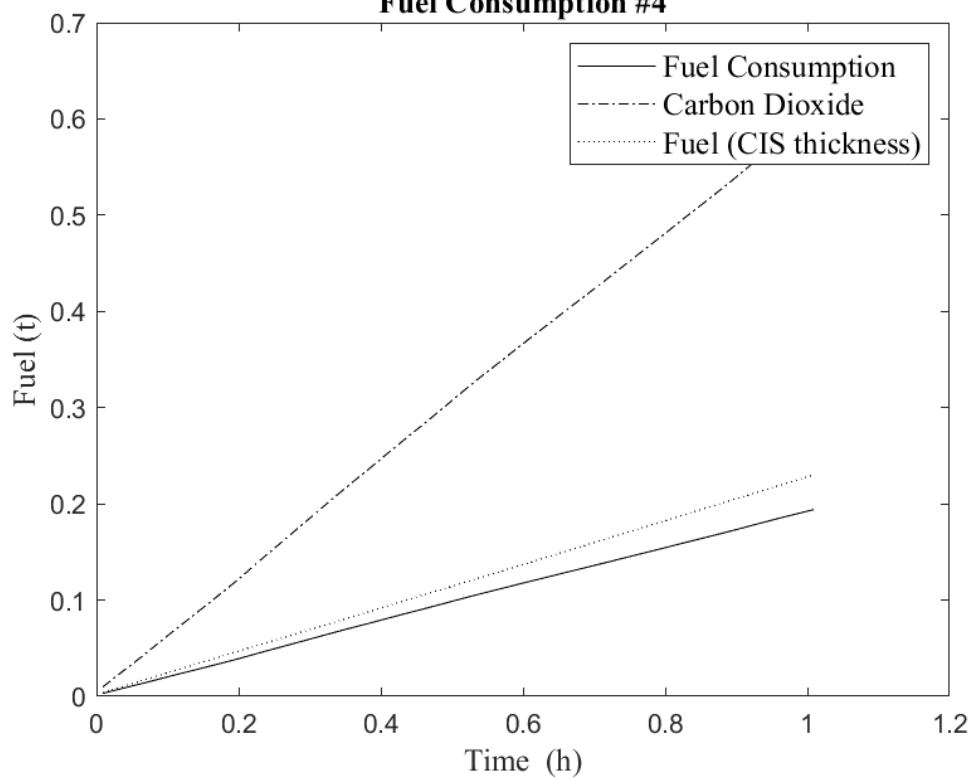
Data Segment #4	
Date	February 3, 2022
Statistical Thickness	0.103m
CIS equivalent thickness	0.15m
First Concentration/ Thickness	3% - 0.225m
Second Concentration/ Thickness	4% - 0.125m
Third Concentration/ Thickness	1% - 0.05m
Ice Type	Grey Ice



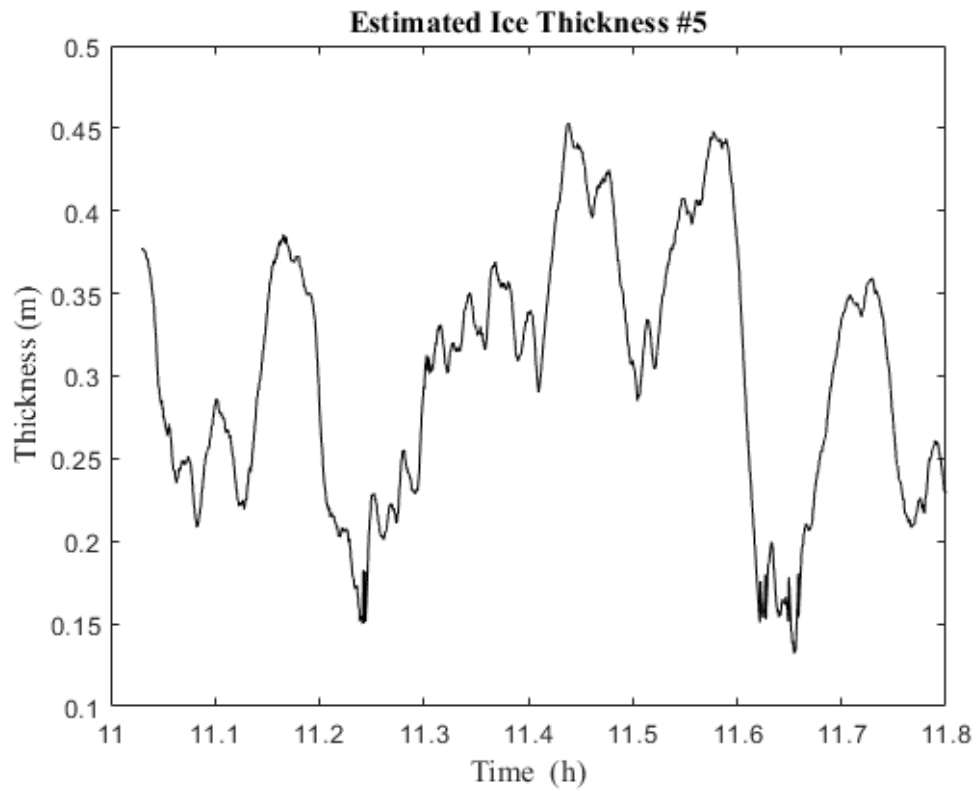
Empirical Ice Resistance #4

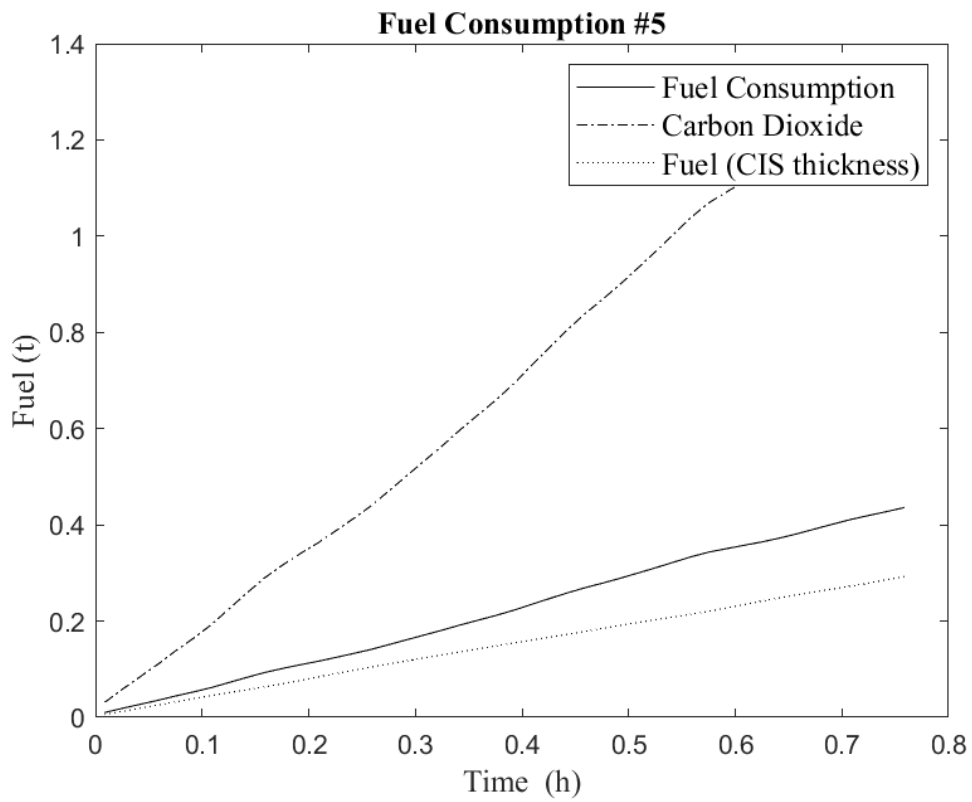
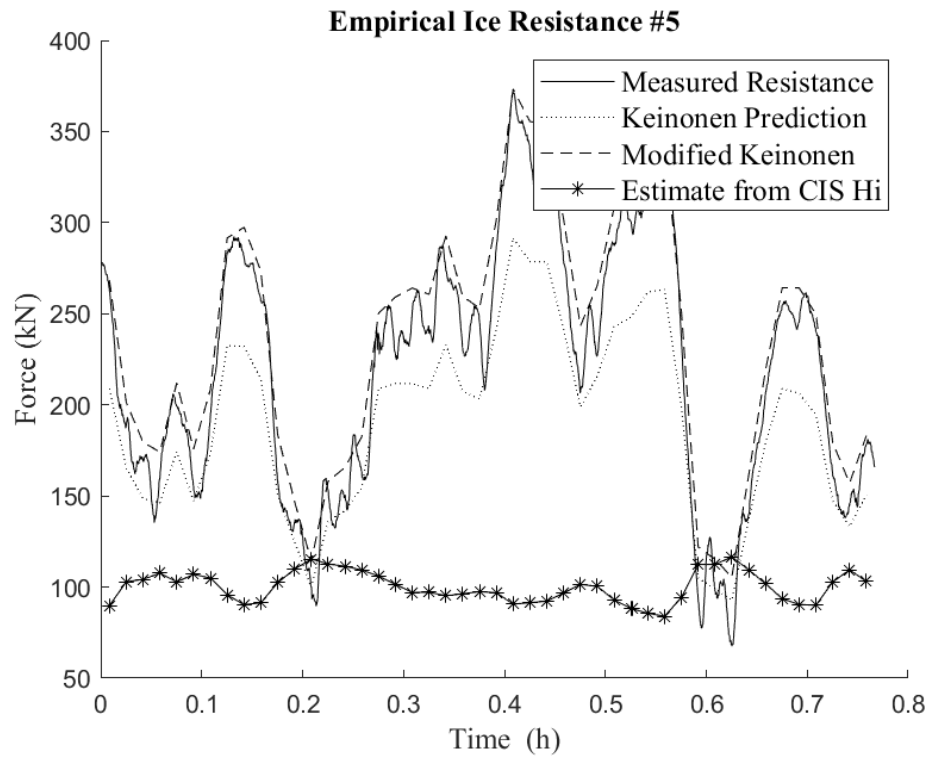


Fuel Consumption #4

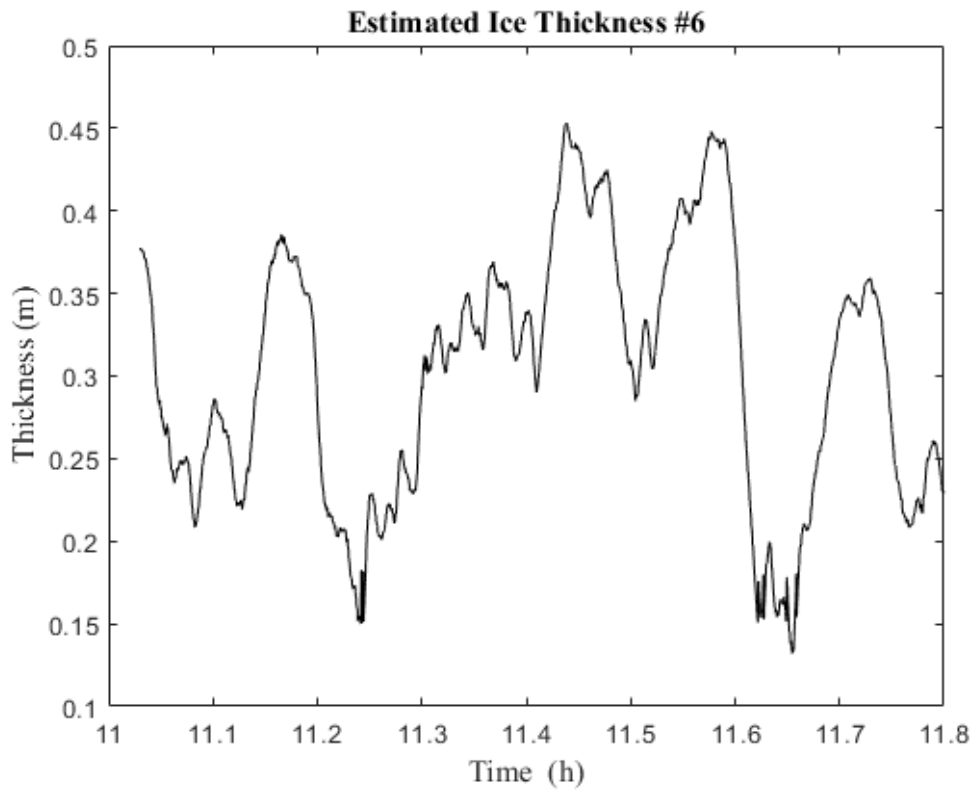


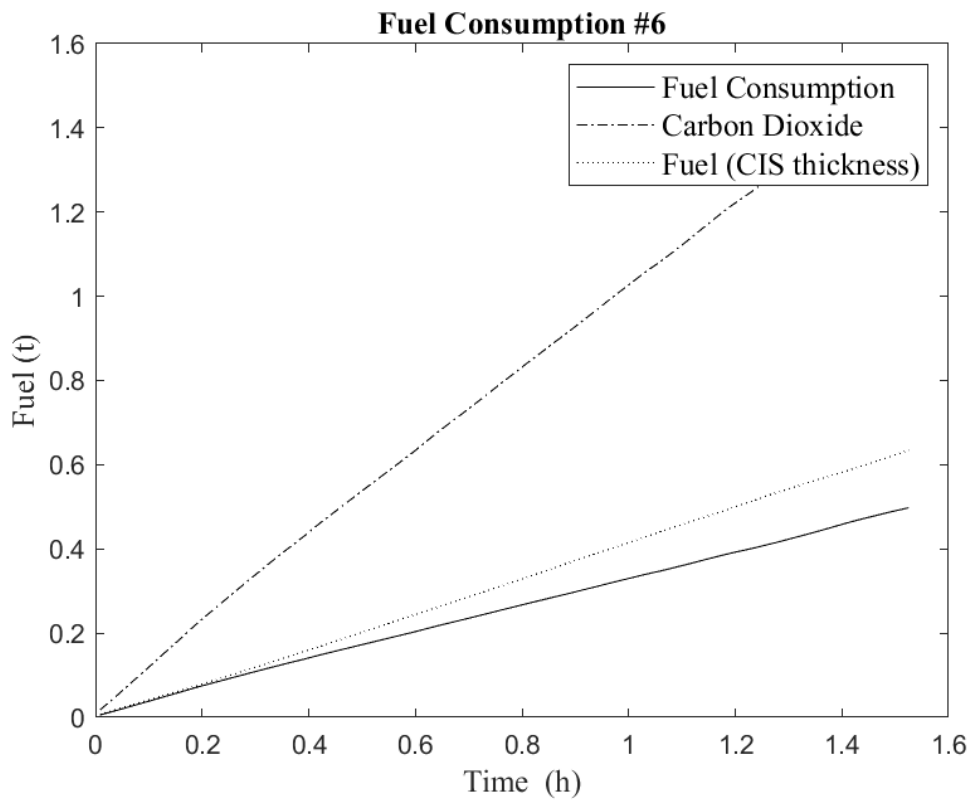
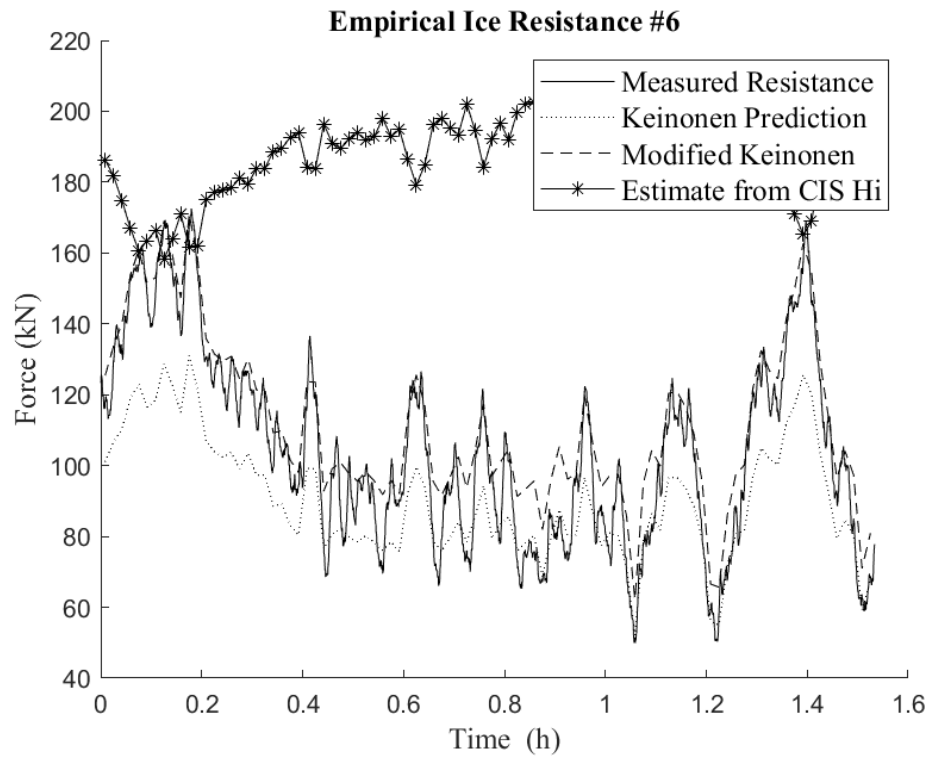
Data Segment #5	
Date	February 20, 2022
Statistical Thickness	0.329m
CIS equivalent thickness	0.17m
First Concentration/ Thickness	4% - 0.225m
Second Concentration/ Thickness	5% - 0.125m
Third Concentration/ Thickness	-
Ice Type	Grey-White Ice



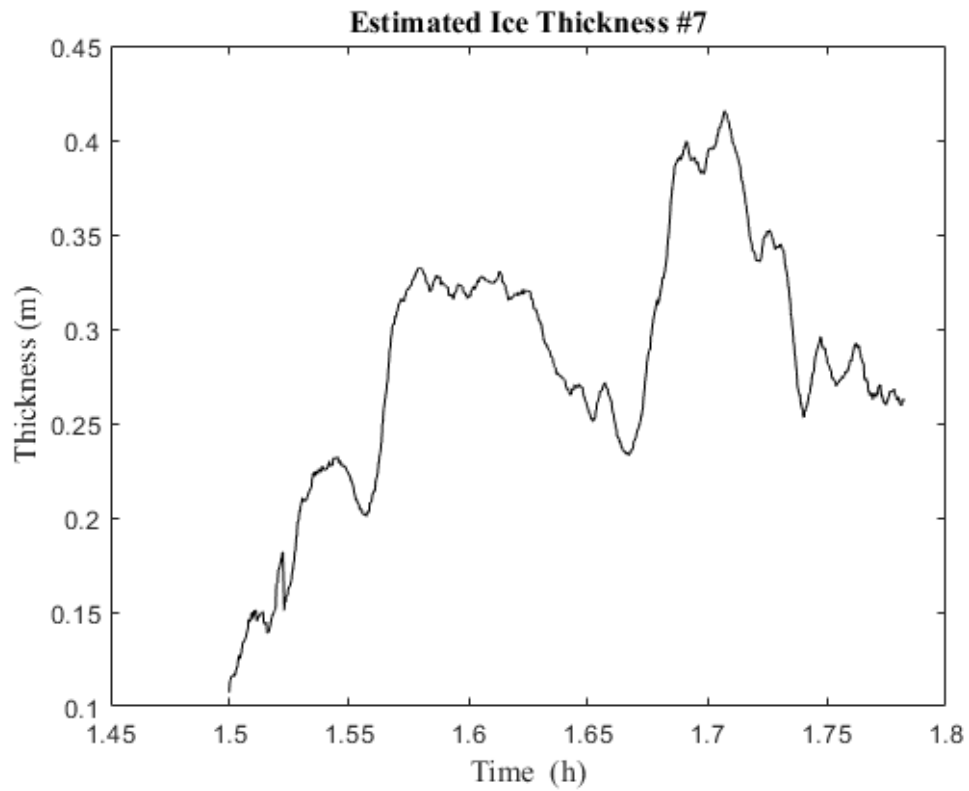
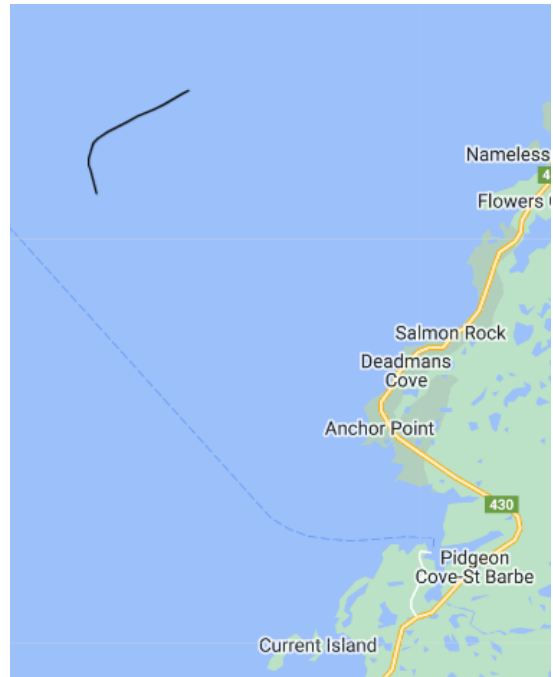


Data Segment #6	
Date	February 21, 2022
Statistical Thickness	0.198m
CIS equivalent thickness	0.26m
First Concentration/ Thickness	2% - 0.5m
Second Concentration/ Thickness	5% - 0.225m
Third Concentration/ Thickness	2% - 0.125m
Ice Type	Grey-White Ice

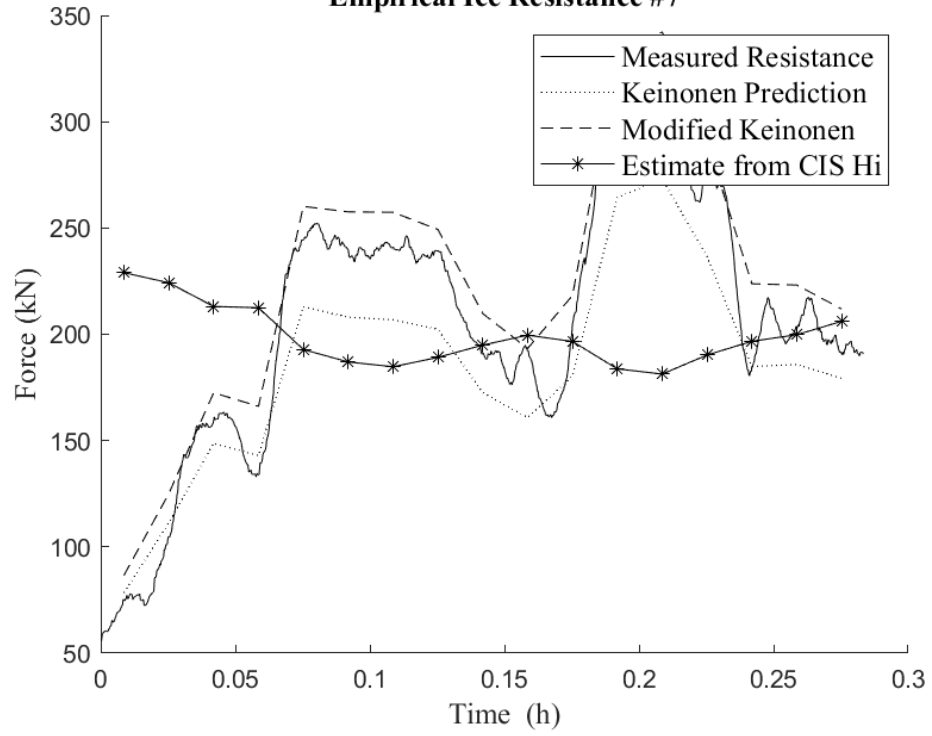




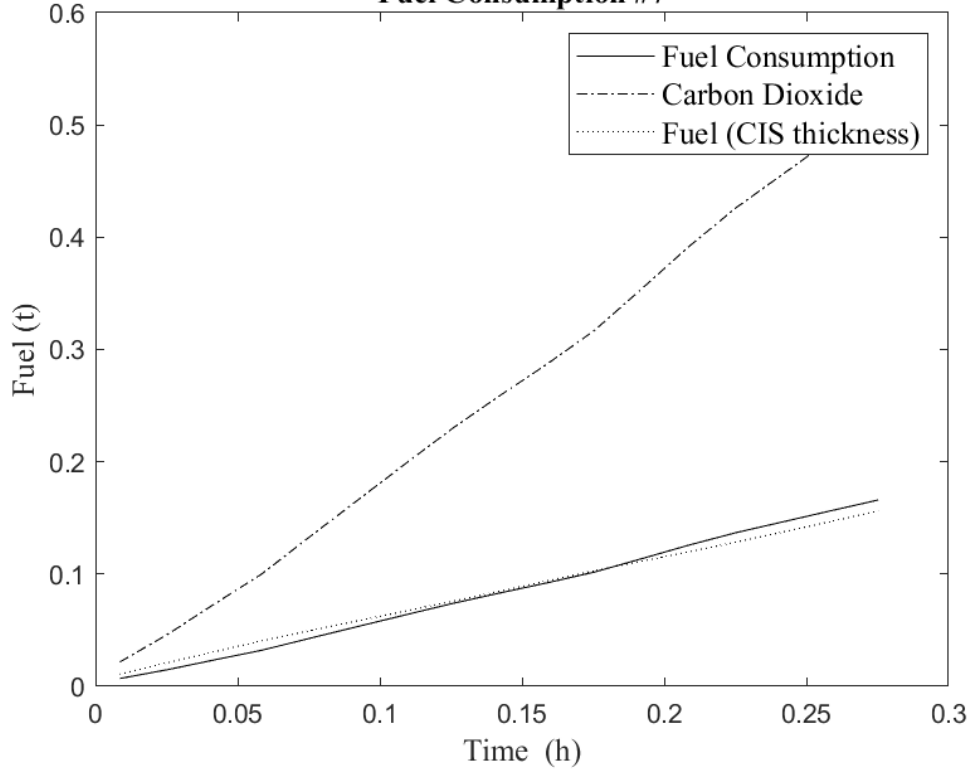
Data Segment #7	
Date	February 21, 2022
Statistical Thickness	0.307m
CIS equivalent thickness	0.26m
First Concentration/ Thickness	2% - 0.5m
Second Concentration/ Thickness	5% - 0.225m
Third Concentration/ Thickness	2% - 0.125m
Ice Type	Thin First Year



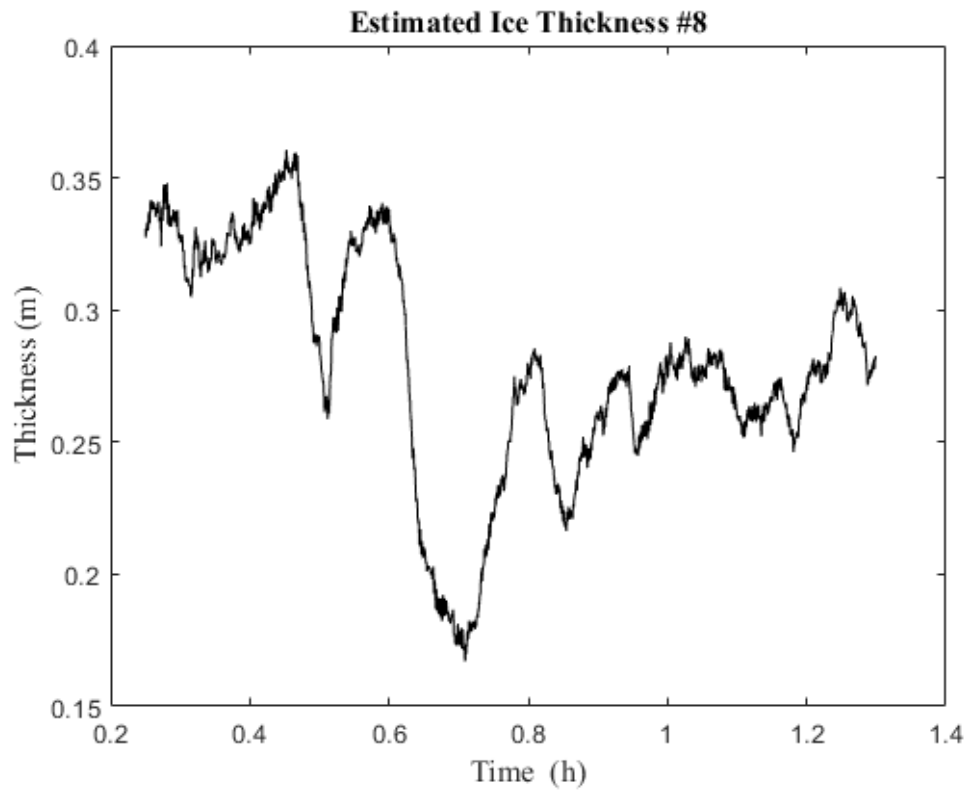
Empirical Ice Resistance #7



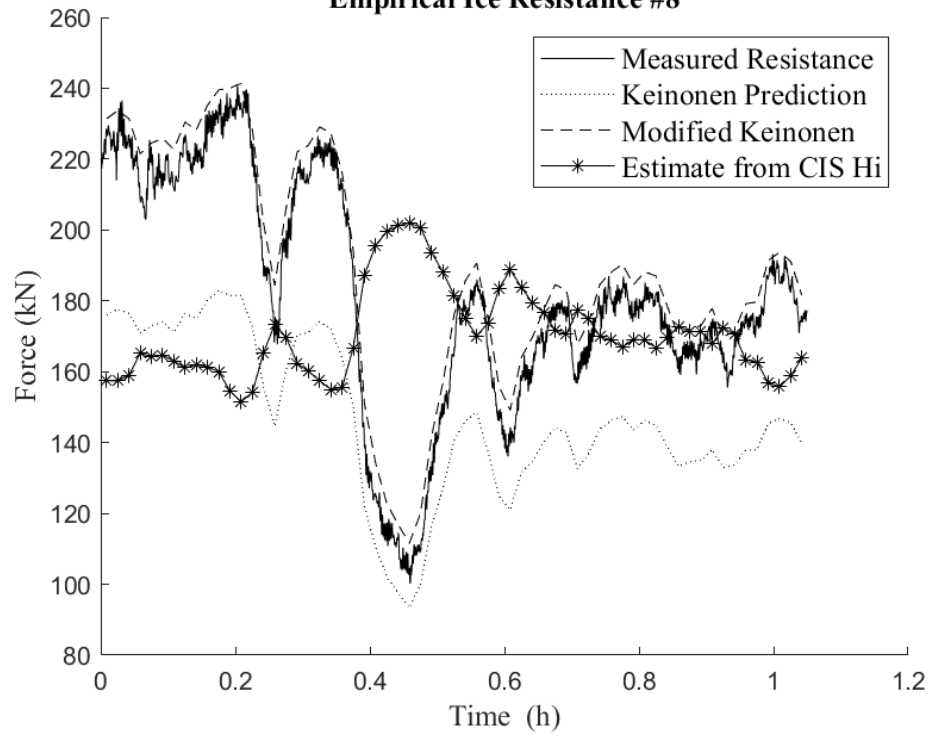
Fuel Consumption #7



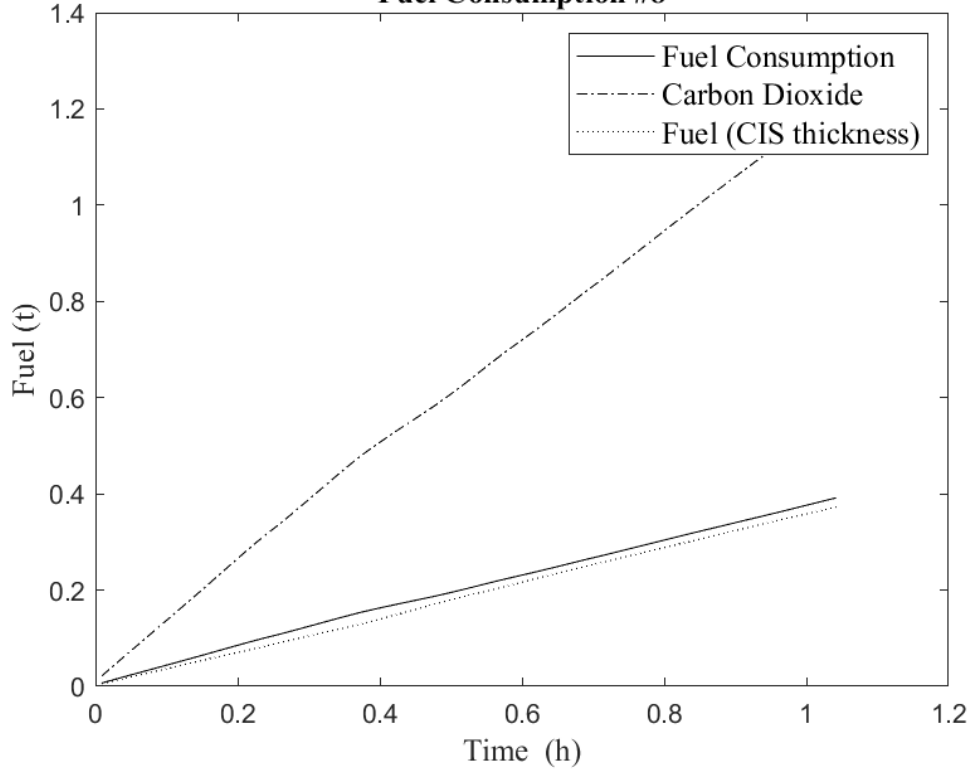
Data Segment #8	
Date	February 21, 2022
Statistical Thickness	0.305m
CIS equivalent thickness	0.26m
First Concentration/ Thickness	2% - 0.5m
Second Concentration/ Thickness	5% - 0.225m
Third Concentration/ Thickness	2% - 0.125m
Ice Type	Thin First Year



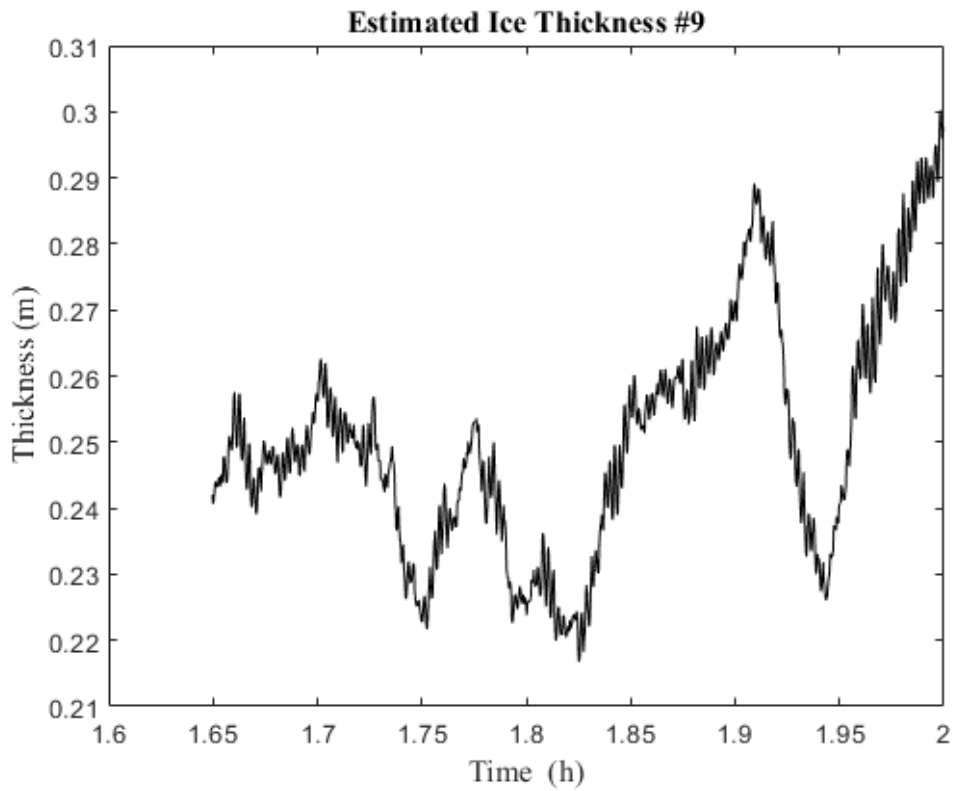
Empirical Ice Resistance #8

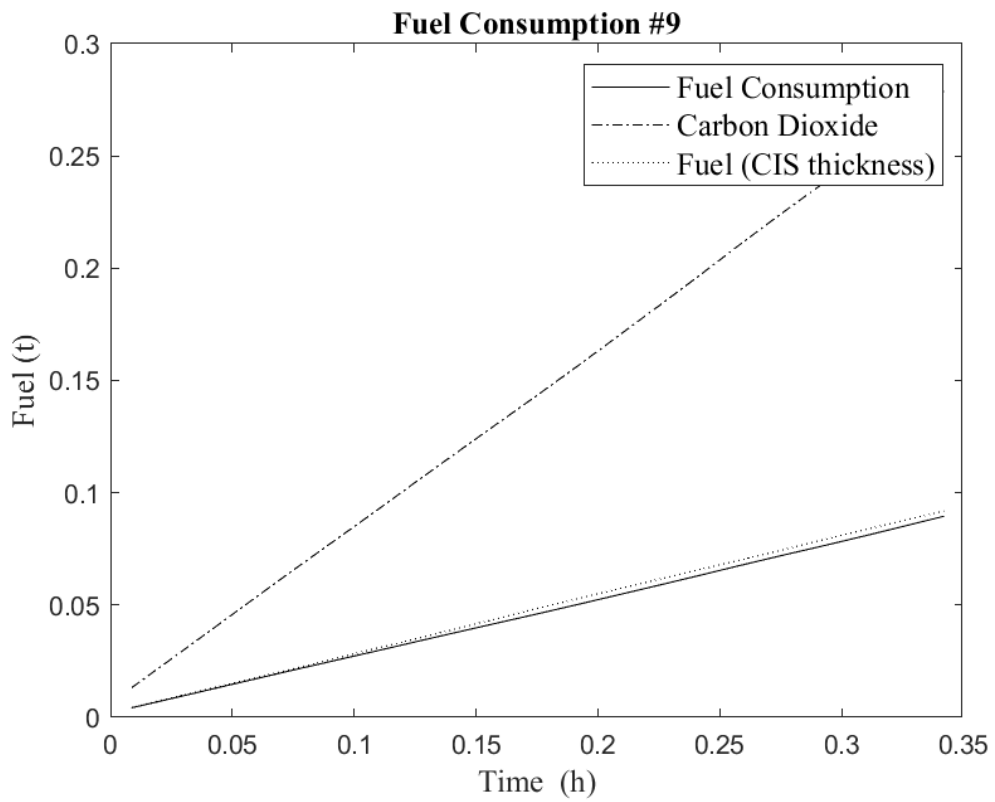
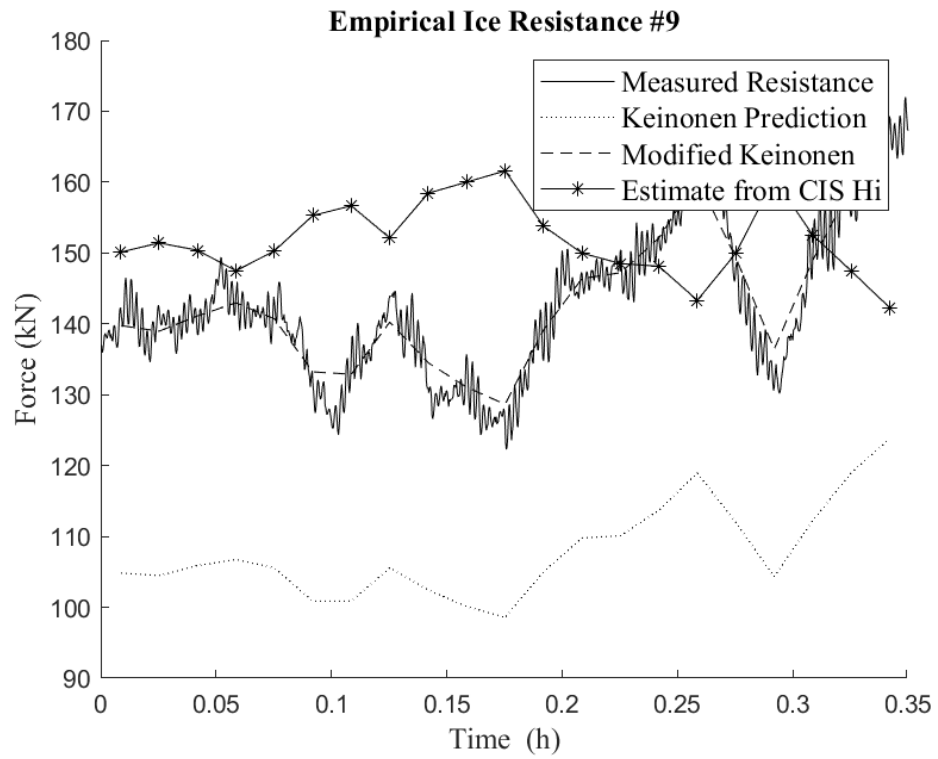


Fuel Consumption #8

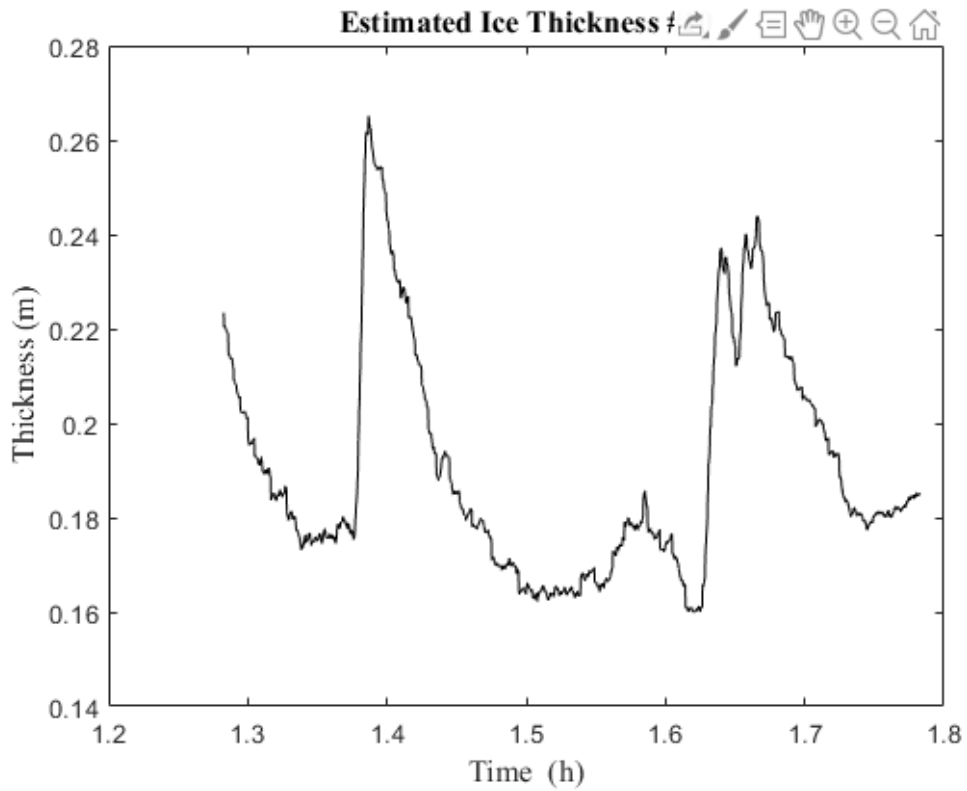
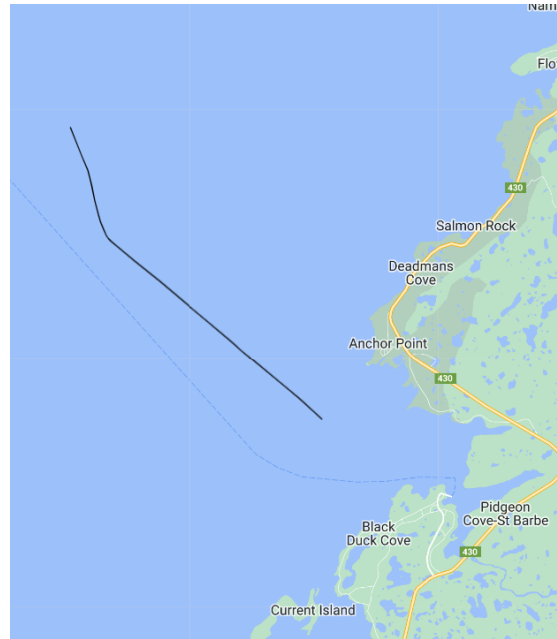


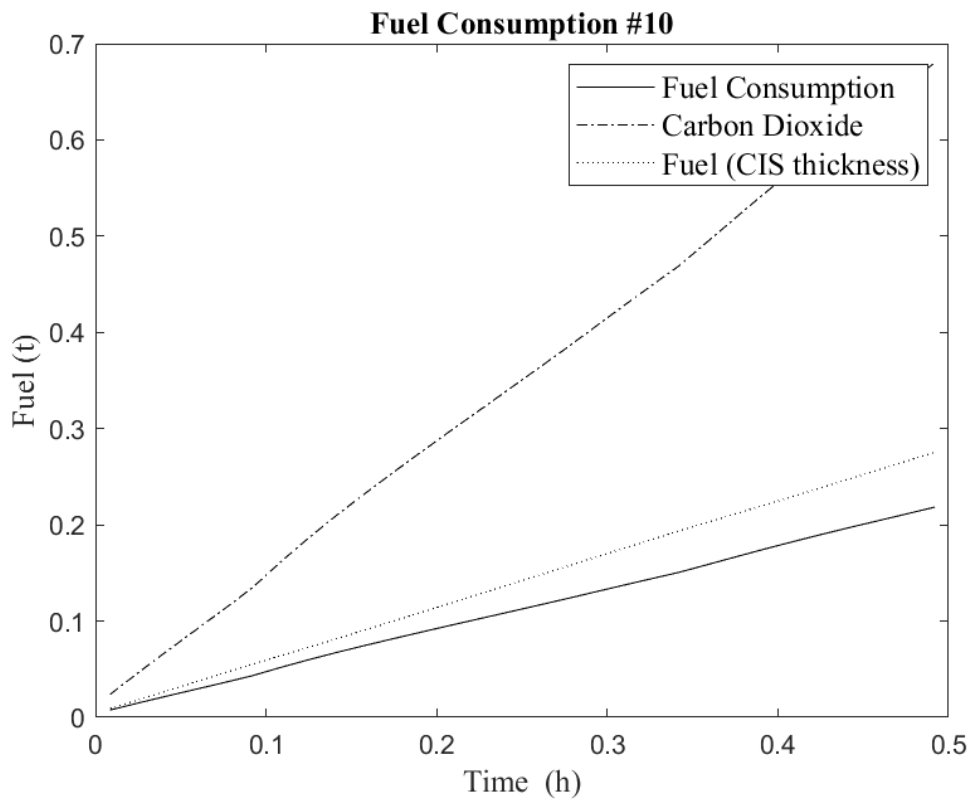
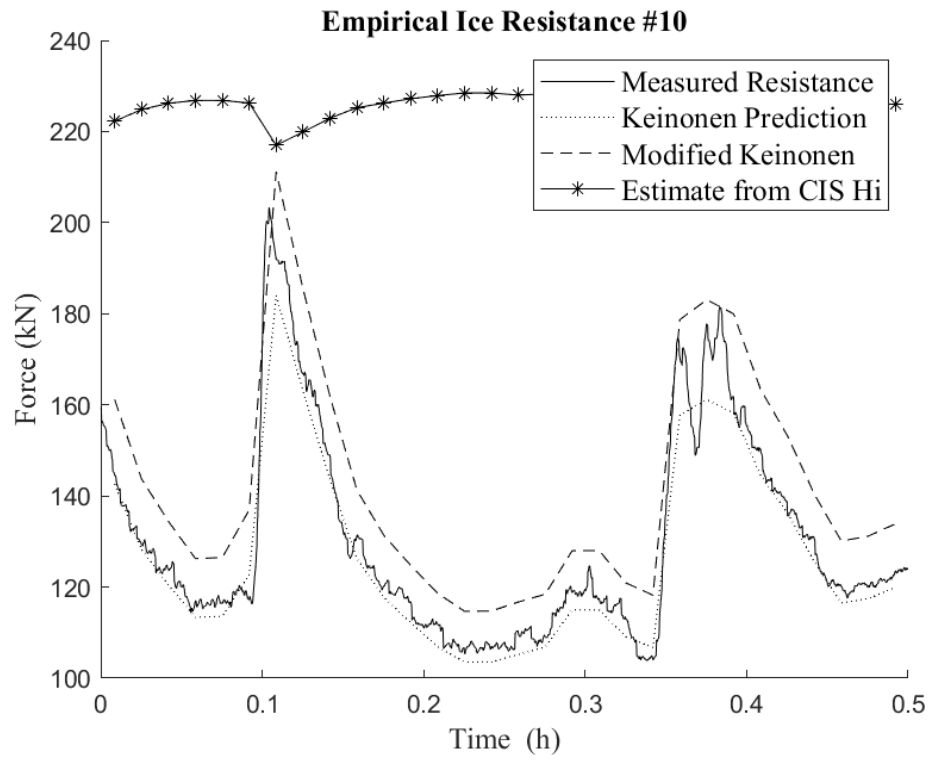
Data Segment #9	
Date	February 21, 2022
Statistical Thickness	0.272m
CIS equivalent thickness	0.26m
First Concentration/ Thickness	2% - 0.5m
Second Concentration/ Thickness	5% - 0.225m
Third Concentration/ Thickness	2% - 0.125m
Ice Type	Grey-White Ice



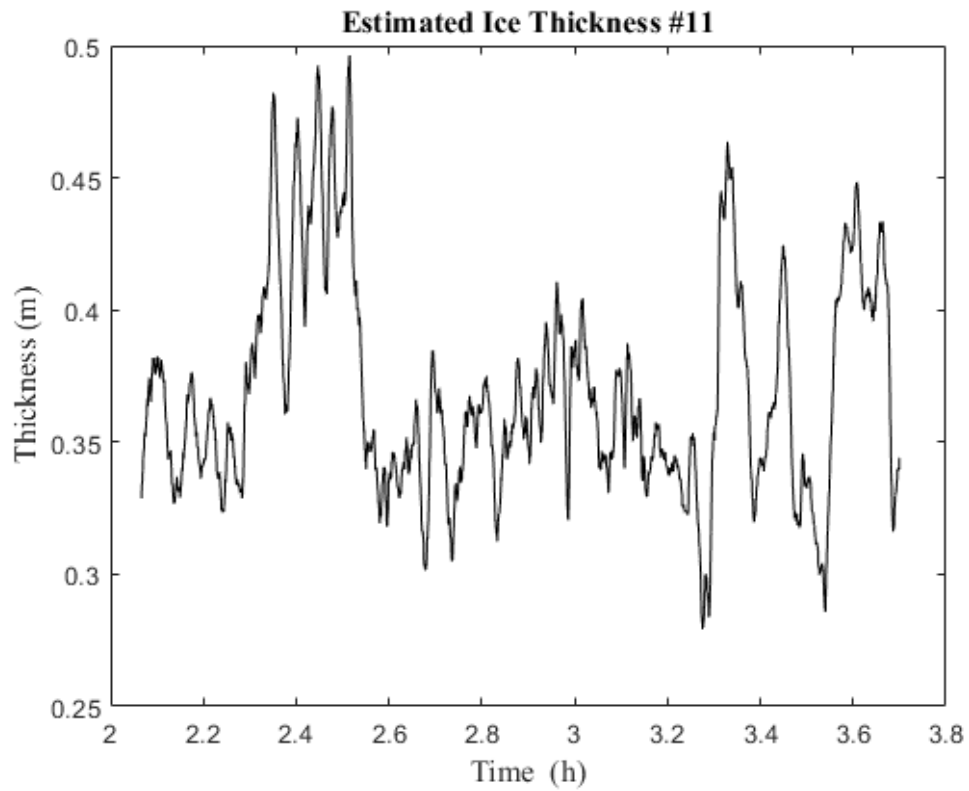


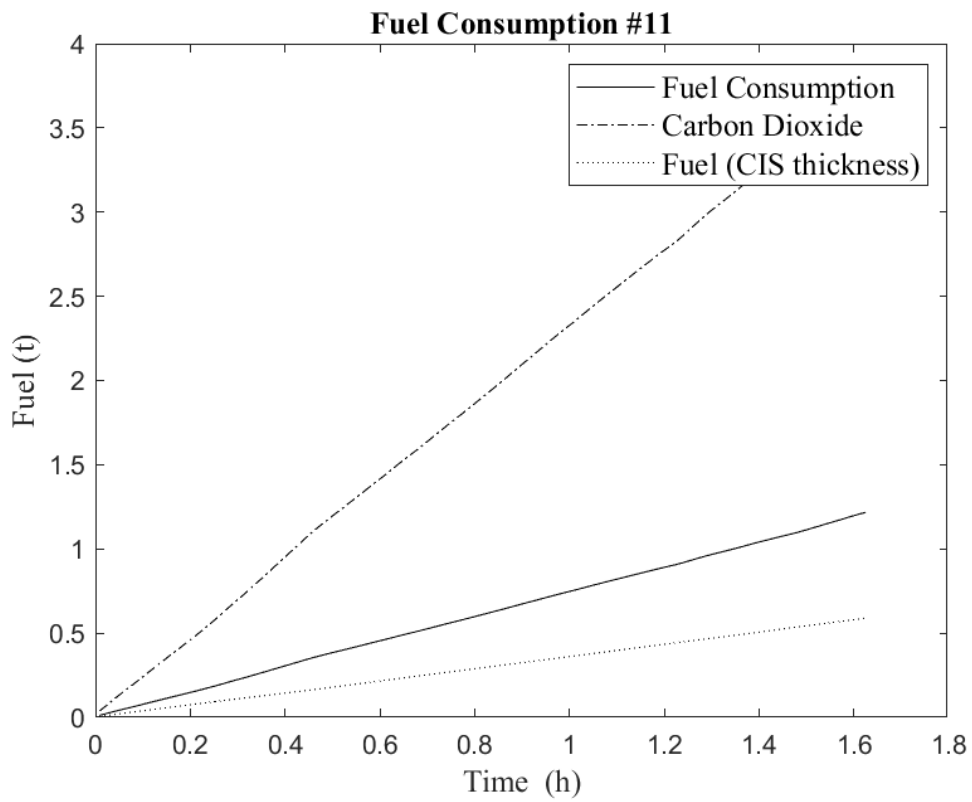
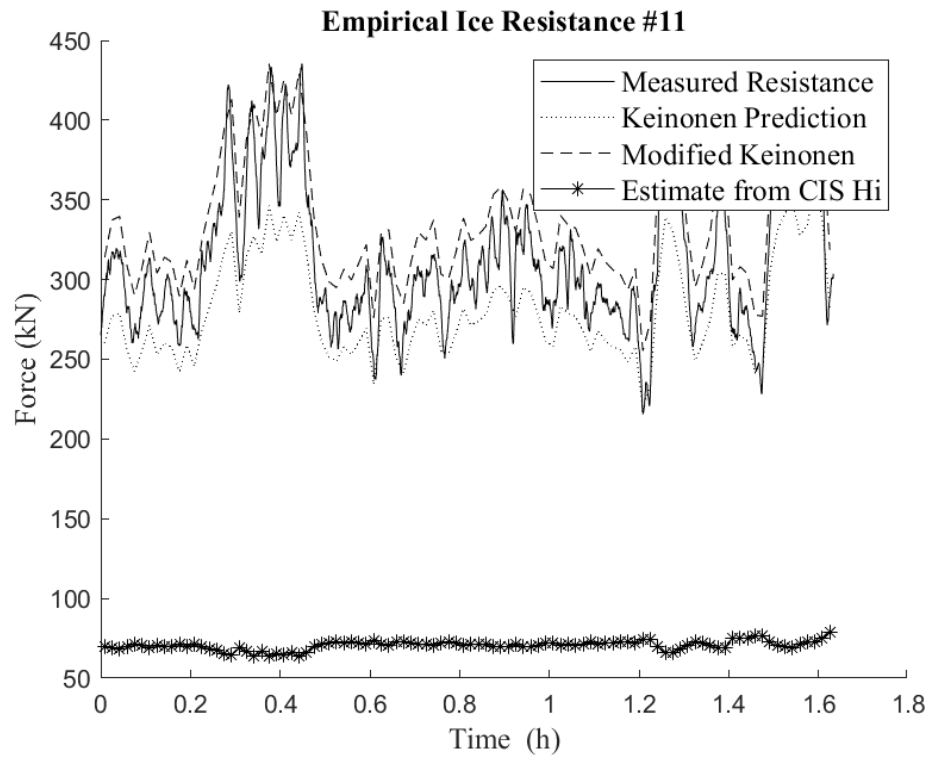
Data Segment #10	
Date	February 23, 2022
Statistical Thickness	0.207m
CIS equivalent thickness	0.26m
First Concentration/ Thickness	2% - 0.5m
Second Concentration/ Thickness	5% - 0.225m
Third Concentration/ Thickness	2% - 0.125m
Ice Type	Gey-white Ice



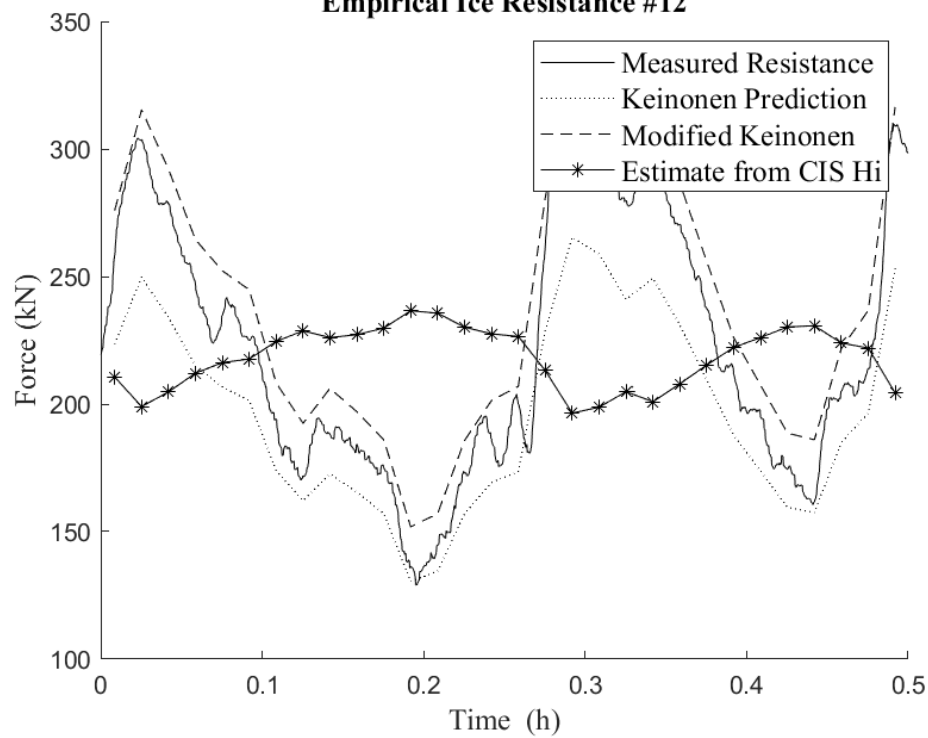


Data Segment #11	
Date	February 24, 2022
Statistical Thickness	0.404m
CIS equivalent thickness	0.13m
First Concentration/ Thickness	2% - 0.225m
Second Concentration/ Thickness	5% - 0.125m
Third Concentration/ Thickness	2% - 0.05m
Ice Type	Outside Range

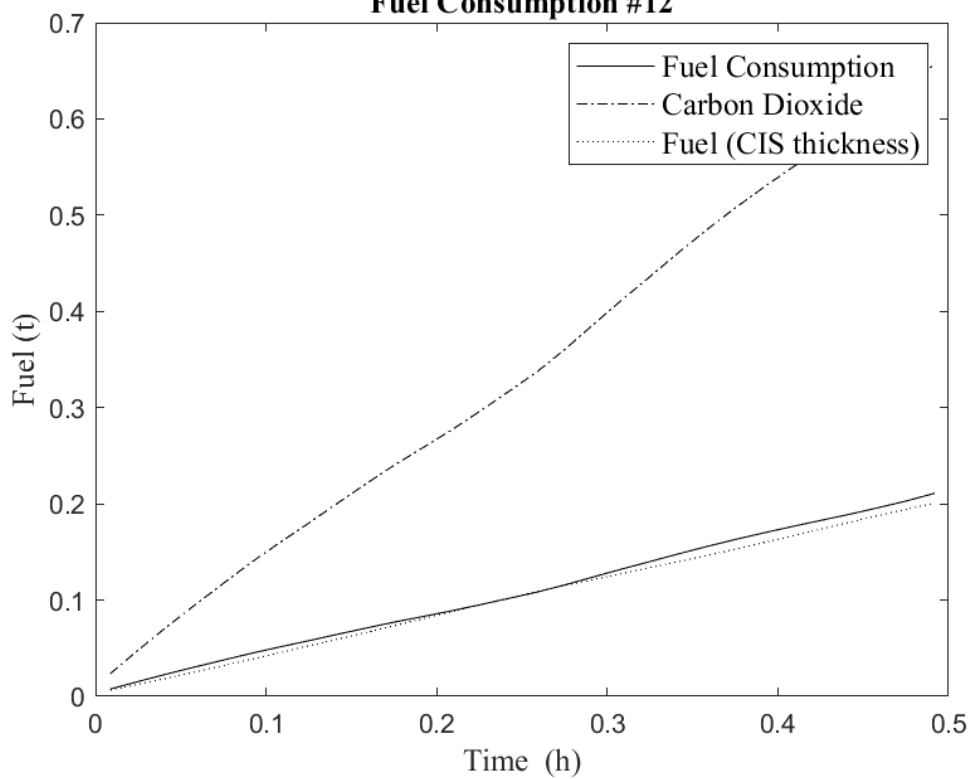




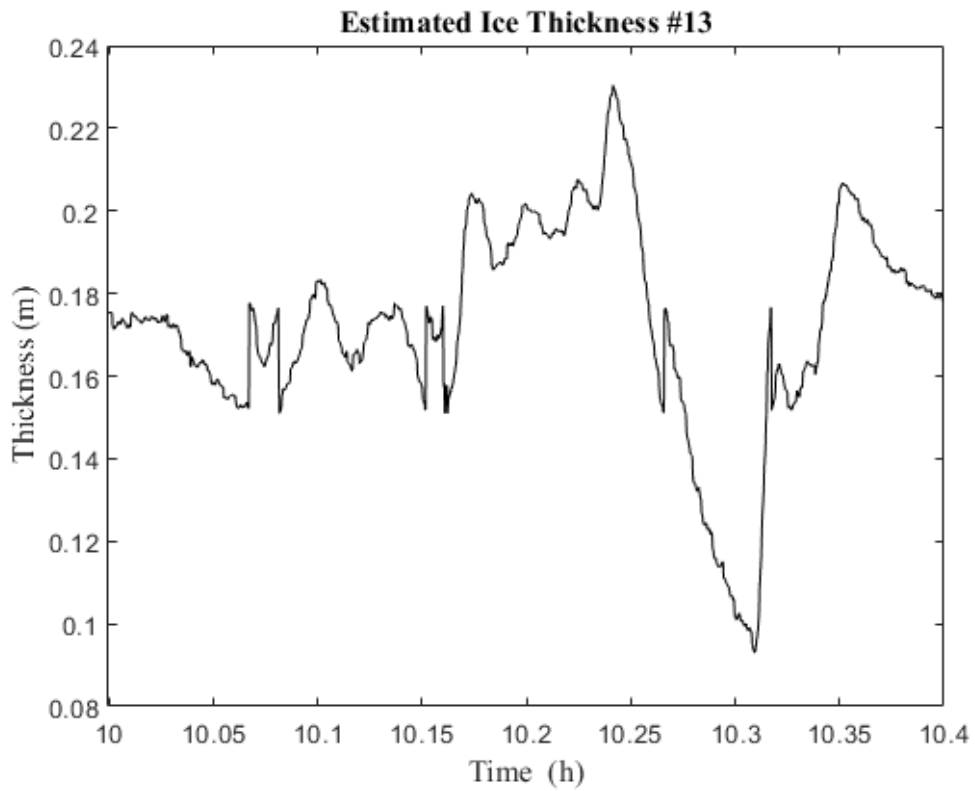
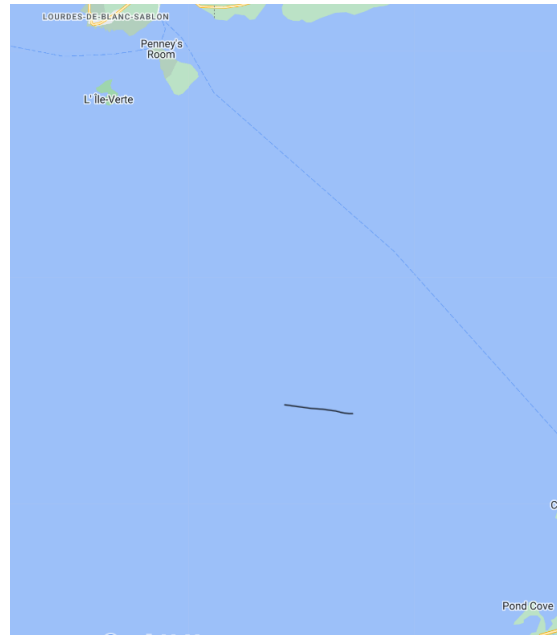
Empirical Ice Resistance #12

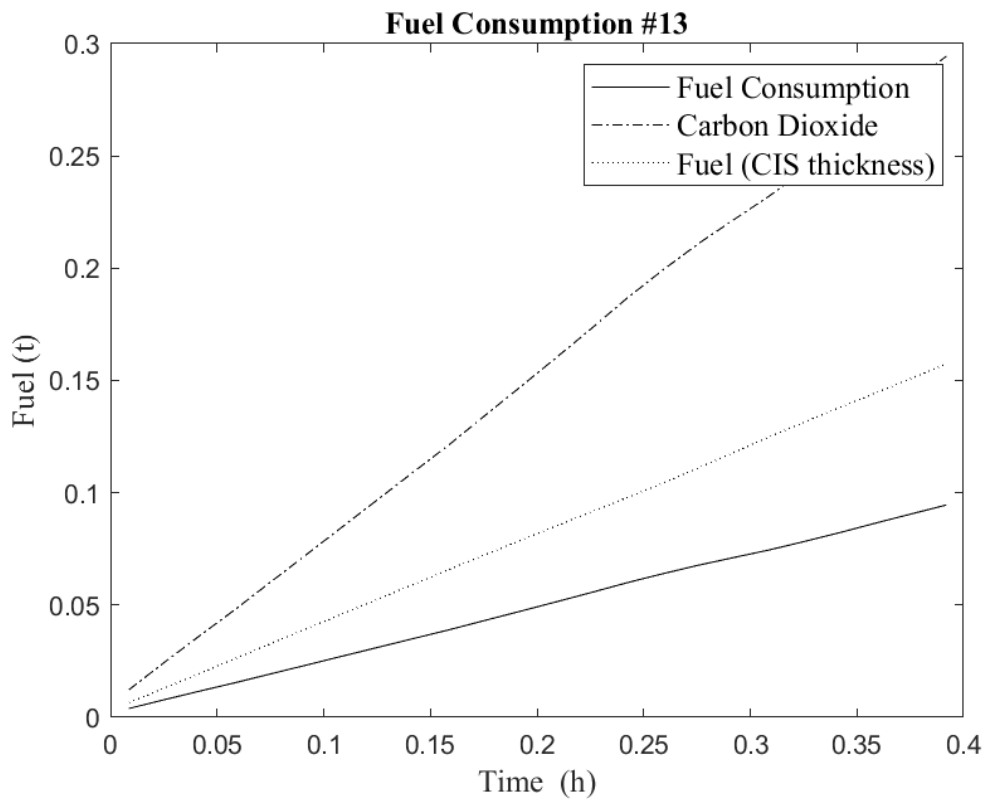
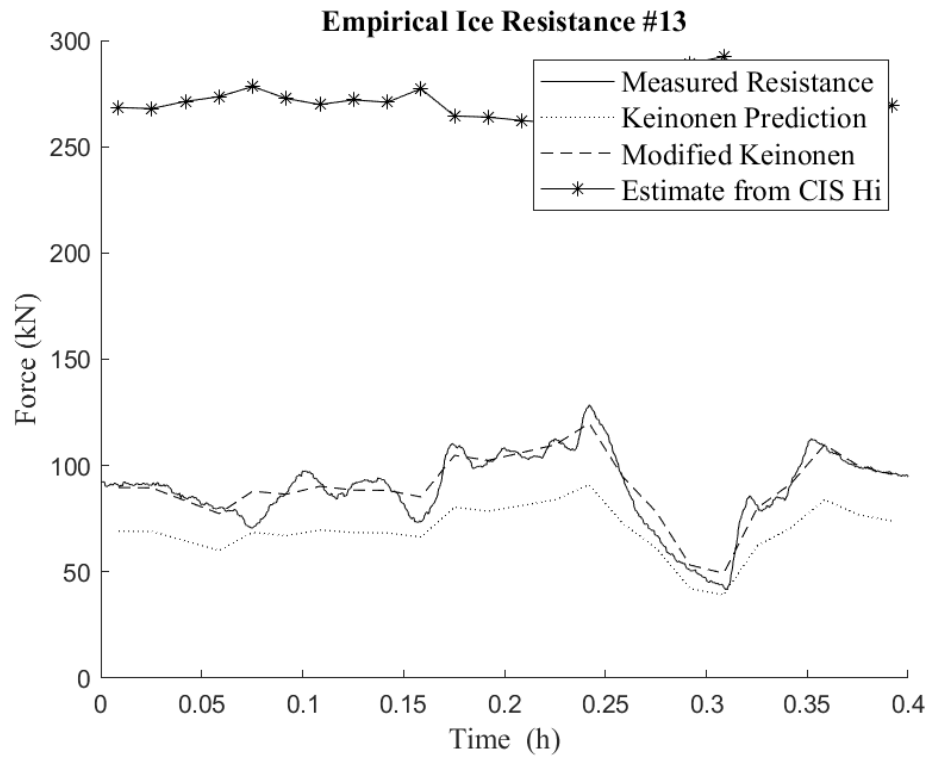


Fuel Consumption #12

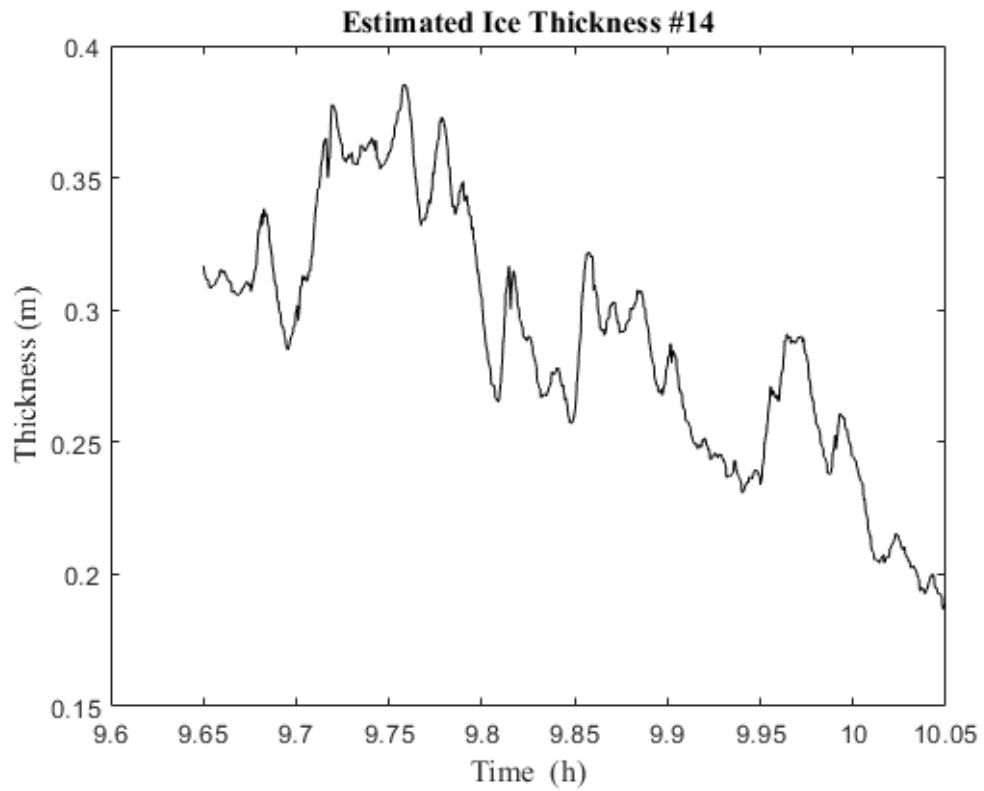


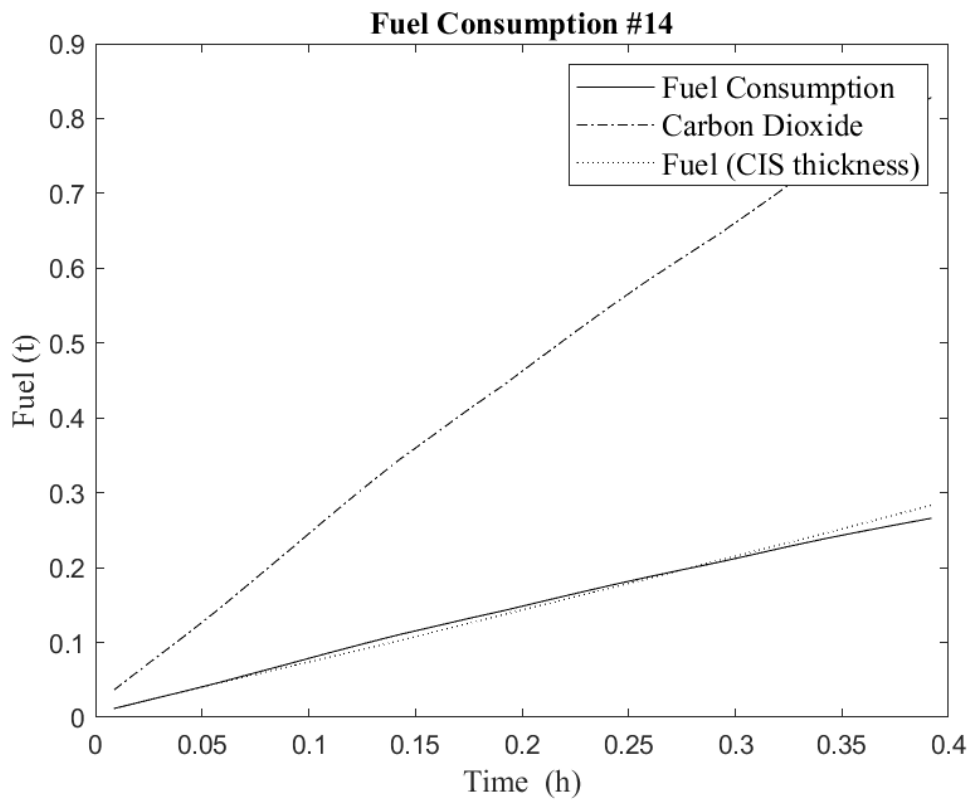
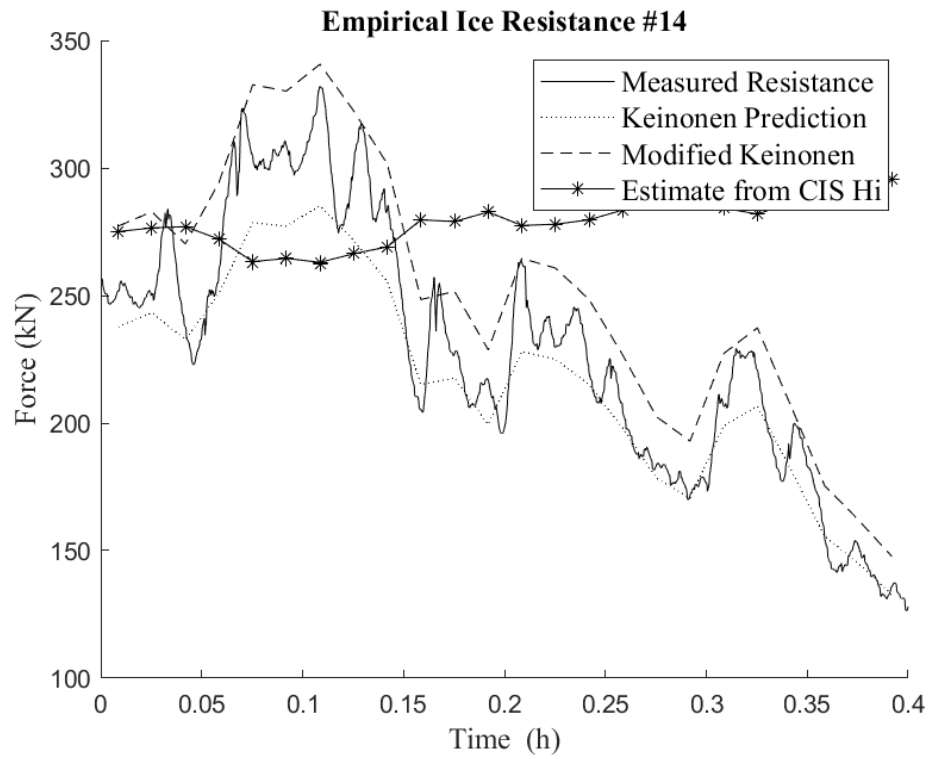
Data Segment #13	
Date	February 27, 2022
Statistical Thickness	0.184m
CIS equivalent thickness	0.36m
First Concentration/ Thickness	5% - 0.5m
Second Concentration/ Thickness	5% - 0.225m
Third Concentration/ Thickness	-
Ice Type	Grey-White Ice



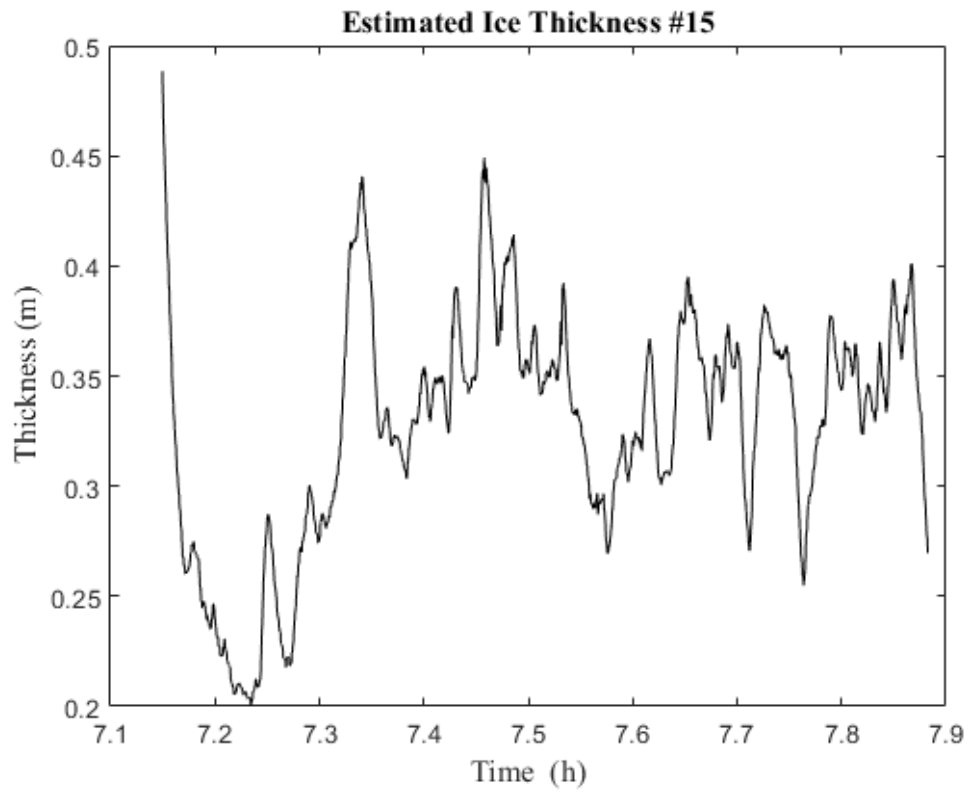


Data Segment #14	
Date	March 2, 2022
Statistical Thickness	0.314m
CIS equivalent thickness	0.31m
First Concentration/ Thickness	3% - 0.5m
Second Concentration/ Thickness	7% - 0.225m
Third Concentration/ Thickness	-
Ice Type	Thin First Year

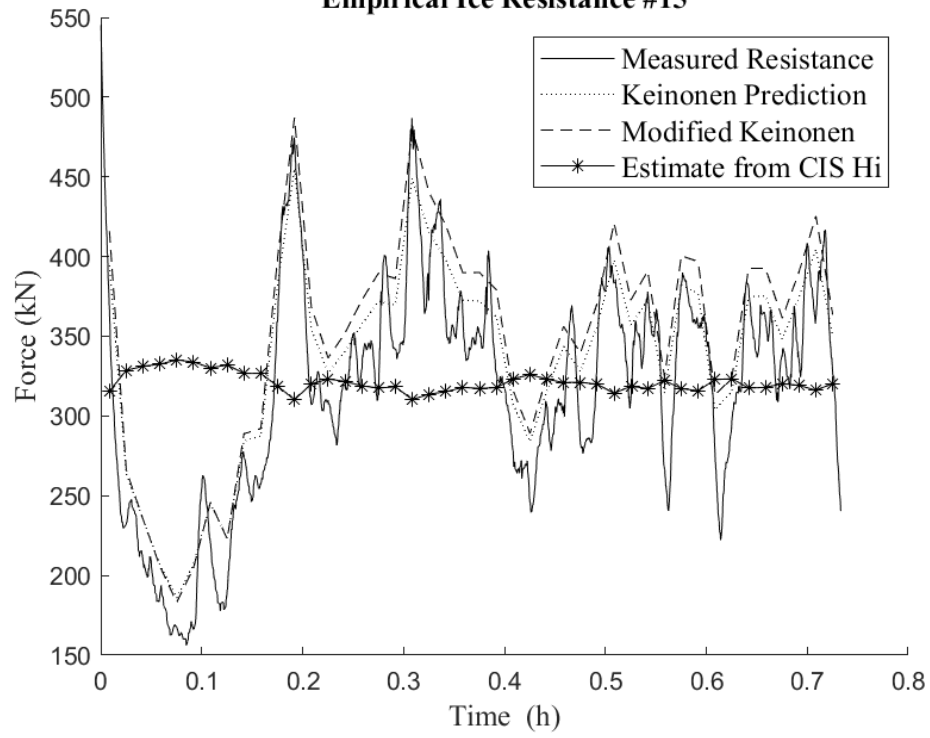




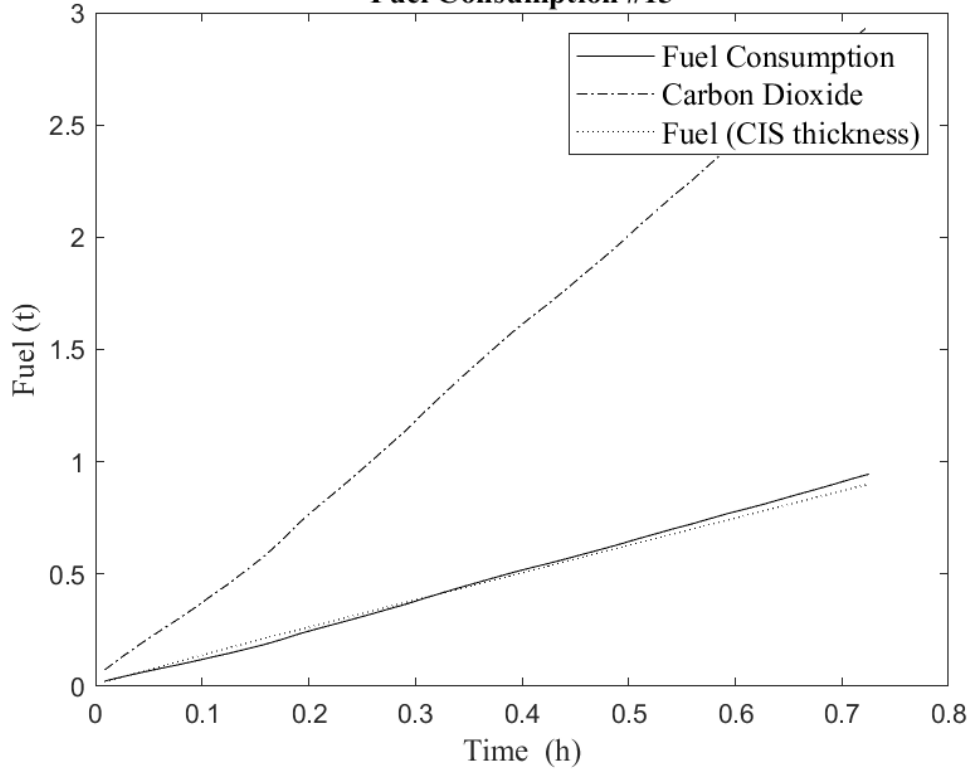
Data Segment #15	
Date	March 3, 2022
Statistical Thickness	0.357m
CIS equivalent thickness	0.31m
First Concentration/ Thickness	3% - 0.5m
Second Concentration/ Thickness	7% - 0.225m
Third Concentration/ Thickness	-
Ice Type	Thin First Year



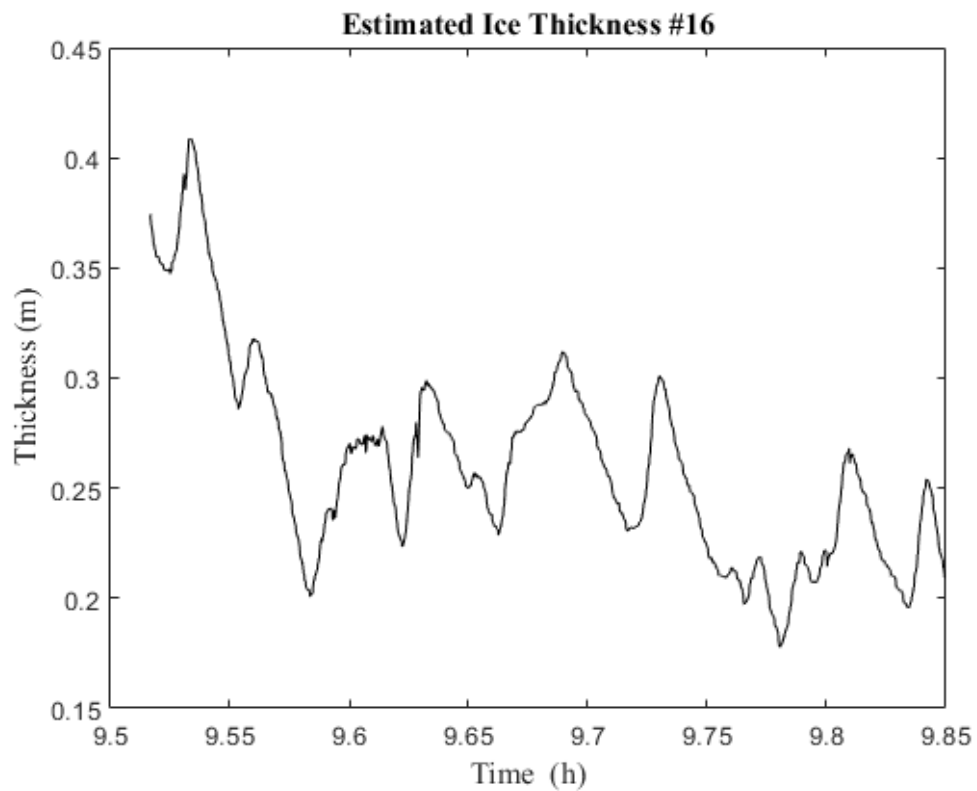
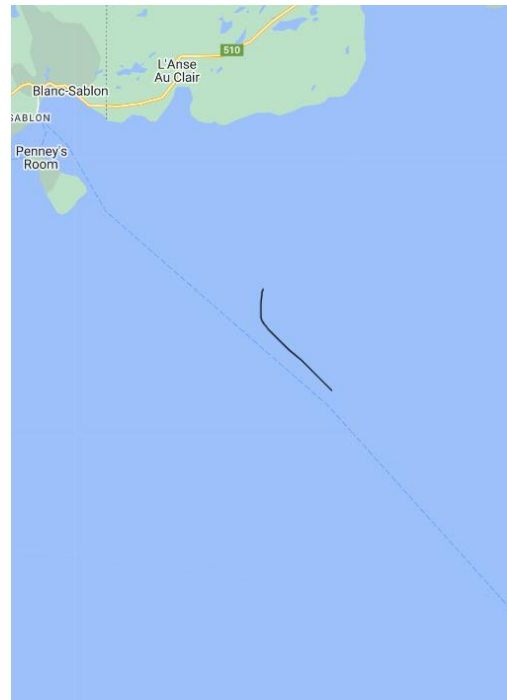
Empirical Ice Resistance #15



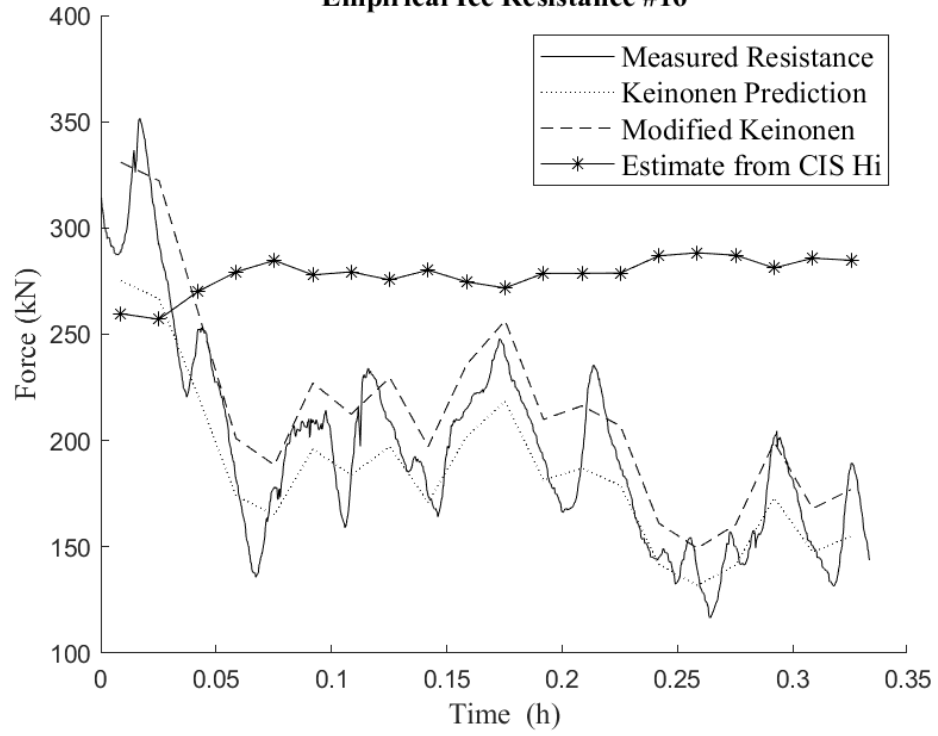
Fuel Consumption #15



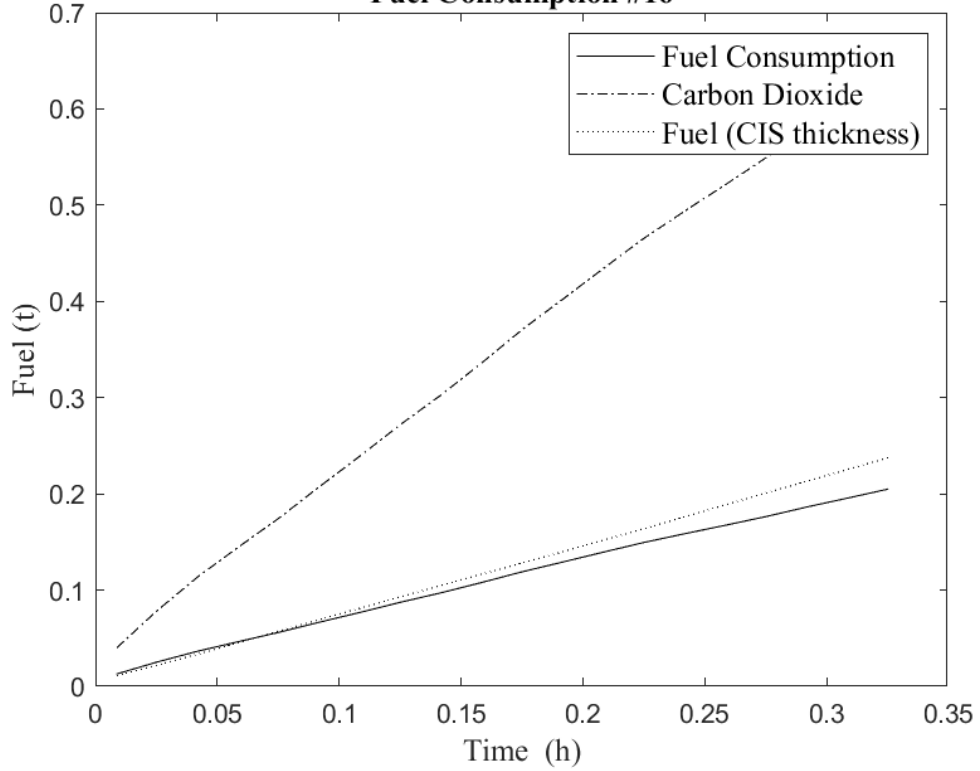
Data Segment #16	
Date	March 3, 2022
Statistical Thickness	0.284m
CIS equivalent thickness	0.31m
First Concentration/ Thickness	3% - 0.5m
Second Concentration/ Thickness	7% - 0.225m
Third Concentration/ Thickness	-
Ice Type	Grey-White Ice



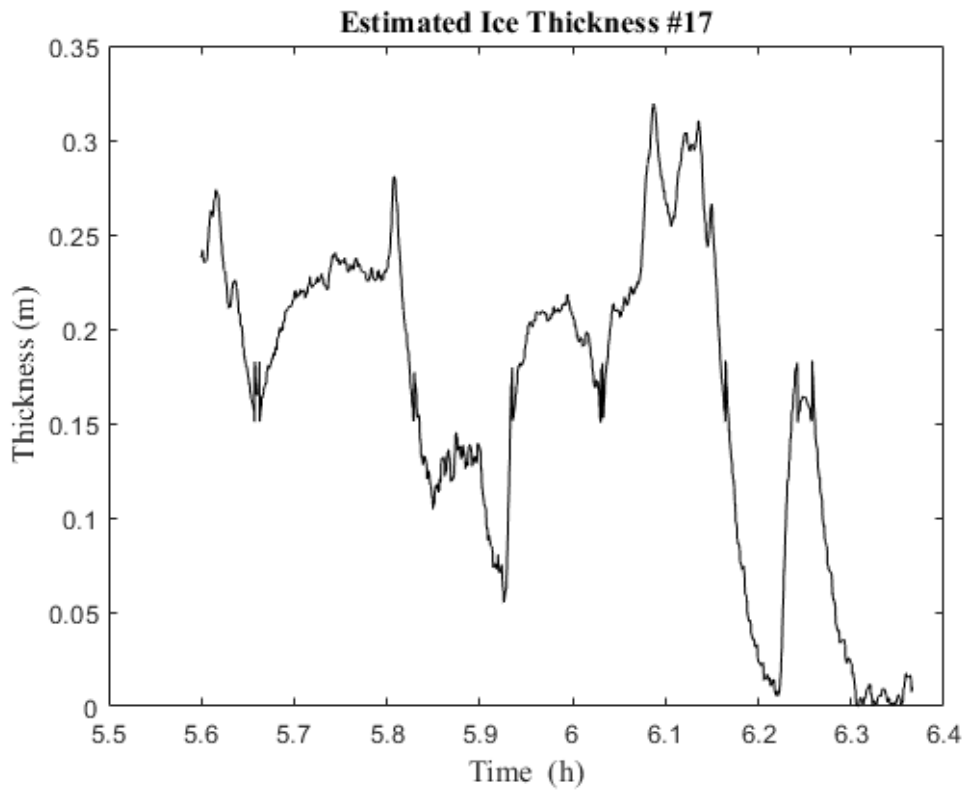
Empirical Ice Resistance #16



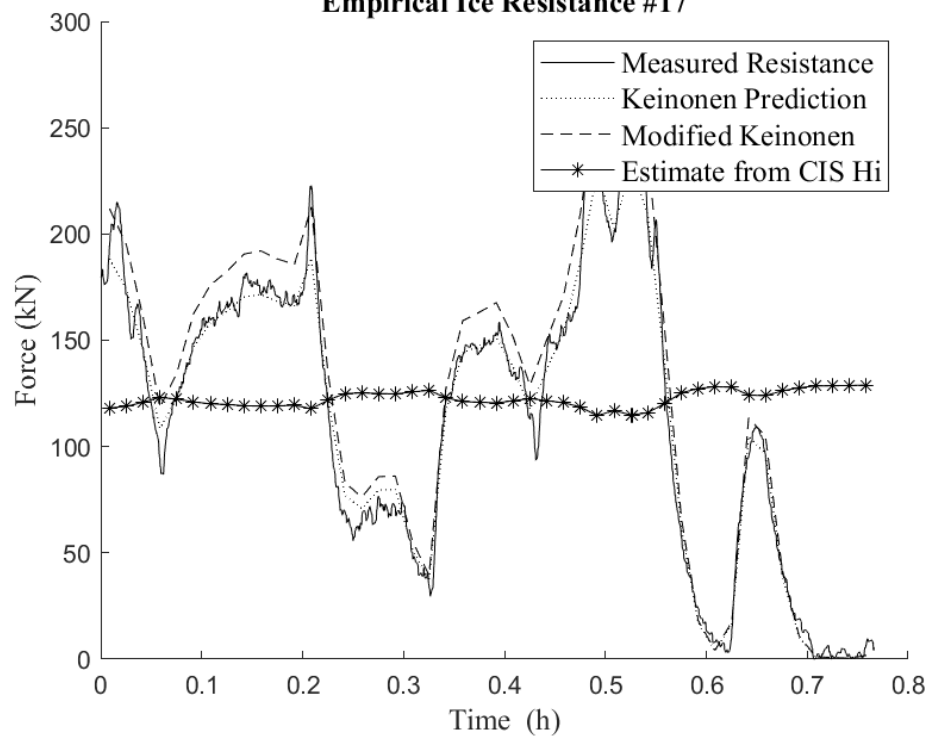
Fuel Consumption #16



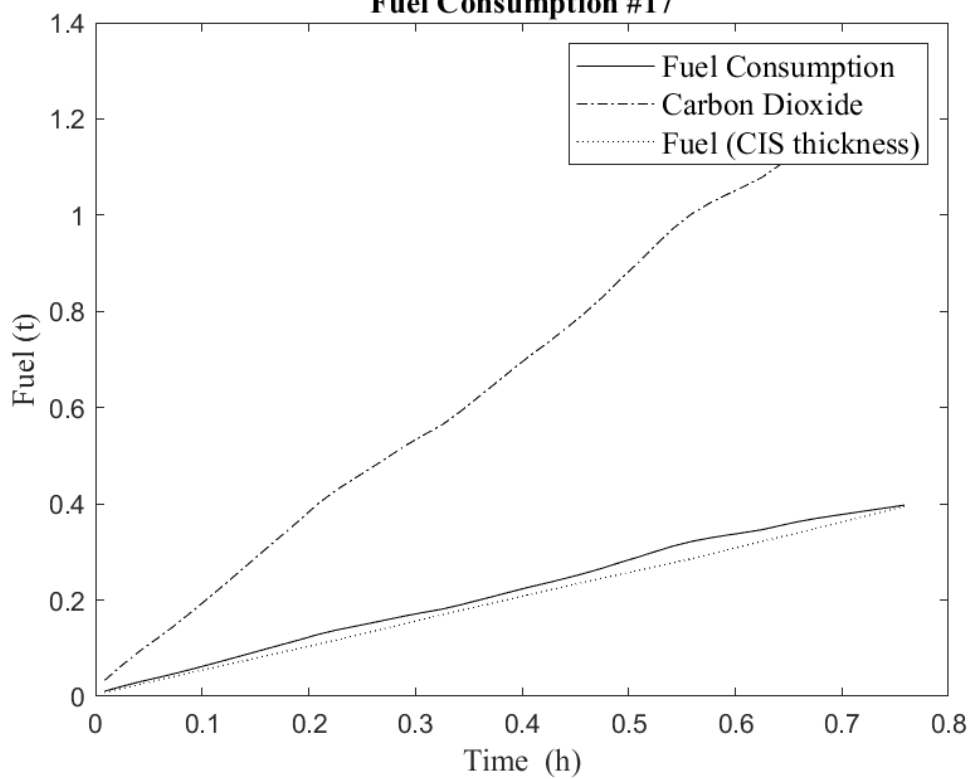
Data Segment #17	
Date	March 4, 2022
Statistical Thickness	0.178m
CIS equivalent thickness	0.17m
First Concentration/ Thickness	4% - 0.225m
Second Concentration/ Thickness	6% - 0.125m
Third Concentration/ Thickness	-
Ice Type	Grey-White Ice



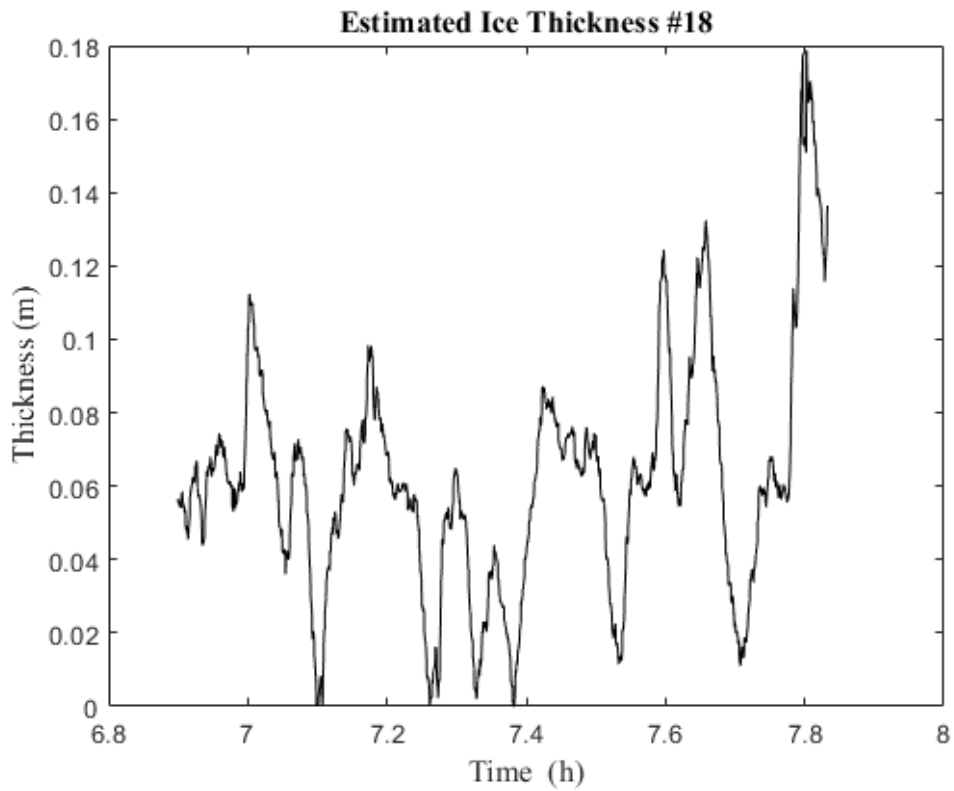
Empirical Ice Resistance #17

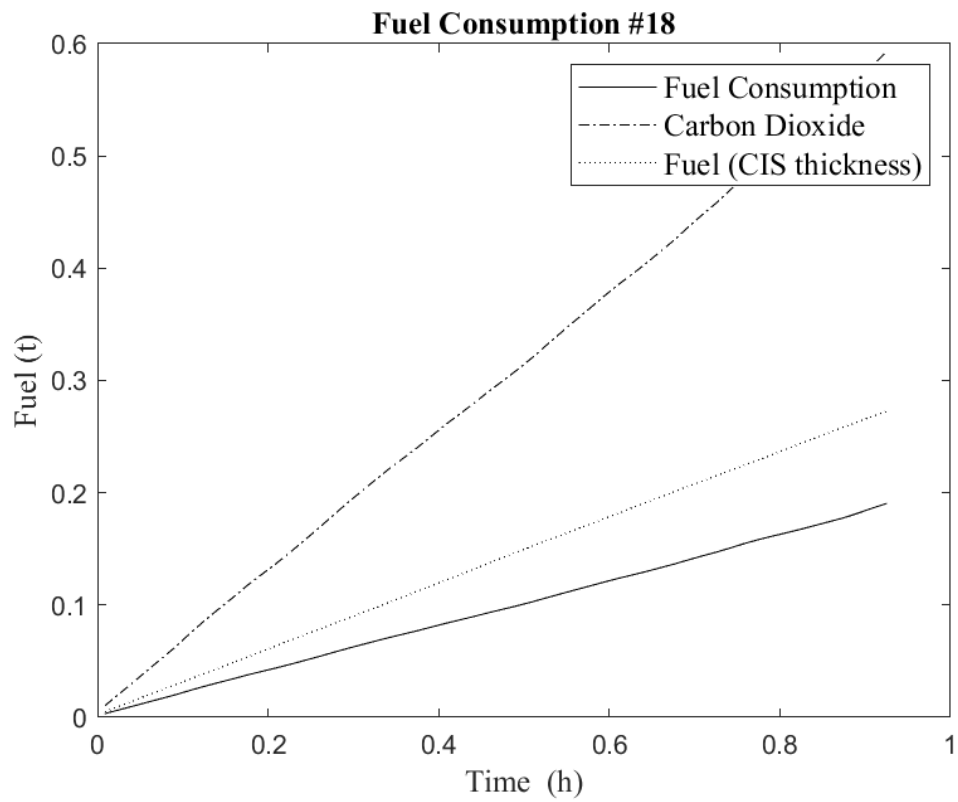
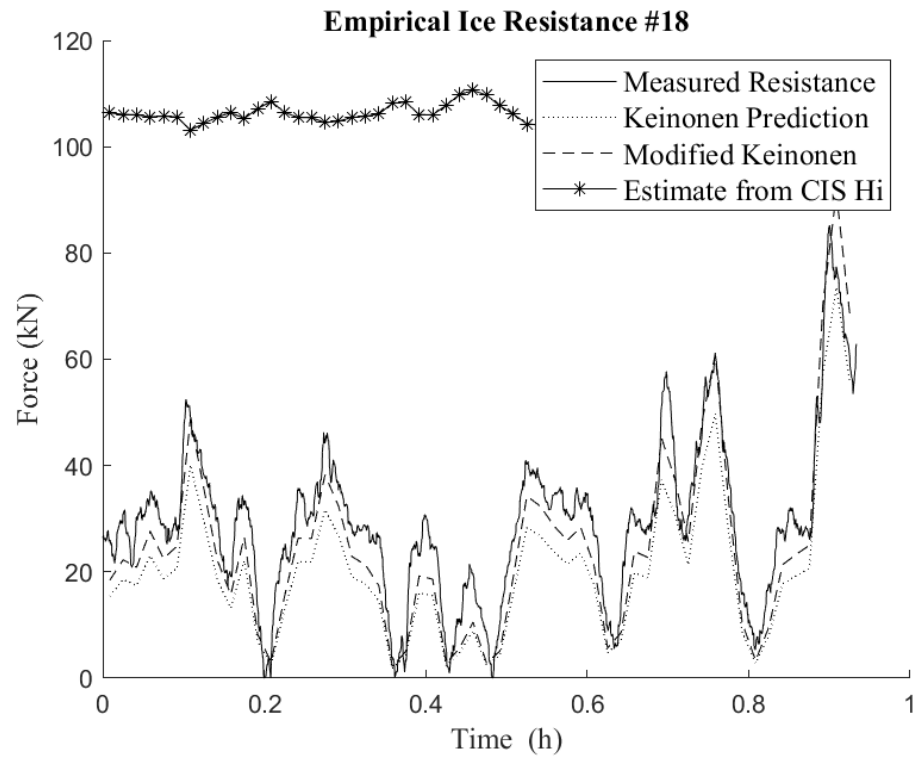


Fuel Consumption #17

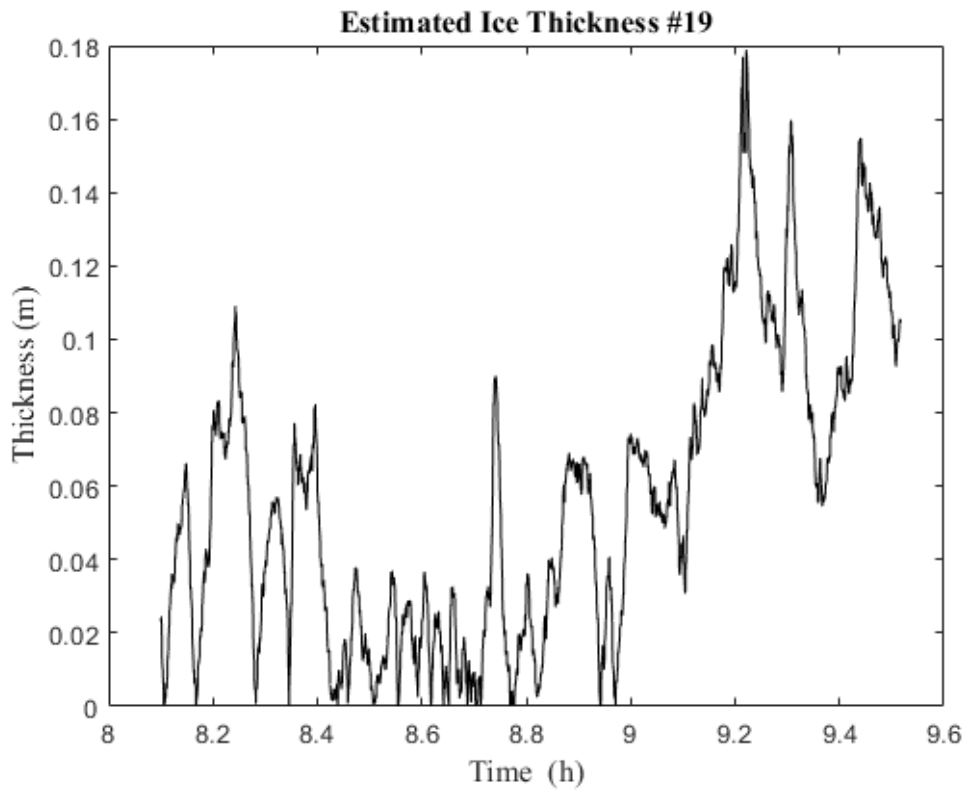


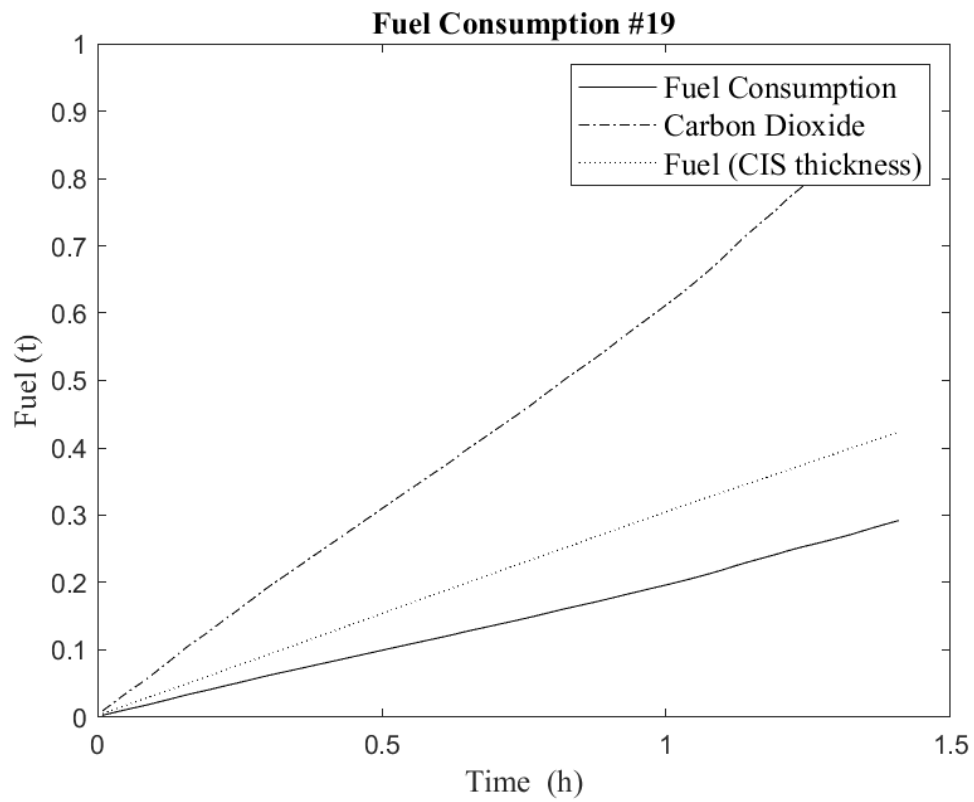
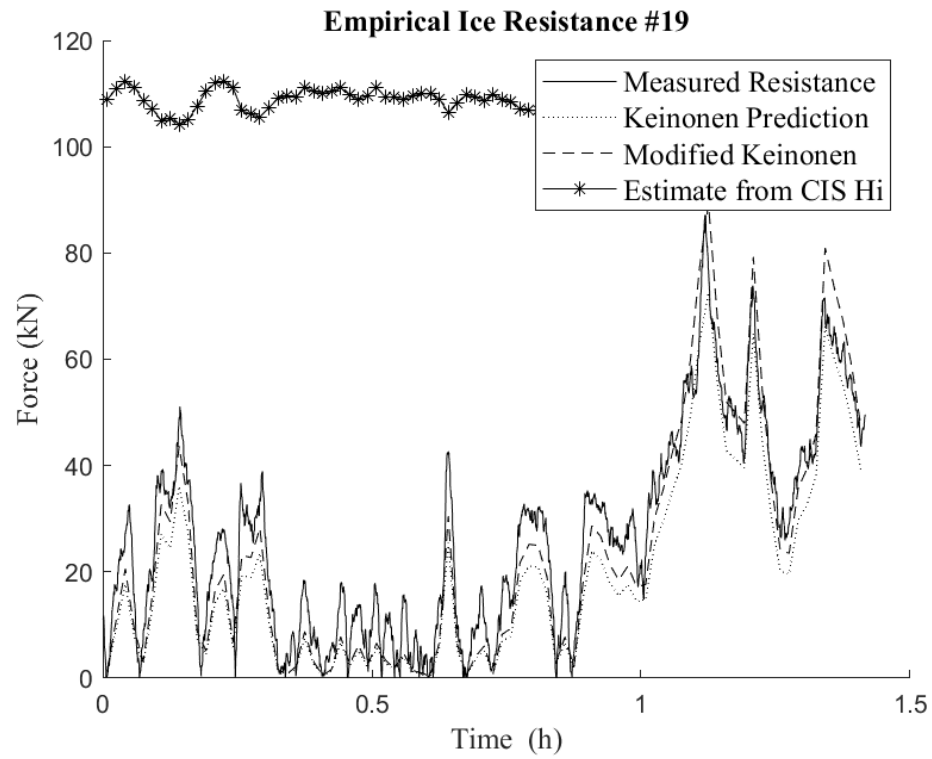
Data Segment #18	
Date	March 4, 2022
Statistical Thickness	0.066m
CIS equivalent thickness	0.17m
First Concentration/ Thickness	4% - 0.225m
Second Concentration/ Thickness	6% - 0.125m
Third Concentration/ Thickness	-
Ice Type	Grey-White Ice



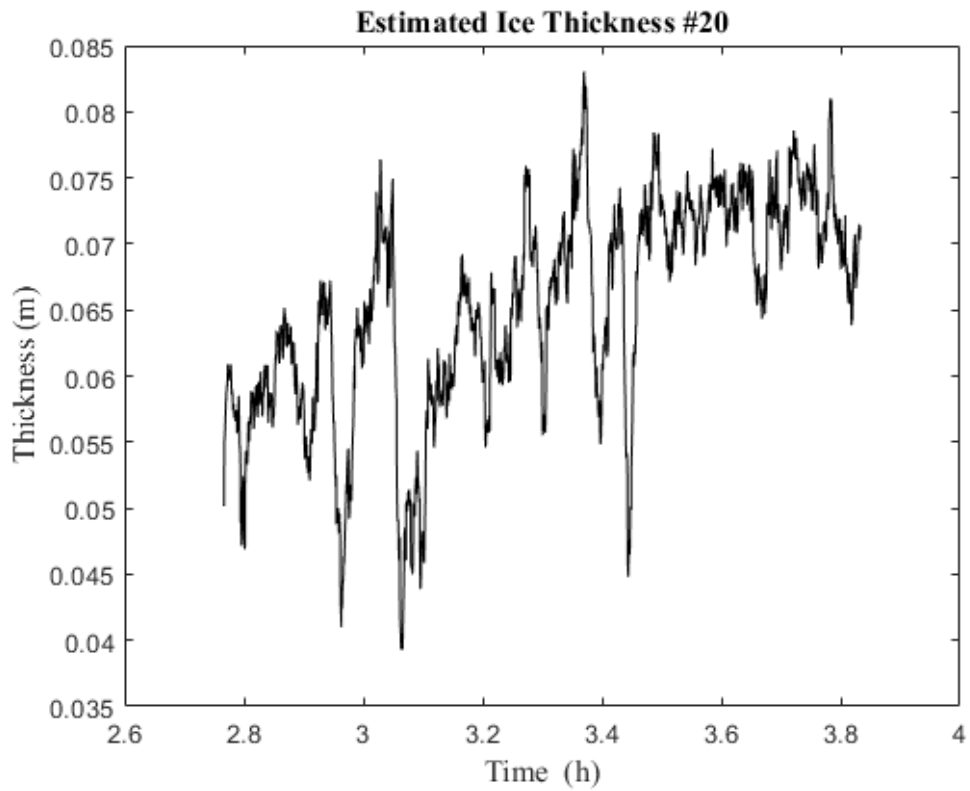
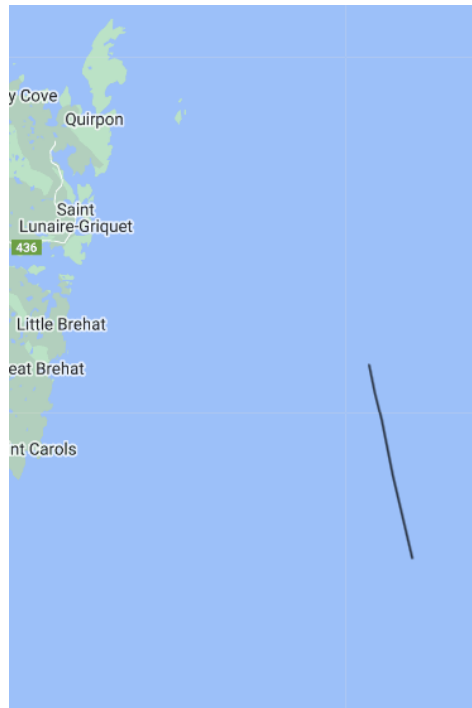


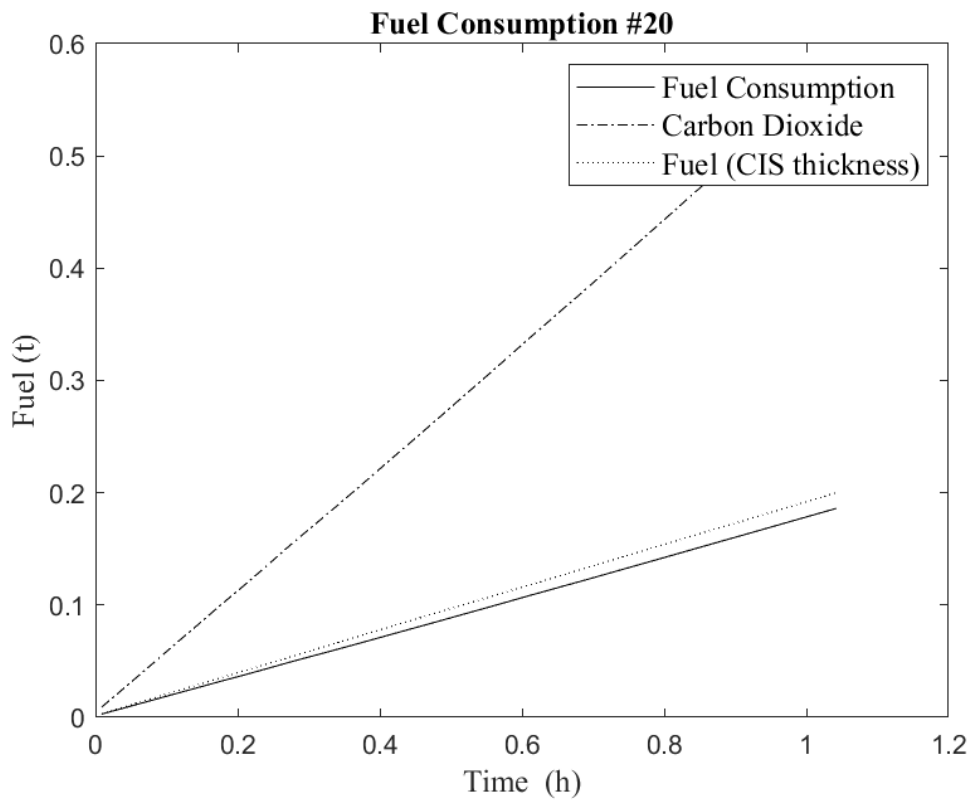
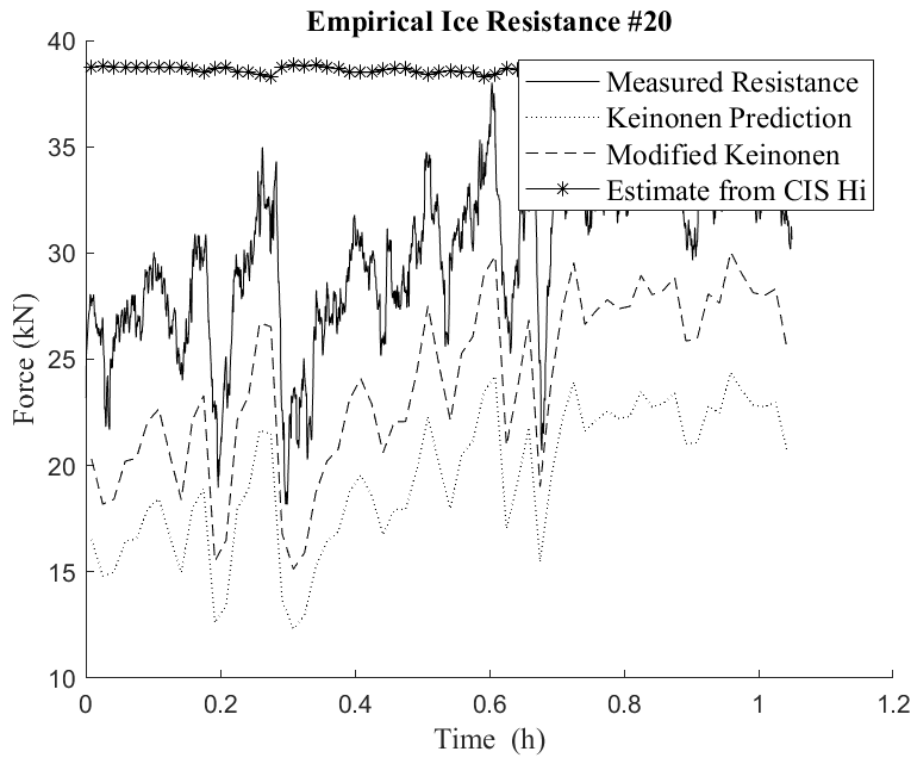
Data Segment #19	
Date	March 4, 2022
Statistical Thickness	0.061m
CIS equivalent thickness	0.17m
First Concentration/ Thickness	4% - 0.225m
Second Concentration/ Thickness	6% - 0.125m
Third Concentration/ Thickness	-
Ice Type	Grey-White Ice



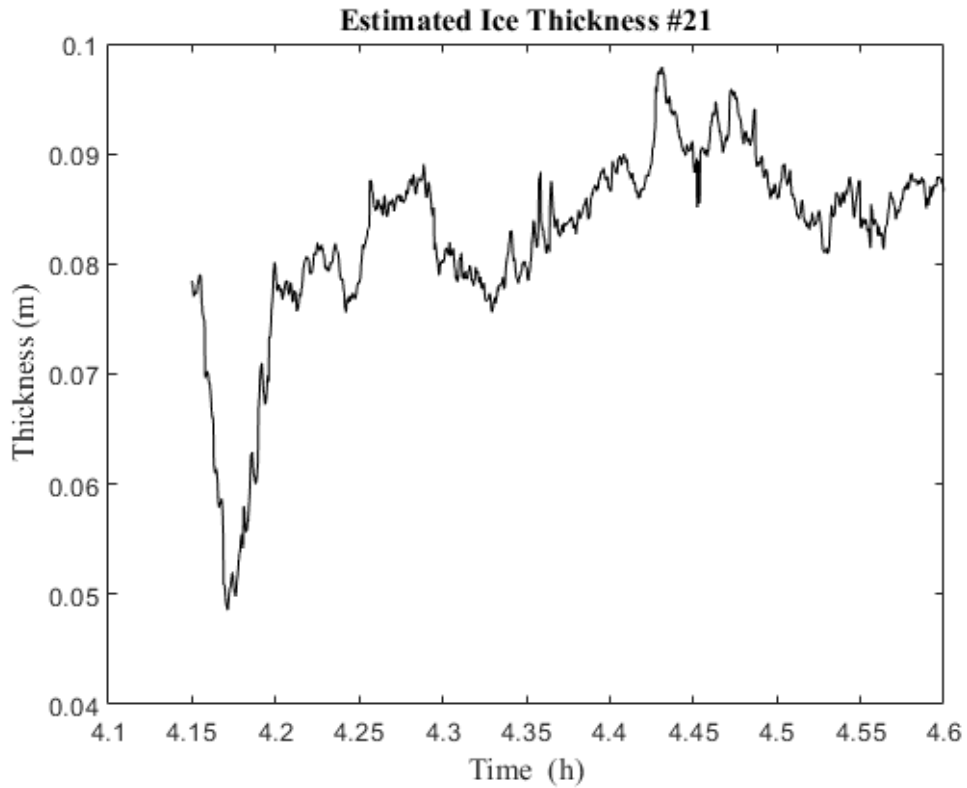


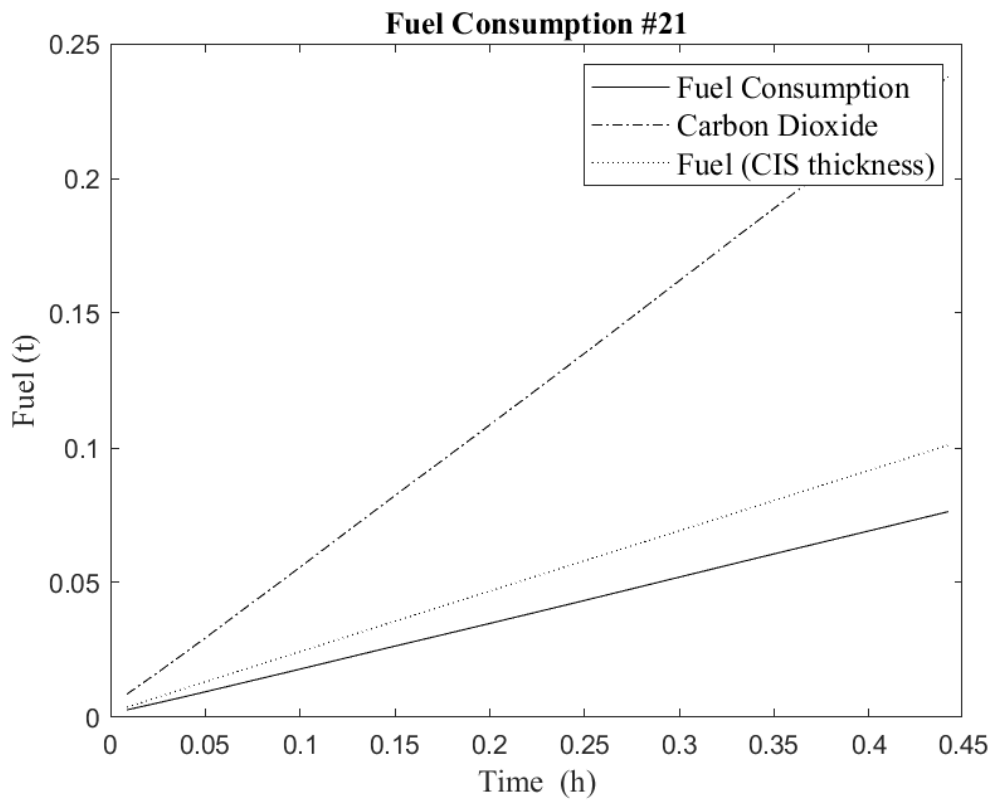
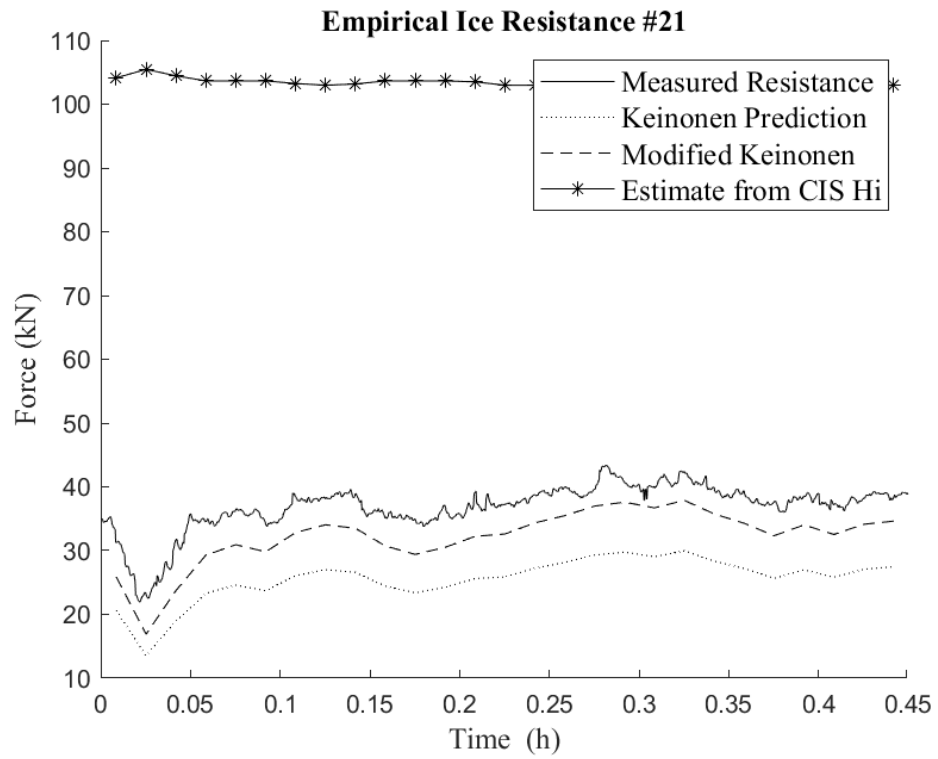
Data Segment #20	
Date	March 4, 2022
Statistical Thickness	0.07m
CIS equivalent thickness	0.18m
First Concentration/ Thickness	6% - 0.225m
Second Concentration/ Thickness	2% - 0.125m
Third Concentration/ Thickness	1% - 0.05m
Ice Type	New Ice



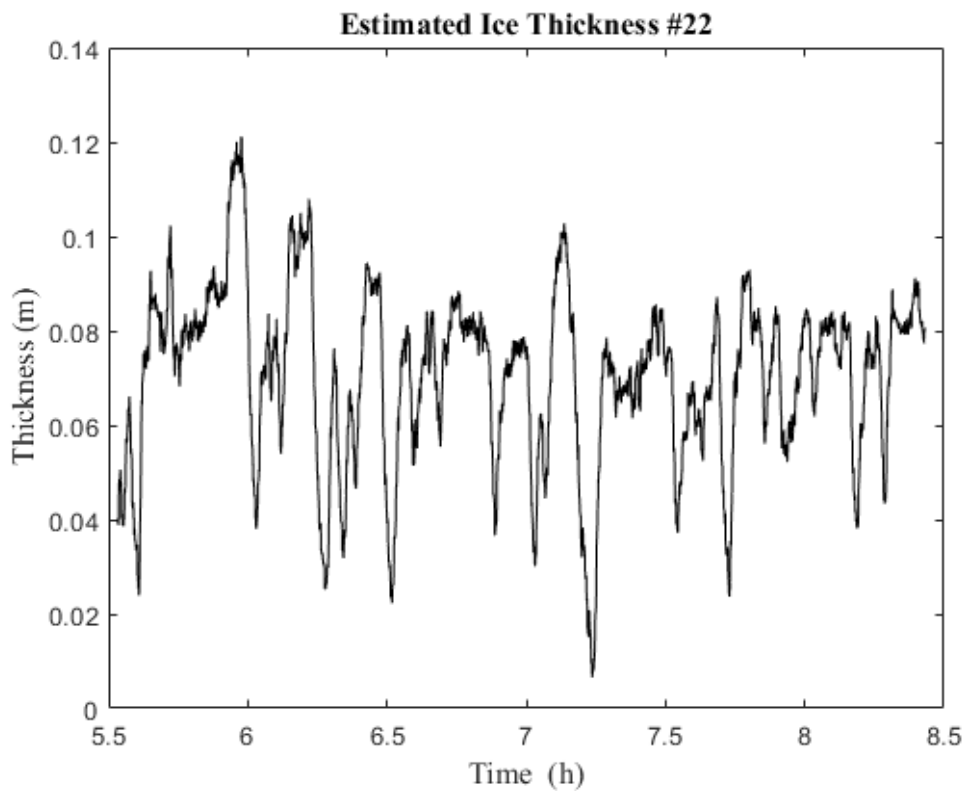


Data Segment #21	
Date	March 4, 2022
Statistical Thickness	0.089m
CIS equivalent thickness	0.18m
First Concentration/ Thickness	6% - 0.225m
Second Concentration/ Thickness	2% - 0.125m
Third Concentration/ Thickness	1% - 0.05m
Ice Type	New Ice

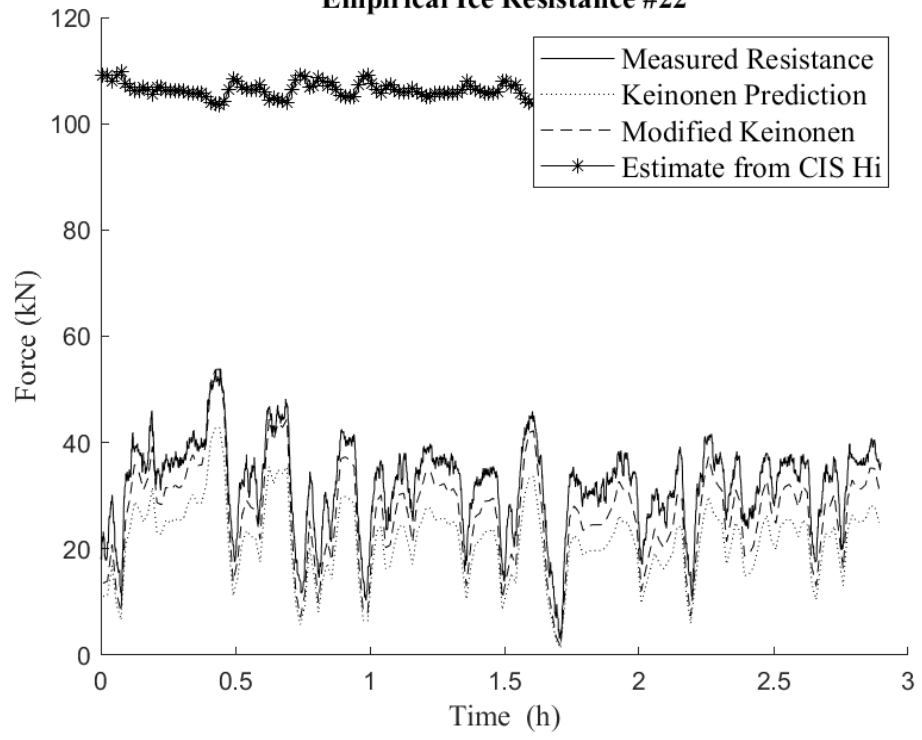




Data Segment #22	
Date	March 4, 2022
Statistical Thickness	0.076m
CIS equivalent thickness	0.18m
First Concentration/ Thickness	6% - 0.225m
Second Concentration/ Thickness	2% - 0.125m
Third Concentration/ Thickness	1% - 0.05m
Ice Type	New Ice



Empirical Ice Resistance #22



Fuel Consumption #22

